

## Characterisation of Fatigue Crack Growth in Adhesive Bonds

Pascoe, John- Alan

**DOI**

[10.4233/uuid:ebbf552a-ce98-4ab6-b9cc-0b939e12ba8b](https://doi.org/10.4233/uuid:ebbf552a-ce98-4ab6-b9cc-0b939e12ba8b)

**Publication date**

2016

**Document Version**

Final published version

**Citation (APA)**

Pascoe, J. A. (2016). *Characterisation of Fatigue Crack Growth in Adhesive Bonds*. [Dissertation (TU Delft), Delft University of Technology]. <https://doi.org/10.4233/uuid:ebbf552a-ce98-4ab6-b9cc-0b939e12ba8b>

**Important note**

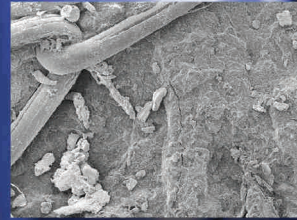
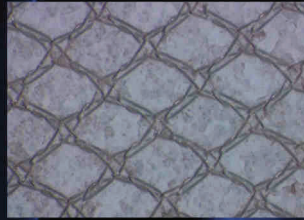
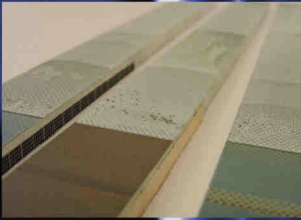
To cite this publication, please use the final published version (if applicable).  
Please check the document version above.

**Copyright**

Other than for strictly personal use, it is not permitted to download, forward or distribute the text or part of it, without the consent of the author(s) and/or copyright holder(s), unless the work is under an open content license such as Creative Commons.

**Takedown policy**

Please contact us and provide details if you believe this document breaches copyrights.  
We will remove access to the work immediately and investigate your claim.



# Characterisation of fatigue crack growth in adhesive bonds

John-Alan Pascoe

# Propositions

accompanying the dissertation

## CHARACTERISATION OF FATIGUE CRACK GROWTH IN ADHESIVE BONDS

by

**John Alan PASCOE**

1. Fatigue crack growth research needs more questions and fewer answers.
2. Most of the *R*-ratio effect that is identified in literature is merely a failure to uniquely describe the applied load cycle.
3. Driving force approaches to fatigue crack growth prediction need to model crack growth behaviour within a single cycle.
4. Using the strain energy release rate does not automatically imply satisfying the first law of thermodynamics.
5. Virtual testing is an oxymoron.
6. The present-day torrent of scientific publications has made the Royal Society's motto of *nullius in verba* untenable.
7. The purpose of democratic elections is not to choose the best solution, but to choose the definition of 'best'.
8. Although we know movies are fictional, we believe what they tell us about the world.
9. Education quality should not be measured by the final level that is achieved, but by the difference between the initial and final levels.
10. To get the fastest response from supervisors and workshop personnel; say you are not in a hurry.

These propositions are regarded as opposable and defensible, and have been approved as such by the supervisor prof. dr. ir. R. Benedictus.

# Stellingen

behorende bij het proefschrift

## CHARACTERISATION OF FATIGUE CRACK GROWTH IN ADHESIVE BONDS

door

**John Alan PASCOE**

1. Het onderzoek naar vermoeingsscheurgroei heeft meer vragen nodig, en minder antwoorden.
2. Het  $R$ -quotiënt effect dat in de literatuur wordt geïdentificeerd, is grotendeels slechts het verzuim een unieke beschrijving te geven van de opgelegde belastings-cyclus.
3. Methodieken voor het voorspellen van vermoeingsscheurgroei gebaseerd op een 'drijvende kracht' - aanpak moeten de scheurgroei binnen een enkele cyclus modelleren.
4. Het gebruik van de rekenergie-afgiftesnelheid impliceert niet automatisch het voldoen aan de eerste wet van de thermodynamica.
5. Virtueel testen is een contradictio in terminis.
6. De huidige stortvloed aan wetenschappelijke publicaties heeft het motto van de *Royal Society* – '*nullius in verba*' – onhoudbaar gemaakt.
7. Het doel van democratische verkiezingen is niet om de beste oplossing te kiezen, maar om de definitie van 'beste' te kiezen.
8. Hoewel we weten dat films fictie zijn, geloven we toch wat ze ons vertellen over de wereld.
9. De kwaliteit van een opleiding zou niet afgemeten moeten worden aan het bereikte eindniveau, maar aan het verschil tussen het begin- en eindniveau.
10. Om de snelste respons te krijgen van begeleiders en werkplaatspersoneel; zeg dat je geen haast hebt.

Deze stellingen worden oponeerbaar en verdedigbaar geacht en zijn als zodanig goedgekeurd door de promotor prof. dr. ir. R. Benedictus.



# **CHARACTERISATION OF FATIGUE CRACK GROWTH IN ADHESIVE BONDS**



# **CHARACTERISATION OF FATIGUE CRACK GROWTH IN ADHESIVE BONDS**

## **Proefschrift**

ter verkrijging van de graad van doctor  
aan de Technische Universiteit Delft,  
op gezag van de Rector Magnificus prof. ir. K. C. A. M. Luyben;  
voorzitter van het College voor Promoties,  
in het openbaar te verdedigen op  
dinsdag 11 oktober 2016 om 15:00 uur

door

**John Alan PASCOE**

Ingenieur Luchtvaart- & Ruimtevaarttechniek,  
Technische Universiteit Delft,  
geboren te Hilversum

Dit proefschrift is goedgekeurd door de

promotor: prof. dr. ir. R. Benedictus

copromotor: dr. ir. R.C. Alderliesten

Samenstelling promotiecommissie:

Rector Magnificus

voorzitter

Prof. dr. ir. R. Benedictus

Technische Universiteit Delft

Dr. ir. R. C. Alderliesten

Technische Universiteit Delft

Onafhankelijke leden:

Prof. dr. ir. L.J. Sluys

Technische Universiteit Delft

Prof. dr. W. Van Paeppegem

Universiteit Gent, België

Prof. dr. M.N. James

Plymouth University, Verenigd Koninkrijk

Prof. dr. M. Hojo

Kyoto University, Japan

Dr. A.P. Vassilopoulos

Ecole Polytechnique Fédérale de Lausanne, Zwitserland

Prof. dr. W. A. Groen,

Technische Universiteit Delft, reservelid



Delft  
University of  
Technology



Nederlandse Organisatie voor Wetenschappelijk Onderzoek

*Keywords:* Adhesive Bonds, Crack Growth, Fatigue, Strain Energy Release

*Printed by:* Gildeprint

*Front & Back:* Test set-ups and fracture surfaces photographed by the author during the course of the research.

Copyright © 2016 by J.A. Pascoe

All rights reserved. No part of this publication may be reproduced, stored in a retrieval system or transmitted in any form or by any means, electronic, mechanical, photocopying, recording or otherwise, without the prior written permission of the author.

This research was supported by the Netherlands Organisation for Scientific Research (NWO) under project number: 017.009.005.

ISBN 978-94-6186-718-6

An electronic version of this dissertation is available at

<http://repository.tudelft.nl/>.

*There is what happens, and what does not happen. There is no 'should'.*

Terry Pratchett, *Nation*



# SUMMARY

Fatigue crack growth (FCG) in adhesive bonds has been studied for a good half a century. However in that time, most efforts have focussed on trying to predict crack growth, rather than understanding it. As a result, although there are many prediction methods available, these are invariably based on empirical correlations, with little regard for the underlying physics. Consequently, in order to use these models, extensive test campaigns are needed to provide sufficient supporting data. Furthermore the limits of validity of the models are not clear, and it is uncertain how to properly take account of test parameters such as the ratio of minimum to maximum load, or the temperature.

Therefore the present thesis does not focus on predicting FCG, but rather on increasing understanding of the crack growth process, by characterising it. The characterisation is done according to a conceptual model of FCG introduced in the thesis. According to this model, the crack growth rate follows from the total amount of available energy and the amount of energy required per unit of crack growth. The energy required per unit of crack growth can also be interpreted as the material's resistance to crack growth. Both the available and required energies depend on the applied load cycle.

Fatigue crack growth experiments were performed on double cantilever beam specimens consisting of two aluminium 2024-T3 arms bonded with FM94 epoxy adhesive. It was found that the amount of energy dissipated per cycle correlated very strongly with the crack growth rate. It was also found that the resistance to crack growth (in terms of energy dissipation per unit of crack growth) was linearly related to the maximum strain energy release rate  $G_{\max}$ , and changed during the course of a fatigue test. At higher load levels more energy is required to generate the same amount of crack growth.

For a given value of the crack growth resistance, the total amount of energy available for crack growth was found to be correlated to the applied cyclic work  $U_{cyc}$ , as well as the strain energy release rate range  $\Delta G$ , and the cyclic strain energy release rate parameter  $\Delta\sqrt{G}$ .

In order to further investigate the relationship between the available and required energy, and the applied load, experiments were performed on specimens with different adhesive layer thicknesses, and at an elevated temperature. It was found that increasing the adhesive thickness did not affect the relationship between the crack growth resistance and the applied load, but did increase the amount of available energy for a given load cycle. Consequently, for a given load cycle, the crack growth was faster if the adhesive layer was thicker.

For the tests at an elevated temperature (80 °C) for 4 out of 6 tests the failure mode changed from cohesive to adhesive, which should be kept in mind when comparing the results. For the specimens that failed adhesively the resistance to crack growth for a given load cycle was higher at 80 °C than at room temperature. If the failure remained cohesive, temperature did not appear to affect the resistance. However there was a large temperature effect on the available energy for a given load cycle, which was much higher



at elevated temperature. The increase in available energy was greater than the increase in resistance, resulting in a greater crack growth rate for a given load cycle at elevated temperature.

Acoustic emission was used to investigate crack growth within a single load cycle. It was found that crack growth occurs both during the loading and the unloading phase of the fatigue cycle, as long as the load (in terms of  $G$ ) is above a certain threshold level. The thresholds for crack growth under quasi-static and fatigue loading appeared to be the same, suggesting it may be possible to derive fatigue properties from a quasi-static test.

In conclusion, this thesis has shown that measuring energy dissipation can be used as a method for characterising FCG. It was shown that the energy required per unit of crack growth depends on maximum load, in terms of  $G_{\max}$ . The amount of energy available for crack growth depends on the load range, in terms of  $U_{cyc}$ ,  $\Delta\sqrt{G}$ , or  $\Delta G$ . Further research is required to clarify the exact relationships between the applied load on the one hand, and the required and available energy on the other.

# SAMENVATTING

Vermoeingscheurgroei in gelijmde verbindingen wordt al een halve eeuw bestudeerd. In die tijd hebben de meeste onderzoeken zich echter gericht op het voorspellen van scheurgroei, in tegenstelling tot het begrijpen ervan. Als gevolg hiervan zijn er weliswaar vele voorspellingmodellen beschikbaar, maar zijn deze onveranderlijk gebaseerd op empirische correlaties en houden ze weinig rekening met de onderliggende fysica. Dit leidt er toe dat er om deze modellen te gebruiken uitgebreide proefprogramma's nodig zijn om voldoende ondersteunende data aan te leveren. Bovendien zijn de geldigheidslimieten van de modellen niet helder. Ook is het onduidelijk hoe rekening te houden met experimentele parameters als de verhouding van minimale tot maximale belasting, of de temperatuur.

Daarom richt dit proefschrift zich niet op het voorspellen van scheurgroei, maar op het vergroten van het begrip van het scheurgroeiproces, door het karakteriseren ervan. De karakterisatie wordt gedaan volgens een conceptueel model van scheurgroei dat in dit proefschrift wordt voorgesteld. Volgens dit model volgt de scheurgroeisnelheid uit de totale hoeveelheid beschikbare energie en de hoeveelheid benodigde energie per eenheid scheurgroei. De benodigde energie per eenheid scheurgroei kan ook worden geïnterpreteerd als de weerstand van een materiaal tegen scheurgroei. Zowel de beschikbare als de benodigde energieën hangen af van de opgelegde belastingscyclus.

Scheurgroeioproeven werden uitgevoerd op *double cantilever beam* proefstukken, bestaande uit twee aluminium 2024-T3 armen, verbonden met FM94 epoxy-lijm. Er werd gevonden dat de hoeveelheid gedissipeerde energie per cyclus zeer sterk correleerde met de scheurgroeisnelheid. Er werd ook gevonden dat de weerstand tegen scheurgroei (in termen van energie dissipatie per eenheid scheurgroei) lineair gerelateerd was aan de maximale rekenergie-afgitesnelheid,  $G_{\max}$ , en veranderde in de loop van een vermoeingsproef. Bij een hogere belasting is er meer energie benodigd om dezelfde hoeveelheid scheurgroei te genereren.

Voor een gegeven waarde van de scheurgroeiweerstand bleek de totale hoeveelheid beschikbare energie voor scheurgroei gecorreleerd aan de opgelegde cyclische arbeid  $U_{cy}$ , alsook aan het bereik van de rekenergie-afgitesnelheid  $\Delta G$ , en de cyclische rekenergie-afgitesnelheidsparameter  $\Delta\sqrt{G}$ .

Om de relatie tussen de beschikbare en benodigde energie enerzijds, en de opgelegde belasting anderzijds, verder te onderzoeken, werden er proeven uitgevoerd op proefstukken met verschillende lijmlaagdiktes, en bij een verhoogde temperatuur. Er werd gevonden dat het verhogen van de lijmlaagdikte geen invloed had op het verband tussen scheurgroeiweerstand en de opgelegde belasting. De hoeveelheid beschikbare energie voor een gegeven belastingscyclus werd wel hoger. Derhalve was voor een gegeven belastingscyclus, de scheurgroeisnelheid hoger als de lijmlaag dikker was.

Voor de proeven bij een verhoogde temperatuur (80 °C) veranderde voor 4 van de 6 proeven de faalmodus van cohesief naar adhesief. Hier moet rekening mee worden ge-

houden bij het vergelijken van de resultaten. Voor de proefstukken die adhesief faalden, was de weerstand tegen scheurgroei hoger bij 80 °C dan bij kamertemperatuur. Als de faalmodus cohesief bleef leek de temperatuur de weerstand niet te beïnvloeden. Er was echter wel een groot temperatuurseffect op de hoeveelheid beschikbare energie voor een gegeven belastingscyclus. Deze was veel hoger bij een hogere temperatuur. De toename van de beschikbare energie was groter dan de toename van de weerstand, wat leidde tot een grotere scheurgroeisnelheid voor dezelfde belastingscyclus bij een hogere temperatuur.

De akoestische-emissie techniek werd ingezet om scheurgroei binnen een enkele belastingscyclus te onderzoeken. Er werd gevonden dat scheurgroei plaatsvindt tijdens zowel tijdens de belastings- als tijdens de ontlastingsfase van de vermoeingscyclus, zolang de belasting (in termen van  $G$ ) groter dan een bepaalde drempelwaarde is. De drempelwaardes voor scheurgroei onder quasi-statische belasting en vermoeingsbelasting leken hetzelfde te zijn. Dit suggereert dat het wellicht mogelijk is om vermoeingseigenschappen af te leiden van een quasi-statische proef.

Dit proefschrift heeft aangetoond dat het meten van energiedissipatie gebruikt kan worden als een methode om vermoeingsscheurgroei te karakteriseren. Er werd aangetoond dat de benodigde hoeveelheid energie per eenheid scheurgroei afhangt van de maximale belasting, in termen van  $G_{\max}$ . De hoeveelheid beschikbare energie voor scheurgroei hangt af van het bereik van de belasting, in termen van  $U_{cyc}$ ,  $\Delta\sqrt{G}$  of  $\Delta G$ . Er is meer onderzoek nodig om het verband op te helderen tussen de opgelegde belasting enerzijds, en de benodigde en beschikbare energie anderzijds.

# PREFACE

In his book *I Shall Wear Midnight*, Sir Terry Pratchett discusses the qualities that good witches should possess. A particularly important set is that of First Sight and Second Thoughts, which he defines as follows:

“First Sight means that you can see what really is there, and Second Thoughts mean thinking about what you are thinking”

Pratchett, T., *I Shall Wear Midnight*, (Random House, London, 2010)

I would argue that not only witches should aspire to these qualities, but also scientists. First sight means remembering which of the parameters we use are actually measured, and which are only proxies for some underlying parameter we can not measure directly. Second thoughts means not being satisfied with an empirical correlation, but trying to find out what this correlation means, and why it should have a certain mathematical form.

Over the past four years I have tried to apply these principles to the problem of fatigue crack growth. Rather than creating yet another prediction model, I have attempted to create more understanding of the crack growth process and the underlying physics. I have tried to highlight where current approaches rely on models and concepts that do not necessarily reflect the actual physics, and have attempted to shed new light on these areas.

It is my hope that this has resulted in a thesis that will inspire a new way of thinking about these problems, and will lead to further research aimed at not just predicting fatigue crack growth, but at actually understanding it.

*John-Alan Pascoe*  
*Delft, June 2016*



# CONTENTS

<b>Summary</b>	<b>vii</b>
<b>Samenvatting</b>	<b>ix</b>
<b>Nomenclature</b>	<b>xvii</b>
<b>1 Introduction</b>	<b>1</b>
1.1 Need for a better understanding of fatigue crack growth in adhesive bonds .	2
1.2 The similitude principle and its application to fatigue crack growth . . . .	3
1.3 Aim and scope of this thesis . . . . .	5
1.4 Thesis outline . . . . .	6
References . . . . .	6
<b>2 Literature Review</b>	<b>9</b>
2.1 Early developments in fracture mechanics . . . . .	10
2.2 Application to fatigue in adhesives and composites . . . . .	12
2.3 Addressing the R-ratio effect . . . . .	14
2.4 Normalisation by the fracture toughness . . . . .	16
2.5 Physical objections to the LEFM based models . . . . .	17
2.6 The configurational force approach . . . . .	18
2.7 Plastic energy dissipation . . . . .	21
2.8 Conclusion . . . . .	23
References . . . . .	23
<b>3 Methodology</b>	<b>31</b>
3.1 Conceptual model of crack growth . . . . .	32
3.2 Definition of terms related to the strain energy . . . . .	33
3.3 Specimen description . . . . .	35
3.4 Test set-up . . . . .	36
3.5 Selection of applied loads . . . . .	37
3.6 Data analysis . . . . .	39
3.6.1 Crack growth rate . . . . .	39
3.6.2 Strain energy release rate . . . . .	39
3.6.3 Energy dissipation . . . . .	40
References . . . . .	41
<b>4 Energy dissipation during fatigue crack growth</b>	<b>43</b>
4.1 Introduction . . . . .	44
4.2 LEFM approach . . . . .	44
4.2.1 R-ratio effect with $G_{\max}$ as similitude parameter . . . . .	46
4.2.2 Suitability of $(\Delta\sqrt{G})^2$ as a similitude parameter . . . . .	46

4.2.3	Interpretation of $(\Delta\sqrt{G})^2$ as crack driving force . . . . .	47
4.2.4	Issues with current driving force approaches . . . . .	48
4.3	Correlation between energy dissipation and crack growth rate . . . . .	48
4.4	Comparison to the conceptual model. . . . .	52
4.4.1	Crack growth resistance . . . . .	53
4.4.2	Available energy . . . . .	56
4.4.3	Existence of a fatigue threshold . . . . .	59
4.4.4	Empirical prediction approach based on current findings . . . . .	60
4.4.5	Explanation of the <i>R</i> -ratio effect when using $\Delta G$ as a similitude parameter . . . . .	62
4.5	Crack growth under quasi-static loading . . . . .	63
4.6	Fractography . . . . .	67
4.7	Conclusion . . . . .	71
	References . . . . .	71
<b>5</b>	<b>Effect of thickness</b>	<b>75</b>
5.1	Introduction . . . . .	76
5.2	Specimens and test set-up . . . . .	76
5.3	Results and discussion . . . . .	78
5.4	Crack growth in glass-fibre composites . . . . .	85
5.4.1	Quasi-static crack growth . . . . .	85
5.4.2	Fatigue crack growth . . . . .	85
5.5	Conclusion . . . . .	88
	References . . . . .	89
<b>6</b>	<b>Effect of temperature</b>	<b>91</b>
6.1	Introduction . . . . .	92
6.1.1	Previous work on the effect of temperature . . . . .	92
6.1.2	Effect of temperature on FM 94 material properties . . . . .	93
6.2	Experimental set-up . . . . .	93
6.3	Results . . . . .	94
6.4	Conclusion . . . . .	99
	References . . . . .	100
<b>7</b>	<b>Fatigue crack growth within a single cycle</b>	<b>103</b>
7.1	Motivation . . . . .	104
7.2	Specimens and experimental set-up . . . . .	105
7.3	Quasi-static experiments . . . . .	107
7.4	Quasi-static threshold. . . . .	112
7.5	Fatigue experiments . . . . .	114
7.6	Fatigue thresholds . . . . .	118
7.7	Discussion . . . . .	120
	References . . . . .	122



<b>8</b>	<b>Conclusions and recommendations</b>	<b>123</b>
8.1	Conclusions. . . . .	124
8.1.1	Physical interpretation of LEFM parameters . . . . .	124
8.1.2	Correlation of energy dissipation and crack growth rate . . . . .	125
8.1.3	Effect of thickness . . . . .	125
8.1.4	Effect of temperature . . . . .	126
8.1.5	Fatigue crack growth in a single cycle . . . . .	126
8.1.6	Final conclusions . . . . .	127
8.2	Recommendations . . . . .	128
8.2.1	Criteria for a good fatigue model. . . . .	128
8.2.2	Future research directions . . . . .	129
8.2.3	Concrete next steps . . . . .	130
	References . . . . .	130
<b>A</b>	<b>Curve fit parameters and additional data</b>	<b>133</b>
	References . . . . .	140
<b>B</b>	<b>Effect of <math>R</math>-ratio for constant <math>(\Delta\sqrt{G})^2</math> and <math>\Delta G</math></b>	<b>141</b>
	<b>Acknowledgements</b>	<b>143</b>
	<b>Curriculum Vitae</b>	<b>145</b>
	<b>List of Publications</b>	<b>147</b>



# NOMENCLATURE

## LATIN SYMBOLS

$A$	Crack surface area	$\text{mm}^2$
$A$	Fit parameter in the Jones model	$\text{mJ}/\text{mm}^2$
$A$	Empirical constant in the Weertman model	-
$a$	Crack length	$\text{mm}$
$C$	Curve fit parameter	unit dependent on $n$
$C$	Compliance	$\text{mm}/\text{N}$
$C_p$	Plasticity influence parameter	-
$\Delta CTOD$	Crack tip opening displacement range	$\text{mm}$
$d$	Displacement	$\text{mm}$
$d_0$	Displacement at zero force	$\text{mm}$
$E$	Young's modulus	$\text{GPa}$
$E_k$	Kinetic energy	$\text{mJ}$
$F$	External work	$\text{mJ}$
$G$	Strain energy release rate	$\text{mJ}/\text{mm}^2$
$G^*$	Energy dissipation per unit crack growth	$\text{mJ}/\text{mm}^2$
$G_c$	Critical strain energy release rate	$\text{mJ}/\text{mm}^2$
$G_R$	Resistance to fatigue crack growth	$\text{mJ}/\text{mm}^2$
$\Delta G$	Strain energy release rate range	$\text{mJ}/\text{mm}^2$
$\Delta\sqrt{G}$	Cyclic strain energy release rate parameter	$\sqrt{\text{mJ}}/\text{mm}$
$J$	J-integral	$\text{mJ}/\text{mm}^2$
$\Delta J$	J-integral range	$\text{mJ}/\text{mm}^2$
$\Delta\sqrt{J}$	Cyclic J-integral parameter	$\text{mJ}/\text{mm}^2$
$K$	Stress intensity factor	$\text{MPa}\sqrt{\text{mm}}$
$\Delta K$	Stress intensity factor range	$\text{MPa}\sqrt{\text{mm}}$
$N$	Number of cycles	-
$n$	Curve fit parameter	-
$n$	Compliance calibration parameter	-
$m$	Number of divisions for determining $G_{\text{avg}}$ in the Atodaria model	-
$P$	Force	$\text{N}$
$Q$	Activation energy	$\text{J}$
$R$	Universal gas constant	$\text{J}/\text{mol}\cdot\text{K}$
$R$	Load ratio	-
$R_p$	Force ratio	-
$R_d$	Displacement ratio	-
$S$	Stress	$\text{MPa}$
$\Delta S$	Stress range	$\text{MPa}$

$s$	Coordinate	mm
$T$	Temperature	°C, K
$\mathbf{t}$	Traction vector	MPa
$U$	Strain energy	mJ
$\mathbf{u}$	Displacement vector	mm
$W$	Energy consumed by crack growth	mJ
$w$	Weight factor in the Atodaria model	-
$w$	Width	mm
$x, y$	Coordinates	mm

## GREEK SYMBOLS

$\alpha$	Ratio between energy flowing to the plastic zone and energy flowing to the end-region in the Broberg model	-
$\alpha, \beta, \gamma$	Curve fit parameters	-
$\Gamma$	Integration path	-
$\Gamma$	Energy per unit area of crack extension	mJ/mm <sup>2</sup>
$\gamma$	Mean stress sensitivity	-
$\gamma$	Effective surface energy	mJ/mm <sup>2</sup>
$\gamma_s$	Surface energy	mJ/mm <sup>2</sup>
$\gamma_p$	Plastic dissipation in the process zone	mJ/mm <sup>2</sup>
$\kappa$	Curve fit parameter	-
$\lambda$	Curve fit parameter	-
$\mu$	Shear modulus	GPa
$\nu$	Poisson's ratio	-
$\xi, \psi$	Curve fit parameters	-
$\sigma$	Stress	MPa
$\Phi$	Energy flow to the end-region in the Broberg model	mJ/mm <sup>2</sup>
$\phi$	Strain energy density	mJ/mm <sup>3</sup>

## SUBSCRIPTS

avg	Average
c	Critical
cyc	Cyclic
i	Index
I, II, III	With respect to mode I, II, III
m	Mean
max	Maximum
min	Minimum
mono	Monotonic
PZ	Plastic zone
pl	Plastic

th	Threshold
tot	Total
y	Yield

## ABBREVIATIONS

AE	Acoustic Emission
ASTM	American Society for Testing and Materials
CAA	Chromic Acid Anodisation
CC	Compliance Calibration
CFRP	Carbon Fibre Reinforced Polymer
CTOD	Crack Tip Opening Displacement
FCG	Fatigue Crack Growth
FEA	Finite Element Analysis
FEM	Finite Element Method
FML	Fibre Metal Laminate
FRP	Fibre Reinforced Polymer
GFRP	Glass Fibre Reinforced Polymer
LEFM	Linear Elastic Fracture Mechanics
MBT	Modified Beam Theory
MCC	Modified Compliance Calibration
PEEK	PolyEther Ether Ketone
RMSE	Root Mean Square Error
QS	Quasi-Static
SERR	Strain Energy Release Rate
SEM	Scanning Electron Microscope
SIF	Stress Intensity Factor



# 1

## INTRODUCTION

*And the crack in the tea-cup opens  
A lane to the land of the dead.*

W.H. Auden, *As I Walked Out One Evening*

*In order to benefit from the advantages offered by adhesive bonding as a joining method for primary aircraft structures, a better understanding of fatigue crack growth is needed. While many models have been developed for predicting fatigue crack growth, prediction and understanding of material behaviour are two different things. The shortcomings of existing models for prediction of crack growth mean that more understanding of the material behaviour is needed. In particular it should be investigated whether the current models for fatigue crack growth are based on the correct similitude principle. Rather than attempting to provide a prediction model, the emphasis should be on increased understanding of material behaviour.*

*This thesis aims to increase understanding of fatigue crack growth in adhesive bonds through the investigation of the relationship between energy dissipation and fatigue crack growth. To avoid differences between materials obscuring the underlying material behaviour, the research was limited to investigating mode I fatigue crack growth in an Al-2024/FM-94 epoxy adhesive bond. To better understand the observed material behaviour, investigations were carried out into the influence of bond-line thickness and of temperature. In addition fatigue crack growth within a single cycle was investigated.*



## 1.1.1. NEED FOR A BETTER UNDERSTANDING OF FATIGUE CRACK GROWTH IN ADHESIVE BONDS

‘*When will it break?*’ is the central question of structural engineering. In order to determine whether a given structure will be able to carry out all its functions reliably, a structural engineer needs to be able to determine under which loads it will fail. There are of course many different materials and possible loading conditions that could be investigated. This thesis will focus specifically on fatigue loading of adhesive bonds.

Adhesive bonding is a very old joining method. There is evidence that birch-bark tar was already in use as an adhesive to join hafts to stone tools as long as 200,000 years ago [1, 2]. Bitumen was used for the same purpose starting at least 70,000 years ago [3]. By 40,000 years ago the first adhesive systems were created by mixing plant resins with ochre [1, 4].

Fast-forwarding to the 20<sup>th</sup> century, adhesive bonding quickly became an important joining method within the aviation industry [5]. Although the switch to all-metal structures around the time of the Second World War made mechanical fastening the dominant joining technique, adhesive bonding remained important. Compared to mechanical fastening, adhesive bonding avoids the need to create holes in the structure, and provides a more uniform load transfer path. Properly designed adhesive bonds therefore create much lower stress concentrations. Consequently they can have a lower weight than mechanically fastened joints. As a lower structural weight reduces an aircraft’s fuel consumption, the use of adhesive bonding can help reduce operational costs, as well as the environmental impact. Additionally, the quest to reduce structural weight has resulted in an increasing use of fibre reinforced polymer (FRP) composites. These are generally not very resistant to bearing pressure, making adhesive bonding a more suitable choice than mechanical fastening.

However, before adhesive bonding can be applied on a large scale to primary aircraft structures, two issues need to be solved. First of all, there is no reliable inspection technique that allows quantification of bond strength in the case of ‘weak’ or ‘kissing’ bonds. Secondly, better prediction models are needed for the behaviour of adhesive bonds under fatigue loading. It is known that cycles of repeated loading will cause cracks to initiate and then propagate within an adhesive bond. However, despite some four decades of research, so far no prediction method has been found that is sufficiently reliable and generally applicable enough to allow certification of adhesive bonding as a primary joining method [6, 7]. In particular, Jones et al. [7] mention the need to account for various test conditions, such as the load ratio and test temperature, as well as the need for better understanding of the growth of ‘short’ cracks. These tend to grow more quickly than would be predicted based on data obtained from tests with ‘long’ cracks. Other issues are how to account for the scatter usually seen in experimental results, and that current methods tend to be based on power-laws with large exponents. This means that even a small uncertainty in applied load translates into a large uncertainty in the resulting crack growth rate.

Thus, at present, manufacturers wishing to use adhesive bonds have to rely on the ‘no-growth’ design philosophy [7], where it must be shown that any damage below a

detectable size will not grow during the entire operational lifetime of the aircraft. This means stresses within the adhesive bond must be kept below the threshold level for fatigue crack growth (FCG), necessitating very heavy designs. Another option is to reinforce the adhesive bond with mechanical fasteners able to carry all the required loads even if the entire bond-line fails. However this imposes a weight penalty, and negates most of the advantages of using an adhesive bond.

The need for a better prediction of FCG in adhesive bonds should now be clear. Ironically, at least part of the reason that better predictions are not yet available is that past studies have focused mainly on prediction, as opposed to *understanding* of material behaviour. As a result, the similitude principle underlying current prediction methods has never been sufficiently examined.

## 1.2. THE SIMILITUDE PRINCIPLE AND ITS APPLICATION TO FATIGUE CRACK GROWTH

**I**N the course of human history, various approaches have been developed to answering the question of when a structure will break. The first ‘structural engineers’ most likely answered this question through a combination of trial-and-error and experience, which was eventually codified into rules-of-thumb and passed down from one generation to the next.

Although one may consider the combination of trial-and-error and rules-of-thumb primitive, this method was used to build many great monuments, such as those of the Egyptian, Greek, Roman, or Mayan civilisations. Even with very little understanding of forces or material behaviour, these civilisations were able to create buildings that are still standing after millennia [8, 9]. The ancient engineers that built these structures were able to predict their strength, at least in a binary fashion (will it break, yes/no?). However, this ability to predict strength *does not imply a deep understanding of the material behaviour*. For example, when dimensioning the foundations of a temple, the Romans relied on rules such as:

“Above ground level, walls should be constructed underneath the columns, half again as thick as the columns are to be, so that the lower parts of the building will be more stable than the upper parts.” [8]

While this rule may result in a temple that can stand the test of time, it does not help one to understand *why* such a structure will not collapse. It also does not help one to figure out whether a slightly different design would work as well.

With the rise of the modern scientific world-view came the desire for a better understanding of material behaviour, pioneered by the experiments of Leonardo da Vinci and Galileo Gallilei [9]. To this scientific quest for better understanding were added the economical imperatives of the Industrial Revolution, which brought new materials and the desire to create new and larger structures. No longer could old rules-of-thumb be relied on to dimension the structures engineers were creating. It was also preferable to have some way of evaluating the performance of new materials, without having to create full-scale structures. This led to the mathematical formulations of stress and strain still in use to day. Additionally, the similitude principle became the most important tool for

engineering predictions.

The similitude principle states that the behaviour of two different structures can be compared by calculating a suitable parameter for (specific locations on) each structure. If this parameter is the same, then the structures will behave in the same way. For example, a truss member will fail under a tensile load that causes a stress, equal to that which causes failure of a specimen of the same material in a laboratory.

This is obviously a very powerful principle, as it allows the prediction of the load-bearing capacity of structures, even when they only exist as designs. It also allows the evaluation of new materials using only small samples, and without leaving the laboratory. However, it is important to remember that the similitude principle is once again a tool for *prediction*, and not necessarily *understanding*. One can predict that a structure will fail at a certain stress, without any understanding of the material processes that actually cause that failure. This means that the similitude principle must be used with caution, and preferably be backed by an understanding of the underlying material behaviour that can identify the limits of the chosen similitude parameter.

An illustrative example is the case of the strength of cracked objects. Initially tensile stress was used as a similitude parameter to predict the tensile strength of structures. If the stress exceeded the value found to cause failure in a laboratory specimen of the same material, then failure would also occur in the structure. While this principle holds for materials without any flaws, it was soon found that cracked structures would fail at much lower values of applied stress. At first the solution was sought in the stress-concentrating effect of notches, as e.g. shown mathematically by Inglis [10]. However, even though it was shown experimentally that Inglis' equations correctly calculated the stress around a notch [11], cracked specimens were still failing before the ultimate stress was reached, even taking into account the stress-concentration. Eventually it was Griffith who used an understanding of the physical material behaviour to show stress was unsuitable as a similitude parameter in this case, and that it was necessary to base similitude on the strain energy within the system [11].

From Griffith's work two similitude parameters were developed [12], i.e. the stress intensity factor (SIF,  $K$ ) and the strain energy release rate (SERR,  $G$ ), which proved to be very successful for predicting the strength of cracked structures under quasi-static load.

For cyclic loading (i.e. fatigue), Wöhler [13] had originally proposed the use of the stress amplitude as the similitude parameter. This parameter could successfully be used to predict fatigue lives, but could not be used to predict the growth rate of fatigue cracks themselves.

Paris et al. [14] therefore proposed the range of the stress intensity factor,  $\Delta K$ , as the correct similitude parameter for FCG rate predictions. Unlike in Griffith's work, the physical justification for  $\Delta K$  as the correct similitude parameter for FCG is much more tenuous. Nevertheless the work of Paris forms the basis of the linear elastic fracture mechanics (LEFM) approach to fatigue, which to this day underlies nearly all FCG prediction models. Although the crack growth rate can in many cases be correlated to some LEFM parameter, there are still issues to be resolved.

For example, the power-law function which is necessary to correlate the crack growth rate to the LEFM parameters, contains two curve-fit parameters of which the physical significance has never adequately been explained. Furthermore, the correlation is sen-

sitive to a number of effects, such as for example changes in the ratio of minimum to maximum stress. Although it is possible to produce good predictions by creating a large test database and interpolating within that, the correct physical explanation of these effects remains controversial [15]. In other words; while the LEFM concept has enabled good *predictions*, it has not produced much *understanding* of FCG behaviour.

Given the issues with the LEFM approach, and the lack of a foundation in an understanding of the underlying physics, it is time to ask whether LEFM has in fact supplied the most appropriate similitude parameter for fatigue. Perhaps a deeper understanding of the material behaviour could produce a better parameter, leading to more accurate and robust predictions of fatigue crack growth.

### 1.3. AIM AND SCOPE OF THIS THESIS

ORIGINALLY the goal of this thesis project was to find a better prediction for FCG rate in adhesive bonds. However during the literature review stage it became clear that while there are many prediction models available in literature, the understanding of the underlying physics is severely lacking. Thus it was decided to make the development of a prediction model a secondary goal, and instead focus on understanding the material behaviour.

As a result of the literature review it was decided that the most promising avenue of research would be to investigate FCG through the lens of an energy-based approach. This lead to the main research question of this thesis:

**Can fatigue crack growth in adhesive bonds be characterised in terms of dissipated strain energy?**

Related to this the following sub-questions were investigated:

- For a given fatigue cycle, what is the driving force or energy available for fatigue crack growth?
- Is the resistance to fatigue crack growth a material constant? If not, what parameters affect it?
- How can the resistance to fatigue crack growth be determined *a priori*?

In order to better understand the obtained test results, the following questions were also examined:

- How does the load ratio affect the relationship between energy dissipation and crack growth rate?
- How does bond-line thickness affect the relationship between energy dissipation and crack growth rate?
- How does temperature affect the relationship between energy dissipation and crack growth rate?
- How does the fatigue crack grow during the course of a single fatigue cycle?

In order to avoid complications caused by differences in behaviour between different materials, one material system was selected for this investigation, i.e. aluminium 2024-T3 bonded with FM-94 epoxy adhesive. Due to time limitations only mode I crack growth was investigated. To create a ‘limit case’ for the thickness investigations, some tests were also performed on an S2-glass/FM94 epoxy composite laminate in two separate projects under the author’s supervision [16, 17].

Despite these constraints on the scope of the research, it is thought that various general principles have been uncovered that are also applicable to other material classes. This will be discussed in more detail in the relevant chapters.

## 1.4. THESIS OUTLINE

A critical reflection on the current approaches to understanding and predicting fatigue crack growth is presented in Chapter 2. The methodology and conceptual model used to examine fatigue crack growth in this thesis are discussed in Chapter 3. Chapter 4 presents the core results obtained in this way. To better understand these results, Chapter 5 examines the effect of bond-line thickness, and Chapter 6 examines the effect of temperature. Chapter 7 discusses the results of an investigation into crack growth behaviour within a single fatigue cycle. The conclusions of the research are summarised in Chapter 8. Chapter 8 also examines how the results of this research can be applied to other materials and how they can inform future efforts to predict fatigue crack growth.

## REFERENCES

- [1] L. Wadley, T. Hodgskiss, and M. Grant, *Implications for complex cognition from the hafting of tools with compound adhesives in the Middle Stone Age, South Africa*, Proceedings of the National Academy of Sciences **106**, 9590 (2009).
- [2] P. P. A. Mazza, F. Martini, B. Sala, M. Magi, M. P. Colombini, G. Giachi, F. Landucci, C. Lemorini, F. Modugno, and E. Ribechini, *A new Palaeolithic discovery: tar-hafted stone tools in a European Mid-Pleistocene bone-bearing bed*, Journal of Archaeological Science **33**, 1310 (2006).
- [3] H. A. Sakhel, H. Valladas, M. Tobey, N. Mercier, D. Jarvie, J. Connan, S. Bonilauri, and E. Boëda, *New evidence for significant use of bitumen in Middle Palaeolithic technical systems at Umm el Tlel (Syria) around 70,000 BP*, Paléorient, 67 (2008), doi:10.3406/paleo.2008.5257.
- [4] S. H. Ambrose, *Chronology of the Later Stone Age and food production in East Africa*, Journal of Archaeological Science **25**, 377 (1998).
- [5] R. J. Schliekelmann, *Introduction*, in *Adhesive bonding of aluminum alloys*, edited by E. W. Thrall and R. W. Shannon (Marcel Dekker, Inc., New York, 1985).
- [6] J. A. Pascoe, R. C. Alderliesten, and R. Benedictus, *Methods for the prediction of fatigue delamination growth in composites and adhesive bonds - a critical review*, Eng Fract Mech **112-113**, 72 (2013).

- [7] R. Jones, W. Hu, and A. J. Kinloch, *A convenient way to represent fatigue crack growth in structural adhesives*, *Fatigue & Fracture of Engineering Materials & Structures* **38**, 379 (2014).
- [8] Vitruvius, *Ten books on architecture* (Cambridge University Press, Cambridge, 1999) English translation by Ingrid D. Rowland.
- [9] S. Timoshenko, *History of strength of materials : with a brief account of the history of theory of elasticity and theory of structures* (McGraw-Hill, New York, 1953).
- [10] C. Inglis, *Stresses in plates due to the presence of cracks and sharp corners*, *Transactions of the Institute of Naval Architects* **55**, 219 (1913).
- [11] A. A. Griffith, *The phenomena of rupture and flow in solids*, *Philosophical Transactions of the Royal Society of London Series A, Containing Papers of a Mathematical or Physical Character* **221**, 163 (1921).
- [12] G. R. Irwin, *Analysis of stresses and strains near the end of a crack traversing a plate*, *ASME Journal of Applied Mechanics* **24**, 361 (1957).
- [13] A. Wöhler, *Ueber die Festigkeits-Versuche mit Eisen und Stahl*. *Zeitschrift für Bauwesen* **XX**, 73 (1870).
- [14] P. Paris, M. Gomez, and W. Anderson, *A rational analytic theory of fatigue*, *The Trend in Engineering* **13**, 9 (1961).
- [15] R. C. Alderliesten, *The explanation of stress ratio effect and crack opening corrections for fatigue crack growth in metallic materials*, *Advanced Materials Research* **891-892**, 289 (2014).
- [16] A. Al Amery, *Strain energy loss per crack growth rate experiment in glass fiber* (Hogeschool InHolland, 2015) BSc thesis.
- [17] J. de Jong and T. van den Hoogenband, *Verschil tussen quasi-statische scheurgroei en scheurgroei door vermoeiing in glasvezelcomposieten met verschillende interfaces.*, Tech. Rep. (Pre-University Leiden, 2015) in Dutch.





# 2

## LITERATURE REVIEW

*Logarithmic plots are a device of the devil*

Charles Richter

*This chapter provides an overview of the literature that formed the background for this thesis. Over the previous 40 years many methods have been developed for the prediction of fatigue crack growth in adhesive bonds and composite materials. A comprehensive review of these methods has been previously published by the author in [1]. In this chapter the focus will be on the work that was directly relevant for the current research.*

*An overview is given of the historical development of the current approaches to prediction of fatigue crack growth. The shortcomings of these methods, in particular the lack of physical underpinning, is highlighted. In addition to a selection of the literature discussed in [1], attention is given to energy dissipation models and configurational force models. These two categories were not discussed in [1], but are worth mentioning here as they provide an alternate approach to the problem of modelling fatigue crack growth. It is concluded that an energy dissipation type model provides the most promising avenue for gaining a better understanding of the physics of the problem.*

### 2.1. EARLY DEVELOPMENTS IN FRACTURE MECHANICS

THE current approaches to understanding fatigue crack growth have their roots in the work of Griffith [2]. Griffith was looking for a theory that would explain the failure of structures containing cracks. At the time it was already understood that failure of specimens without flaws could be predicted by the concept of ultimate stress. However, this concept was unable to predict when cracked structures would fail, even if one took into account the stress concentrating effect of cracks or notches [2].

Griffith's breakthrough was to take energy, rather than stress, as the controlling parameter. Griffith recognised that in order to grow a crack, new surfaces must be created, for which energy is required. The required amount of energy is equal to the surface energy of the material, multiplied by the area of the newly created crack surfaces.

Although crack growth requires energy, the extension of a crack will also release strain energy from the surrounding material. Thus Griffith proposed that the critical stress at which a crack would extend, could be derived from the balance between released and consumed energy [2]. It should be emphasised here that Griffith derived the conditions under which a crack could propagate without disturbing the overall equilibrium of the object, i.e. assuming fixed-grip and quasi-static load conditions.

In perfectly brittle materials formation of new surfaces is the only mechanism consuming energy and Griffith's theory works. However, in other materials there will always be plastic deformation in the vicinity of the crack tip, which also dissipates energy. To account for this, Orowan and Irwin independently proposed the use of an effective surface energy  $\gamma$ ; defined as the sum of the actual surface energy  $\gamma_s$ , and the energy dissipated by plastic deformation in the vicinity of the crack tip  $\gamma_p$  [3–5], i.e.:

$$\gamma = \gamma_s + \gamma_p \quad (2.1)$$

Especially for metals,  $\gamma_p \gg \gamma_s$ , which is important for the theories discussed in section 2.7

Griffith's concept was further developed and mathematically formalised by Irwin and Kies [6–9], who formulated the energy balance as [7]:

$$\frac{dF}{dA} - \frac{dU}{dA} = \frac{dW}{dA} + \frac{dE_k}{dA} \quad (2.2)$$

where  $F$  is the work done on a body by external forces,  $U$  is the strain energy in the body,  $W$  is the energy consumed by crack growth (i.e. surface energy and plastic deformation),  $E_k$  is the kinetic energy, and  $A$  is the crack surface area. Note that in [7] the left hand term of equation 2.2 shows an addition, whereas here it contains a subtraction. This is because Irwin and Kies originally formulated equation 2.2 in terms of the reduction in strain energy, which is the additive inverse of the change in strain energy  $dU/dA$ .

The derivative of kinetic energy with respect to crack surface is assumed to be zero. The derivatives of external work and strain energy can be combined into the parameter known as the strain energy release rate (SERR) according to [10]:

$$G = \frac{d(F - U)}{dA} \quad (2.3)$$

The SERR is thus equal to difference between the reduction of strain per unit of crack growth and the external work performed per unit of crack growth. If this difference exceeds the amount of energy required per unit of crack growth,  $dW/dA$ , then unstable fracture can occur. In other words, equation 2.2 can be restated as a stability criterion. Crack growth will occur if:

$$G \geq G_c \quad (2.4)$$

where  $G_c$  is a critical SERR value. By comparison of equations 2.2 - 2.4  $G_c$  is in theory equal to the amount of energy consumed by any form of crack growth. In practice however  $G_c$  is equal to the value of  $G$  at which crack propagation is determined to occur *under quasi-static loading*, as for example codified in the ASTM D5528 test standard [11]. It is assumed that under these conditions  $G = G_c$ . While this is a reasonable assumption, it is important to remember that  $G_c$  implicitly refers to quasi-static loading conditions.

Apart from formalising the expressions for  $G$ , Irwin also demonstrated the equivalence of the SERR and the stress intensity factor (SIF,  $K$ ) [8, 9], according to:

$$G = \frac{K^2}{E'} \quad (2.5)$$

$$E' = E \quad \text{plane stress} \quad (2.6)$$

$$E' = \frac{E}{1 - \nu^2} \quad \text{plane strain} \quad (2.7)$$

where  $E$  is the Young's modulus of the material, and  $\nu$  is the Poisson ratio.

The consequence of equation 2.5 is that  $K$  and  $G$  can be used interchangeably in fracture mechanics analyses. So for example a stability criterion like equation 2.4 can be written in terms of  $K$ , rather than  $G$ . Equation 2.5 was also used to adapt fatigue crack growth (FCG) models originally developed for metals so they could be used for FCG in adhesive bonds and composites. This will be discussed in the next section. In principle equation 2.5 was derived for quasi-static loading conditions in a linear elastic material. However, it is usually assumed to also hold for fatigue loading and for ductile materials, as long as the amount of plastic deformation is sufficiently small.

The work of Griffith and Irwin formed the basis of the field now known as LEFM. Before continuing with the application of this theory to FCG in composites and adhesives, there is an important conceptual point to be made about these theories. In equation 2.5 Irwin has equated the stress-based and the energy-based approaches to the crack growth problem. Through the Williams solution [12] to the Westergaard equations [13]  $K$  describes the stress around a crack tip [8], whereas  $G$  describes the strain energy configuration within an object. Thanks to equation 2.5 however,  $K$  can be interpreted as saying something about the strain energy configuration and  $G$  can be interpreted as indicative of the crack tip stress. Thus regardless of whether one takes stress or energy as the basis for similitude, one can use either  $K$  or  $G$ . However, this interchangeability of stress and energy has obscured what basis of similitude is actually being relied on in a given FCG model.

Due to the difficulty of calculating  $K$  for non-homogeneous materials,  $G$  is often used in models for FCG in adhesives and composites. However, because the models used were

originally developed using  $K$ ,  $G$  in this case is interpreted as indicative of the crack-tip stress field, rather than as an energy parameter. This has caused various issues with these models to go unnoticed. Issues that are clearly highlighted if one looks instead through the lens of a strain energy based approach. This will be further discussed in section 2.5.

## 2.2. APPLICATION TO FATIGUE IN ADHESIVES AND COMPOSITES

WITH equation 2.4 it is possible to predict when a crack will grow under quasi-static loading conditions. However under fatigue loading crack growth will occur even if the maximum  $G$  value reached remains well below the  $G_c$  measured in quasi-static loading tests. Various methods for predicting FCG have been proposed, of which the method of Paris is currently the most successful.

Paris started from Wöhler's observation that fatigue life is governed by the stress amplitude [14]. For FCG Paris then reasoned that it is not the far-field stress that is important, but rather the stress at the crack tip, as described by the SIF. Consequently Paris and various different co-workers published a series of papers [15–17] in which the SIF range  $\Delta K = K_{\max} - K_{\min}$  was proposed as a similitude parameter for FCG. By curve-fitting of available crack growth data, Paris et al. proposed the relationship [15–17]:

$$\frac{da}{dN} = C \Delta K^n \quad (2.8)$$

where  $a$  is the crack length,  $N$  is the number of cycles, and  $C$  and  $n$  are curve fitting parameters.

This approach was first applied to metals, but was soon adapted to use in fatigue delamination and crack growth in composites and adhesive bonds. The first application of equation 2.8 to these classes of materials was by Roderick et al. [18] who proposed the equation:

$$\frac{da}{dN} = C G_{\max}^n \quad (2.9)$$

for debonding of carbon fibre reinforced polymer (CFRP) and glass fibre reinforced polymer (GFRP) layers bonded to aluminium as reinforcement (what would now be called a fibre metal laminate (FML) or hybrid joint). Making use of equation 2.5 the SIF was replaced by the SERR as the similitude parameter, based on the fact that it is easier to compute the SERR for a non-homogeneous material.

It is noteworthy that the direct equivalent of  $\Delta K$  would be  $\Delta\sqrt{G}$ , defined as:

$$\Delta\sqrt{G} = \left( \sqrt{G_{\max}} - \sqrt{G_{\min}} \right)^2 \quad (2.10)$$

yet Roderick et al. chose to use  $G_{\max}$  instead. In [18] this choice was not explicitly motivated, but in a follow-up research project [19] various formulations of  $G$  were investigated, based on the maximum applied stress  $S_{\max}$ , the stress range  $\Delta S$ , and a combined parameter  $S_{\max}\Delta S$ . The first two of these formulations are equivalent to respectively  $G_{\max}$  and  $\Delta G$ . Based on the correlation with test results Roderick et al. concluded that which formulation of  $G$  was best suited depended on the material system.

Concurrent with the investigations of Roderick et al., Mostovoy and Ripling put forward the equation [20]:

$$\frac{da}{dN} = C \Delta G^n = C (G_{\max} - G_{\min})^n \quad (2.11)$$

to describe fatigue crack growth in adhesive bonds. Mostovoy and Ripling motivate this choice of model as follows:

“... the methods [sic] used to define flaw tolerance to cyclic loading is patterned after that used for metals. That is crack-growth-per-cycle,  $da/dN$ , is plotted as a function of  $G_i$  which is defined as the difference between the maximum and minimum value of  $G_i$ ” [20].

Note that the physics of the problem are not considered, only that this equation is also used for metals. Furthermore application of equation 2.5 shows that  $\Delta G$  is in fact not equivalent to  $\Delta K$ . This does not mean that equation 2.11 is necessarily wrong, but it does mean that the basis of similitude has been changed with respect to equation 2.8 [21].

The basic concept employed in equations 2.9 and 2.11, i.e. correlation of the crack growth rate with some function of the SERR, was also found to hold in fibre reinforced polymers (FRPs). This was first shown by Wang and Wang [22], and O’ Brien [23, 24]. Again Wang and Wang only offer as justification the success of this concept in other material systems, while O’ Brien just notes the existence of this correlation without any attempt at physical justification.

In summary, the models proposed for fatigue crack growth in adhesives and composites were selected by applying the same concept that had previously worked in metals. This is a reasonable approach and has indeed resulted in models that can successfully correlate experimental data. However, it should be realised that the underlying model for FCG in metals, i.e. equation 2.8, is itself also no more than an empirical correlation.  $\Delta K$  was chosen as a correlating parameter because Paris et al. expected a correlation between crack-tip stress range and FCG rate. While it has been firmly established that such a correlation exists, the question of why there should be a power-law relationship between  $\Delta K$  and  $da/dN$  has not been satisfactorily answered. In fact, it is usually not even asked.

This would not be a problem if equations 2.9 or 2.11 could offer adequate predictions for all loading conditions and  $C$  and  $n$  could be treated as material properties. However, there are a wide variety of factors that can influence the correlation between FCG rate and SERR, for example: mode-mix, loading ratio ( $R$ ), and temperature. Rather than account for these factors from an understanding of the physics, researchers have attempted to deal with them through modifications of the basic equations. This has produced a well-stocked library of empirical correlations and curve-fit models, but no fundamental explanation of the the underlying phenomena. Nor is there a proven model for general crack growth predictions.

A comprehensive overview of the models that have been developed since the pioneering work of Roderick et al. and Mostovoy and Ripling has been provided in [1]. This chapter will focus on the models that were developed in order to deal with the so-called ‘R-ratio effect’, and models that make use of normalisation by the fracture toughness,

as they provide a good illustration of the issues caused by a lack of consideration of the physics.

### 2.3. ADDRESSING THE R-RATIO EFFECT

It was already noted by Paris [15, 16] that the correlation given in equation 2.8 depends on the mean stress. Equivalently one can state that the correlation depends on the  $R$ -ratio, which is defined as:

$$R = \frac{S_{\min}}{S_{\max}} \quad (2.12)$$

Paris suggested that this effect could be accounted for by making the coefficient  $C$  a function of the mean stress [16]. Later researchers found this suggestion insufficient, and a variety of other models have been suggested.

Hojo et al. [25, 26] observed that for a given  $da/dN$

$$\Delta K (1 - R)^\gamma = \text{constant} \quad (2.13)$$

where  $\gamma$  is a material parameter, representing the sensitivity to the mean stress. Based on this observation Hojo et al. derived the relationship:

$$\frac{da}{dN} = C \Delta K^{(1-\gamma)n} K_{\max}^{\gamma n} \quad (2.14)$$

as a model for the prediction of the FCG rate for any  $R$ -ratio. In terms of the SERR, this can be rewritten as [21]:

$$\frac{da}{dN} = C' \left( \Delta \sqrt{G} \right)^{(1-\gamma')n'} G_{\max}^{\gamma' n'} \quad (2.15)$$

with

$$\Delta \sqrt{G} = \left( \sqrt{G_{\max}} - \sqrt{G_{\min}} \right)^2 \quad (2.16)$$

Atodaria et al. arrived at a similar equation (originally in terms of the SIF, but later also derived in terms of the SERR), but replaced  $G_{\max}$  by  $G_{\text{avg}}$ , giving [27–29]:

$$\frac{da}{dN} = C \left[ \left( \sqrt{G} \right)_{\text{avg}}^\gamma \left( \Delta \sqrt{G} \right)^{1-\gamma} \right]^n \quad (2.17)$$

with

$$\sqrt{G_{\text{avg}}} = \left[ \frac{1}{m} \sum_{\sqrt{G_{\text{th}}}}^{\sqrt{G_{\max}}} \left( \sqrt{G} \right)^w \right]^{\frac{1}{w}} \quad (2.18)$$

where  $m$  is the number of divisions into which the range  $\sqrt{G_{\text{th}}}$  to  $\sqrt{G_{\max}}$  is divided,  $G_{\text{th}}$  is the threshold value of  $G$ , below which no crack growth is assumed to occur, and  $w$  is an experimentally determined weight factor. This equation was proposed on the basis that for a fixed  $K_{\max}$  the crack growth rate decreases as  $R$  increases (due to the decrease of  $\Delta K$ ), whereas for a fixed  $\Delta K$  the opposite happens: the growth rate increases with increasing  $R$  (due to the increase in  $K_{\max}$ ).

Khan [30] proposed a superposition of  $\Delta G$  and  $G_{\max}$ , based on fractographic observations. The resulting equation has the form:

$$\frac{da}{dN} = C_1 \Delta G^{n_1} + C_2 G_{\max}^{n_2} \quad (2.19)$$

Andersons et al. [31] combined the work of Hojo et al. [25, 26] with a Priddle / Hartman-Schijve type equation [32, 33] to propose the model

$$\frac{da}{dN} = C \left( \frac{\Delta K - \Delta K_{th}}{K_c - K_m} \right)^b \quad (2.20)$$

where  $K_c$  is the critical  $K$  value at which quasi-static crack growth occurs, and  $K_m$  is the mean SIF.

In the Andersons model the  $R$ -ratio is accounted for by the equation:

$$\Delta K_{th} = \Delta K_{th0} (1 - R)^\gamma \quad (2.21)$$

where  $\Delta K_{th0}$  is the value of  $K_{th}$  for  $R = 0$ . This basically represents an extension of the Hojo model to the regions of non-loglinear crack growth behaviour in the vicinity of the threshold and critical load values.

A similar model has been suggested by Jones et al. [34–37]. Jones et al. also use a Priddle type equation, viz:

$$\frac{da}{dN} = C \left[ \frac{\Delta \sqrt{G} - \Delta \sqrt{G_{th}}}{\sqrt{1 - \sqrt{\frac{G_{\max}}{A}}}} \right]^n \quad (2.22)$$

where  $A$  is a fit parameter. Originally Jones et al. used  $G_c$  rather than  $A$  [34], implying a physical relationship between the crack growth rate and the fracture toughness. Even in ref. [34] however, this was considered a fitting parameter, rather than an independently determinable physical quantity. In the most recent work [36, 37] Jones et al. argue that any scatter can be accounted for by varying  $\Delta \sqrt{G_{th}}$ , effectively creating an equation with 4 fit parameters, 2 of which are supposedly physical quantities.

A different approach has been proposed by Allegri et al. [38], who suggested the equation:

$$\frac{da}{dN} = C \left( \frac{G_{II\max}}{G_{IIc}} \right)^{\frac{n}{(1-R)^2}} \quad (2.23)$$

Although this equation was put forward for the case of mode II growth, one could imagine a similar equation for mode I growth. Allegri et al. discuss the correspondence between their proposed equation and the phenomenological features of a series of crack growth experiments; i.e. how the crack growth vs SERR curves rotate as a function of  $R$ . Beyond this however, they do not provide an underlying physical theory that justifies the chosen form of their equation.

This is an objection that can be raised to all the crack growth models discussed in this section. The form of the equations has been chosen so that the shape of the graphs they

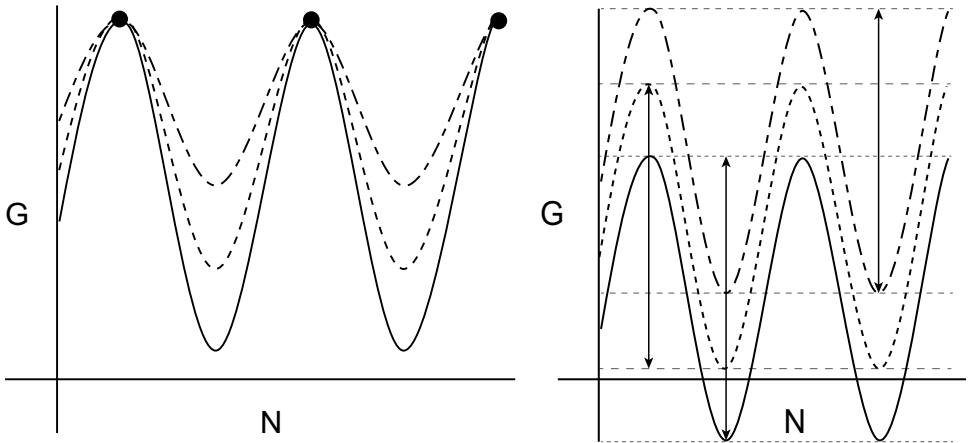


Figure 2.1: For a given  $G_{\max}$  many different load cycles can be defined. Likewise, for a given  $\Delta G$  there are many possible load cycles. Thus  $G_{\max}$  or  $\Delta G$  alone are insufficient to uniquely define a load cycle, and thus are not a sufficient basis for an FCG model.

produce mimics the behaviour seen during tests. While care has been taken to get the mathematics to match, none of the authors seem to have considered what their models are implying about the physical process of fatigue crack growth.

This lack of attention to the physics can even be seen in the term '*R*-ratio effect'. This terminology implies that there is some kind of fundamental material behaviour that is then modified by the *R*-ratio. This fundamental material behaviour can supposedly be described by the correlation between  $da/dN$  and some function of the SERR, e.g.  $G_{\max}$  or  $\Delta G$ . However it is a simple fact of mathematics that  $G_{\max}$  or  $\Delta G$  alone are insufficient to uniquely describe a load cycle, as illustrated in figure 2.1. Since there are many different possible load cycles for a given value of  $G_{\max}$ , it should come as no surprise that there is no unique relationship between  $G_{\max}$  and  $da/dN$ . Of course this same line of reasoning also holds for  $\Delta G$ .

In other words, the '*R*-ratio effect' is at least in part an artefact of the choice of an insufficient number of parameters to describe the load cycle. This needs to be accounted for, before any physical basis for the *R*-ratio effect can be identified.

It may sometimes be useful to examine the effect of mean load and load range separately. However it is important to acknowledge that these parameters should be given equal weight conceptually, even if some materials may be more sensitive to one or the other.

## 2.4. NORMALISATION BY THE FRACTURE TOUGHNESS

VARIOUS researchers have suggested that to correctly model fatigue crack growth one should consider the crack driving force in relation to the material resistance; usually interpreted as the relation of  $G_{\max}$  or  $\Delta G$  to  $G_c$ . This was first suggested by Wang et al.



[39, 40], in the form:

$$\frac{da}{dN} = C \left( \frac{\Delta\sqrt{G}}{G_c} \right)^n \quad (2.24)$$

This principle of normalising the ‘driving force’ with respect to the fracture toughness has been used in many different models [38, 41–45].

In all of these models the fatigue resistance is assumed to be constant. Because  $C$  is determined by curve fitting, the constancy of the fatigue resistance means there is no way of experimentally comparing the performance of a normalised equation such as equation 2.24 with that of a non-normalised equation. Any constant value (in this case  $1/G_c^n$ ) can be ‘extracted’ from  $C$  and placed separately into the equation without affecting the validity of the fit. Thus normalisation can only be justified on the grounds of the underlying physical model of the material behaviour, but little justification is given in the cited papers.

Furthermore one must ask whether the *quasi-static* parameter  $G_c$  is a correct measure of the crack growth resistance during fatigue, especially as FCG will occur for  $G < G_c$ . There have been several attempts to find a better representation of fatigue resistance, following the approach of Poursartip [46]. Poursartip proposed the fatigue resistance parameter  $G_R(a)$ , which is explicitly a function of crack length  $a$ . This type of parameter has been adopted by Shivakumar, Chen, and co-workers [47, 48], Zhang, Peng, and co-workers [49, 50], and Murri [51, 52]. Even with this approach however, the issue remains that  $G_R$  is determined based on a quasi-static test. Therefore it is not necessarily representative for crack growth resistance in fatigue. For example Murri [51, 52] used  $G_R$  as a way of accounting for fibre bridging in mode I delamination in CFRP. However Yao et al. have recently shown that a pre-crack produced by quasi-static loading does not produce the same fibre bridging effect on FCG as a pre-crack produced by fatigue loading [53]. In other words: fracture toughness does not equal fatigue resistance.

If one does accept, for the sake of argument, that a correct representation of the fatigue resistance can be found, the question becomes why  $da/dN$  depends on  $G_{\max}/G_c$  or  $G_{\max}/G_R$  in a non-linear manner. If the driving force is twice as strong compared to the resistance, why is the crack growth (much) more than twice as fast? No physical justification for this could be found in the literature. One can also ask why normalisation by the fatigue resistance is the correct procedure, rather than some other mathematical operation.

Ultimately normalisation by the fatigue resistance suffers from the same issue as that which plagued the models described in section 2.3: a lack of grounding in an understanding of the underlying physical behaviour.

## 2.5. PHYSICAL OBJECTIONS TO THE LEFM BASED MODELS

IN sections 2.1 and 2.2 it was already discussed that thanks to equation 2.5 the SIF and SERR are often treated as interchangeable on a conceptual level. Strictly speaking the SERR is an *energy* parameter. However, due to the historical development of FCG models for adhesive bonds and composites, as developments of the Paris relation, the SERR is often implicitly regarded as being descriptive of the crack tip *stress*. According to equation 2.5 this is perfectly allowable. However, let us see what happens if we do think

of the SERR as an energy parameter, and keep the Griffith energy balance principle in mind.

As originally derived,  $G$  is the amount of energy released *as a consequence of* crack growth. This would imply there is no  $G$  if there is no crack growth (as there will be no energy release). However presently  $G$  is usually treated more as a virtual parameter, that has a value regardless of whether there is a crack growth increment or not.

In both cases  $G$  is a function of load and geometry. This has two implications. Firstly, although a  $G$  value can be calculated for the load at any point in the fatigue cycle, there will only be an actual release of energy if there is in fact an increment of crack growth. Secondly, during a fatigue load cycle  $G$  is continuously changing. This raises some important questions regarding the validity of equations 2.9 and 2.11 and by extension any models based on these equations.

If  $G$  is continuously changing, then why would only the value of  $G$  at maximum load (i.e.  $G_{\max}$ ) be of importance for the FCG rate? Griffith's energy balance (and the first law of thermodynamics) demand that the energy consumed by crack growth in one entire cycle be equal to the energy released during *that entire cycle*. The energy released by crack growth increments that do not occur at maximum load must therefore also be considered. Thus a simple explanation for the ' $R$ -ratio effect' in this view, is that only using  $G_{\max}$  as a controlling parameter ignores the crack growth happening in the rest of the fatigue cycle.

Now let us consider  $\Delta G$  as a controlling parameter.  $\Delta G$  is defined as  $G_{\max} - G_{\min}$ . Therefore, taking  $\Delta G$  as a controlling parameter implies giving physical relevance to  $G_{\min}$ . According to the standard definition of the SERR,  $G_{\min}$  is the amount of energy released by a crack growth increment at the minimum fatigue load. But is there in fact a crack growth increment at minimum load? If crack growth does occur at the minimum fatigue load, then why does the crack not keep growing if fatigue cycling is stopped and the load held at the minimum level? On the other hand, if  $G_{\min}$  has no physical meaning, then what is the physical meaning of  $\Delta G$ ?

Even if both  $G_{\max}$  and  $G_{\min}$  do have physical meaning, the question remains, why would it be the difference between these two values that is the controlling parameter for FCG? Why shouldn't the absolute values of the energy being released at maximum and minimum load also be considered, rather than only the difference between these values? Again this provides an explanation for the ' $R$ -ratio effect'; the absolute energy release is ignored by choosing only  $\Delta G$  as the controlling parameter.

Based on the discussion above it is clear that on grounds of physical principles all the single-parameter LEFM-based models must be rejected as general descriptions for FCG. To have a model that is valid for more than one  $R$ -ratio, two parameters are necessary. Various two-parameter models have been discussed in section 2.3, but no physical justification for the chosen equations has been provided. Although they may provide usable predictions, these models can not be regarded as a theoretical framework that explains fatigue crack growth.

## 2.6. THE CONFIGURATIONAL FORCE APPROACH

THE models described in the previous section all rely on LEFM. However, there are other approaches to understanding crack growth. One example is the configura-

tional force approach recently championed by Ochensberger and Kolednik [54–57]. The concept of configurational forces was proposed by Eshelby [58–60] within the framework of continuum mechanics. Eshelby showed that the integral over a closed surface of the normal component of the energy-momentum tensor, can be interpreted as a force on any discontinuities (e.g. cracks) within that surface [60]. This type of force is now commonly called a configurational force. For a two-dimensional crack, the component of the configurational force parallel to the crack extension is equal to the J-integral [59, 60]. The J-integral is a path-independent integral defined by Rice [61] as:

$$J = \int_{\Gamma} \left( \phi dy - \mathbf{t} \cdot \frac{\partial \mathbf{u}}{\partial x} ds \right) \quad (2.25)$$

Here  $\Gamma$  is the integration path, with coordinate  $s$  along that path,  $\phi$  is the energy density,  $\mathbf{t}$  is the traction on the enclosed surface,  $\mathbf{u}$  is the displacement vector, and  $x$  and  $y$  are Cartesian coordinates, see also figure 2.2. If the material is perfectly linear elastic the J-integral is equal to the SERR.

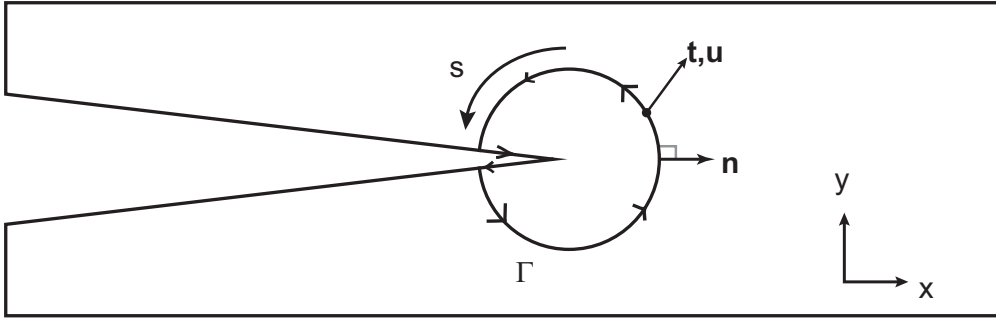


Figure 2.2: Definition of the terms in the calculation of the J-integral (see equation 2.25). The J-integral is calculated over the path  $\Gamma$  surrounding the crack tip, and integrates the difference between the strain energy and the dot product of the traction vector  $\mathbf{t}$ , and the partial derivative w.r.t.  $x$  of the displacement vector  $\mathbf{u}$ .

Simha et al. [62, 63], developed this concept further for elastic-plastic materials. In that case the J-integral is no longer path-independent. Using the configurational force concept Simha et al. were able to derive the relationship between a J-integral evaluated for an integration path near the crack-tip,  $J_{\text{tip}}$ , and one evaluated for a far-field integration path  $J_{\text{far}}$ :

$$J_{\text{tip}} = J_{\text{far}} + C_p \quad (2.26)$$

$C_p$  is introduced by Simha et al. as a ‘plasticity influence term’ which represents the configurational force due to plasticity. A  $C_p < 0$  implies that plasticity has a shielding effect, reducing the crack driving force at the crack tip.

Ochensberger and Kolednik performed further numerical investigations into the nature of the elastic-plastic J-integral formulation developed by Simha, especially considering how to deal with its path-dependence [54, 55]. They concluded that the correct parameter to evaluate crack growth is a J-integral evaluated on a contour that completely encloses the crack-tip plastic zone, denoted  $J_{\text{PZ}}^{\text{ep}}$ . The superscript ‘ep’ indicates that this

J-integral was formulated in such a way that it is also valid for elastic-plastic materials. As long as the integration path only goes through elastically deformed material, this detail can be ignored however, as the conventional and elastic-plastic J-integral are equal in that case [55].

$J_{PZ}^{ep}$  is interpreted by Ochensberger and Kolednik as the driving force on the crack plus its surrounding process zone; crack extension will occur if  $J_{PZ}^{ep}$  equals or exceeds the crack growth resistance. For fatigue crack growth Ochensberger and Kolednik [55, 56] claim that the driving force is given by a cyclic J-integral defined as

$$J_{\max} + J_{\min} - 2\sqrt{J_{\max}J_{\min}} = \left(\sqrt{J_{\max}} - \sqrt{J_{\min}}\right)^2 \quad (2.27)$$

Rather confusingly Ochensberger and Kolednik (following common practice in literature) denote this quantity as  $\Delta J$ , despite it not being equal to the range of the J-integral. Thus the quantity defined by equation 2.27 will be denoted as  $\Delta\sqrt{J}$  in this thesis. This also serves to highlight its similarity to the quantity  $\Delta\sqrt{G}$  discussed by Rans et al. [21].

Confusing notations aside, there is a more fundamental issue regarding the interpretation of  $\Delta\sqrt{J}$  as the driving force for FCG. That  $J$  can be interpreted as a driving force for propagation of a crack under quasi-static load follows by derivation from fundamental principles of (continuum) mechanics. Crack growth occurs when this driving force exceeds some critical value, which one can call the crack growth resistance. However, as Ochensberger and Kolednik note, under cyclic loading crack growth occurs for driving force values well below the crack growth resistance measured under quasi-static load.

One possible explanation is that for some reason the resistance to fatigue crack growth is lower than the resistance to quasi-static growth. However, Ochensberger and Kolednik instead conclude that it is the driving force description that is lacking [55, 56]. They claim that for the case of fatigue loading it is necessary to introduce new driving force terms such as  $\Delta K$  and  $\Delta\sqrt{J}$ , even if, as they acknowledge:

“these terms are not necessarily real driving force terms in the thermodynamic sense.” [56]

According to Ochensberger and Kolednik this lack of reality is acceptable, as long as the ‘fatigue driving force’ allows prediction of the crack growth rate. Based on experimental observations of Pippan et al. [64], Ochensberger and Kolednik claim that the fatigue crack growth rate is proportional to the range of the crack tip opening displacement ( $\Delta CTOD$ ). Supported by numerical simulations they then argue that  $\Delta\sqrt{J}$  is proportional to  $\Delta CTOD$  and therefore should be interpreted as the driving force for FCG.

With this line of argument Ochensberger and Kolednik have abandoned the physical justification for the use of  $J$ . While the interpretation of  $J$  as a driving force for quasi-static crack growth is physically sound, how and why  $\Delta\sqrt{J}$  should be interpreted as a ‘fatigue driving force’ is unclear. As Ochensberger and Kolednik themselves point out,  $\Delta K$  and  $\Delta CTOD$  are nothing other than parameters that have empirically been found to have a correlation with the crack growth rate. There has been so far no explanation of the physical mechanisms that would justify labelling these terms as a ‘driving force’. Accepting  $J$ , and by extension  $G$  and  $K^2$ , as a crack driving force immediately raises the question why simply taking the range of the applied force cycle would give a ‘cyclic driving force’.

At first sight some kind of integration procedure would seem to be more appropriate, although by analogy to classical mechanics, it would be more appropriate to call such a quantity the ‘driving impulse’.

Even if one does accept  $\Delta\sqrt{J}$  as a driving force, the question remains how to determine the FCG rate based solely on the driving force. Any theory of fatigue crack growth needs to be able to explain how far a crack will grow during one cycle. Merely knowing the driving force is insufficient to do this. To provide an analogy: to calculate the final velocity of a rocket, it is not sufficient to only know the thrust of the rocket (i.e. the rocket’s ‘driving force’), one also needs to know the mass of the rocket, the duration during which the rocket engine fires, and the atmospheric drag on the rocket. In terms of a fatigue crack, one needs to know not only how large the driving force is, but also for ‘how long’ this force is applied, and what the material’s resistance to fatigue crack growth is. Simply finding an empirical relationship between a ‘driving force’ and crack growth rate may produce an useful prediction model for engineering purposes, but not a correct constitutive material model.

## 2.7. PLASTIC ENERGY DISSIPATION

RATHER than attempting to find a driving force by means of LEFM or configurational forces, some researchers have attempted to relate the crack growth rate to energy dissipation. In essence, this is a return to the energy balance as proposed by Griffith and Irwin & Kies. Only very recently has this approach been applied to non-metallic materials [65–71], so this section will make a brief excursion into the field of FCG in ductile metals.

In metals FCG is considered to be strongly related to plastic deformation. Furthermore the energy  $\gamma_p$  consumed by plastic dissipation near to a crack tip is usually orders of magnitude greater than the surface energy  $\gamma_s$  of the material. Thus the energy approaches for FCG in metals tend to focus on relating the crack growth rate to the dissipation of energy due to plasticity. The first to suggest such an approach were Rice [72, 73] and Weertman [74, 75]. Weertman’s model forms the basis for many of the current energy-based models of FCG and is usually formulated as [76]:

$$\frac{da}{dN} = A \frac{\Delta K^4}{\sigma_y^2 \mu \Gamma} \quad (2.28)$$

where  $A$  is a dimensionless constant (determined empirically),  $\sigma_y$  is the yield stress,  $\mu$  is the shear modulus and  $\Gamma$  is the required energy per unit area of crack extension. It is noteworthy that Weertman himself considered this to be a stress-based model, with a critical stress controlling the crack growth [75], even though it is presently thought of as an energy-based model. Another notable feature is the fourth order dependence on  $\Delta K$  in equation 2.28. This matches experimental results in metals, but not in FRPs or adhesives, where (when converted to a  $\Delta K$  dependence) exponents as high as 16 have been found [36].

Another important contribution was made by Bodner et al. [77], who proposed think-

ing about FCG in terms of the equation

$$\frac{da}{dN} = \frac{da}{dU_{pl}} \frac{dU_{pl}}{dN} \quad (2.29)$$

where  $dU_{pl}/dN$  is the plastic energy dissipation per cycle and  $da/dU_{pl}$  is the crack advance per unit of energy dissipation. This is of course a restatement of the first law of thermodynamics, applied to fatigue crack growth. Calculation of  $dU_{pl}/dN$  can be done relatively easily with the finite element method (FEM), but finding the correct expression for  $da/dU_{pl}$  is less obvious.

Klingbeil proposed using the critical SERR  $G_c$  as  $(da/dU_{pl})^{-1}$  giving [76, 78]

$$\frac{da}{dN} = \frac{1}{G_c} \frac{dU_{pl}}{dN} \quad (2.30)$$

Good correlation was found for data from crack growth experiments in a variety of metals [76]. However the use of  $G_c$  as controlling parameter is questionable. As discussed earlier  $G_c$  is found during quasi-static tests, and its applicability to FCG is unclear. For example Ranaganathan et al. [79] present experimental evidence that  $da/dU_{pl}$  depends on  $\Delta K$ , especially for near-threshold crack growth. Ranaganathan et al. argue this is reflective of changes in the micro-mechanical crack-growth mechanisms. Thus Smith [80] adopted the Klingbeil model, but used an empirically determined value of  $da/dU_{pl}$  (which turned out to be three times the fracture toughness value reported in literature). With this approach good correlation between the model and experimental data was found. It was also shown to be possible to accurately predict the crack growth retardation produced by a tensile overload.

A different approach was developed by Cojocaru and Karlsson [81, 82] and developed further by Nittur et al. [83]. In this approach a dissipation domain is defined around the crack tip, and fixed to advance along with it. The cumulative plastic dissipation (over several cycles, if necessary) is calculated. If the cumulative plastic dissipation exceeds an empirically determined critical value the crack is advanced. The cumulative plastic dissipation is then evaluated and compared to the critical value in this new region. The process is repeated until the plastic dissipation becomes less than the critical value, at which point one or more new load cycles are applied. Comparison with test results showed good correlation. It should be noted that Nittur et al. assumed a constant value of the critical dissipation value.

In summary, the plastic dissipation models produce good results and are consistent with physical principles. Questions that remain are whether it is still appropriate to only consider the plastic dissipation for material classes other than metals, where very different plastic zones may be generated. This is especially questionable for configurations where cracks propagate within a constrained volume of material, e.g. crack growth in adhesive bonds or delamination in FRPs. That delamination growth rates are generally not proportional to  $\Delta K^4$  indicates that other sources of energy dissipation may need to be considered in these cases.

## 2.8. CONCLUSION

An overview has been given of the most important models for predicting and understanding FCG in composite materials and adhesive bonds. The models most commonly used at present are those based on LEFM. Although these can provide useful predictions, they are invariably based on empirical curve fitting. This means they are of limited validity, and extensive (and expensive) test programmes are required to generate sufficient material data. From a scientific point of view, the physical justification of these models is severely lacking, and provides little understanding of fatigue crack growth.

A question that was raised when examining the LEFM-based models was how to interpret the SERR. Due to the history of FCG models in adhesive bonds and composites being based on the Paris relationship, which was developed for metals, the SERR is usually implicitly considered to be a description of the crack tip stress. However the SERR was originally derived as the amount of energy released by an increment of crack growth. Returning to this interpretation of the SERR highlights various issues with the LEFM-based models, as discussed in section 2.5.

Rather than interpreting  $G$  as the energy release, the configurational force approach also allows one to interpret  $G$  as the driving force for crack growth (assuming conditions are such that  $J = G$  is valid). Note that these interpretations conflict in cases where there is no crack growth increment. The driving force exists irrespective of crack growth occurring, but energy will only be released if the crack does in fact grow.

That  $J$  should be regarded as the driving force for crack growth of a quasi-static crack has been shown quite convincingly on the basis of physical principles. How this should be related to FCG remains unclear however. The choice to consider  $\Delta\sqrt{J}$  as the driving force for FCG, as proposed by some researchers, is based purely on empirical correlations, and in defiance of the fact that  $\Delta\sqrt{J}$  does not in fact represent a thermodynamical driving force. Thus it would seem to be better to regard the correct definition of the driving force for fatigue crack growth as an open question.

The FCG models that have the most physical justification are those based on plastic energy dissipation. Questions that remain to be resolved are whether it is appropriate to only consider *plastic* dissipation in the case of non-metallic materials, and how to determine the dissipation per unit of crack growth. In particular it must be investigated whether this last parameter is a constant or not.

This thesis aims to answer these questions for the case of fatigue crack growth in a metal-to-metal epoxy adhesive bond, with the expectation that the results can be generalised to larger classes of fatigue crack growth.

## REFERENCES

- [1] J. A. Pascoe, R. C. Alderliesten, and R. Benedictus, *Methods for the prediction of fatigue delamination growth in composites and adhesive bonds - a critical review*, Eng Fract Mech **112-113**, 72 (2013).
- [2] A. A. Griffith, *The phenomena of rupture and flow in solids*, Philosophical Transactions of the Royal Society of London Series A, Containing Papers of a Mathematical or Physical Character **221**, 163 (1921).



- [3] E. Orowan, *Fracture and strength of solids*, Rep Prog Phys **12**, 185 (1949).
- [4] E. Orowan, *Fundamentals of brittle behavior in metals*, in *Fatigue and Fracture of Metals*, edited by W. Murray (Massachusetts Institute of Technology and John Wiley & Sons, New York, 1952) pp. 139–167.
- [5] G. R. Irwin, *Fracture dynamics*, in *Fracturing of Metals*, edited by G. Sachs (American Society for Metals, Cleveland, 1948).
- [6] G. R. Irwin and J. Kies, *Fracturing and fracture dynamics*, Welding Journal - Research Supplement **31**, 95s (1952).
- [7] G. R. Irwin and J. Kies, *Critical energy rate analysis of fracture strength*, Welding Journal - Research Supplement **33**, 193s (1954).
- [8] G. R. Irwin, *Analysis of stresses and strains near the end of a crack traversing a plate*, ASME Journal of Applied Mechanics **24**, 361 (1957).
- [9] G. R. Irwin, *Fracture mechanics*, in *Proceedings of the First Symposium on Naval Structural Mechanics* (1958) pp. 557–594.
- [10] N. Perez, *Fracture Mechanics* (Springer US, Boston, 2004).
- [11] ASTM Standard D 5528/ D 5528-01, *Standard test method for mode I interlaminar fracture toughness of unidirectional fiber-reinforced polymer matrix composites*, (2007), ASTM International, West Conshohocken, PA, USA.
- [12] M. L. Williams, *On the stress distribution at the base of a stationary crack*, J Appl Mech **24**, 109 (1957).
- [13] H. Westergaard, *Bearing pressures and cracks*, J Appl Mech **61**, A49 (1939).
- [14] A. Wöhler, *Ueber die Festigkeits-Versuche mit Eisen und Stahl*. Zeitschrift für Bauwesen **XX**, 73 (1870).
- [15] P. Paris, M. Gomez, and W. Anderson, *A rational analytic theory of fatigue*, The Trend in Engineering **13**, 9 (1961).
- [16] P. Paris, *The fracture mechanics approach to fatigue*, in *10th Sagamore Army Materials Research Conference* (Syracuse University Press, 1964) pp. 107–132.
- [17] P. Paris and F. Erdogan, *A critical analysis of crack propagation laws*, J Basic Eng **85**, 528 (1963).
- [18] G. Roderick, R. Everett, and J. Crews Jr, *Debond Propagation in Composite Reinforced Metals*, Tech. Rep. NASA TM X-71948 (NASA, 1974).
- [19] G. L. Roderick, R. A. Everett Jr., and J. H. Crews Jr, *Cyclic Debonding of Unidirectional Composite Bonded to Aluminum Sheet for Constant-Amplitude Loading*, Tech. Rep. NASA TN D-8126 (NASA, 1976).



- [20] S. Mostovoy and E. Ripling, *Flaw tolerance of a number of commercial and experimental adhesives*, in *Adhesion Science and Technology*, Polymer Science and Technology 9B, edited by L.-H. Lee (Plenum Press, New York, 1975) pp. 513–562.
- [21] C. Rans, R. C. Alderliesten, and R. Benedictus, *Misinterpreting the results: How similitude can improve our understanding of fatigue delamination growth*, *Compos Sci Technol* **71**, 230 (2011).
- [22] S. S. Wang and H. T. Wang, *Interlaminar crack growth in fiber reinforced composites during fatigue*, *J Eng Mater Technol* **101**, 34 (1979).
- [23] T. O'Brien, *Characterization of Delamination Onset and Growth in a Composite Laminate*, Tech. Rep. NASA Technical Memorandum 81940 (NASA, 1981).
- [24] T. K. O'Brien, *Characterization of delamination onset and growth in a composite laminate*, in *Damage in Composite Materials*, ASTM STP 775, edited by K. Reifsnider (American Society for Testing and Materials, Philadelphia, 1982) pp. 140–167.
- [25] M. Hojo, K. Tanaka, C. G. Gustafson, and R. Hayashi, *Effect of stress ratio on near-threshold propagation of delamination fatigue cracks in unidirectional CFRP*, *Compos Sci Technol* **29**, 273 (1987).
- [26] M. Hojo, S. Ochiai, C.-G. Gustafson, and K. Tanaka, *Effect of matrix resin on delamination fatigue crack growth in CFRP laminates*, *Eng Fract Mech* **49**, 35 (1994).
- [27] D. R. Atodaria, S. K. Putatunda, and P. K. Mallick, *A fatigue crack growth model for random fiber composites*, *J Compos Mater* **31**, 1838 (1997).
- [28] D. R. Atodaria, S. K. Putatunda, and P. K. Mallick, *Delamination growth behavior of a fabric reinforced laminated composite under mode I fatigue*, *J Eng Mater Technol* **121**, 381 (1999).
- [29] D. R. Atodaria, S. K. Putatunda, and P. K. Mallick, *Fatigue crack growth model and mechanism of a random fiber SMC composite*, *Polym Compos* **20**, 240 (1999).
- [30] R. Khan, *Delamination Growth in Composites under Fatigue Loading*, Phd thesis, Delft University of Technology (2013), <http://doi.org/10.4233/uuid:dbd8025c-c660-452b-8b0b-391c8ad3a89f>.
- [31] J. Andersons, M. Hojo, and S. Ochiai, *Empirical model for stress ratio effect on fatigue delamination growth rate in composite laminates*, *Int J Fatigue* **26**, 597 (2004).
- [32] E. Priddle, *High cycle fatigue crack propagation under random and constant amplitude loadings*, *International Journal of Pressure Vessels and Piping* **4**, 89 (1976).
- [33] A. Hartman and J. Schijve, *The effects of environment and load frequency on the crack propagation law for macro fatigue crack growth in aluminium alloys*, *Eng Fract Mech* **1**, 615 (1970).

- [34] R. Jones, S. Pitt, A. J. Bunner, and D. Hui, *Application of the Hartman-Schijve equation to represent mode I and mode II fatigue delamination growth in composites*, Compos Struct **94**, 1343 (2012).
- [35] R. Jones, S. Stelzer, and A. J. Brunner, *Mode I, II and mixed mode I/II delamination growth in composites*, Compos Struct **110**, 317 (2014).
- [36] R. Jones, W. Hu, and A. J. Kinloch, *A convenient way to represent fatigue crack growth in structural adhesives*, Fatigue & Fracture of Engineering Materials & Structures **38**, 379 (2014).
- [37] W. Hu, R. Jones, and A. Kinloch, *Computing the growth of naturally-occurring disbonds in adhesively-bonded patches to metallic structures*, Eng Fract Mech (2015), in Press.
- [38] G. Allegri, M. I. Jones, M. R. Wisnom, and S. R. Hallett, *A new semi-empirical model for stress ratio effect on mode II fatigue delamination growth*, Composites Part A **42**, 733 (2011).
- [39] A. Wang, P. Chou, and S. Lei, *A stochastic model for the growth of matrix cracks in composite laminates*, J Compos Mater **18**, 239 (1984).
- [40] A. Wang, M. Slomiana, and R. Bucinell, *Delamination crack growth in composite laminates*, in *Delamination and Debonding of Materials*, ASTM STP 876, edited by W. Johnson (American Society for Testing and Materials, Philadelphia, 1985) pp. 135–167.
- [41] W. Chan and A. Wang, *Free-edge delamination characteristics in S2/CE9000 glass/epoxy laminates under static and fatigue loads*, in *Composite Materials: Fatigue and Fracture, Second Volume*, ASTM STP 1012, edited by P. A. Lagace (American Society for Testing and Materials, Philadelphia, 1989) pp. 270–295.
- [42] N. Blanco, E. K. Gamstedt, L. E. Asp, and J. Costa, *Mixed-mode delamination growth in carbon-fibre composite laminates under cyclic loading*, Int J Solids Struct **41**, 4219 (2004).
- [43] R. Ramkumar and J. Whitcomb, *Characterization of mode I and mixed-mode delamination growth in T300/5208 graphite/epoxy*, in *Delamination and Debonding of Materials*, ASTM STP 876, edited by W. Johnson (American Society for Testing and Materials, Philadelphia, 1985) pp. 315–335.
- [44] A. Russell and K. Street, *Predicting interlaminar fatigue crack growth rate in compressively loaded laminates*, in *Composite Materials: Fatigue and Fracture, Second Volume*, ASTM STP 1012, edited by P. A. Lagace (Philadelphia, Philadelphia, 1989) pp. 162–178.
- [45] G. Allegri and M. R. Wisnom, *A non-linear damage evolution model for mode II fatigue delamination onset and growth*, Int J Fatigue **43**, 226 (2012).

- [46] A. Poursartip, *The characterization of edge delamination growth in laminates under fatigue loading*, in *Toughened Composites*, ASTM STP 937, edited by N. J. Johnston (American Society for Testing and Materials, Philadelphia, 1987) pp. 222–241.
- [47] K. Shivakumar, H. Chen, F. Abali, D. Le, and C. Davis, *A total fatigue life model for mode I delaminated composite laminates*, *Int J Fatigue* **28**, 33 (2006).
- [48] H. Chen, K. Shivakumar, and F. Abali, *A comparison of total fatigue life models for composite laminates*, *Fatigue Fract Eng Mater Struct* **29**, 31 (2006).
- [49] L. Peng, J. Zhang, L. Zhao, R. Bao, H. Yang, and B. Fei, *Mode I delamination growth of multidirectional composite laminates under fatigue loading*, *J Compos Mater* **45**, 1077 (2011).
- [50] J. Zhang, L. Peng, L. Zhao, and B. Fei, *Fatigue delamination growth rates and thresholds of composite laminates under mixed mode loading*, *Int J Fatigue* **40**, 7 (2012).
- [51] G. B. Murri, *Evaluation of delamination onset and growth characterization methods under mode I fatigue loading*, in *American Society for Composites, 27th Technical Conference* (DEStech Publications, Inc., Arlington, TX, 2012) pp. 601–620.
- [52] G. B. Murri, *Evaluation of Delamination Onset and Growth Characterization Methods under Mode I Fatigue Loading*, Tech. Rep. NASA/TM-2013-217966 (NASA, 2013).
- [53] L. Yao, R. Alderliesten, M. Zhao, and R. Benedictus, *Bridging effect on mode I fatigue delamination behavior in composite laminates*, *Composites Part A* **63**, 103 (2014).
- [54] O. Kolednik, R. Schönggrundner, and F. D. Fischer, *A new view on J-integrals in elastic-plastic materials*, *Int J Fract* **187**, 77 (2014).
- [55] W. Ochensberger and O. Kolednik, *A new basis for the application of the J-integral for cyclically loaded cracks in elastic-plastic materials*, *Int J Fract* **189**, 77 (2014).
- [56] W. Ochensberger and O. Kolednik, *Physically appropriate characterization of fatigue crack propagation rate in elastic-plastic materials using the J-integral concept*, *Int J Fract* **192**, 25 (2015).
- [57] W. Ochensberger and O. Kolednik, *Overload effect revisited - investigation by use of configurational forces*, *Int J Fatigue* **83**, Part 2, 161 (2016).
- [58] J. D. Eshelby, *The force on an elastic singularity*, *Philosophical Transactions of the Royal Society of London A: Mathematical, Physical and Engineering Sciences* **244**, 87 (1951).
- [59] J. D. Eshelby, *Energy relations and the energy-momentum tensor in continuum mechanics*, in *Inelastic behaviour of solids*, edited by M. Kanninen, W. Adler, A. Rosenfield, and R. Jaffee (McGraw-Hill, New York, 1970).
- [60] J. D. Eshelby, *The elastic energy-momentum tensor*, *Journal of Elasticity* **5**, 321 (1975).

- [61] J. Rice, *A path independent integral and the approximate analysis of strain concentration by notches and cracks*, J Appl Mech **35**, 379 (1968).
- [62] N. K. Simha, F. D. Fischer, O. Kolednik, and C. R. Chen, *Inhomogeneity effects on the crack driving force in elastic and elastic-plastic materials*, J Mech Phys Solids **51**, 209 (2003).
- [63] N. K. Simha, F. D. Fischer, G. X. Shan, C. R. Chen, and O. Kolednik, *J-integral and crack driving force in elastic-plastic materials*, J Mech Phys Solids **56**, 2876 (2008).
- [64] R. Pippan, C. Zelger, E. Gach, C. Bichler, and H. Weinhandl, *On the mechanism of fatigue crack propagation in ductile metallic materials*, Fatigue & Fracture of Engineering Materials & Structures **34**, 1 (2011).
- [65] L. Yao, R. C. Alderliesten, M. Zhao, and R. Benedictus, *Discussion on the use of the strain energy release rate for fatigue delamination characterization*, Composites Part A **66**, 65 (2014).
- [66] L. Yao, R. C. Alderliesten, and R. Benedictus, *Interpreting the stress ratio effect on delamination growth in composite laminates using the concept of fatigue fracture toughness*, Composites Part A **78**, 135 (2015).
- [67] L. Yao, *Mode I fatigue delamination growth in composite laminates with fibre bridging*, Ph.D. thesis, Delft University of Technology (2015).
- [68] L. Amaral, L. Yao, R. Alderliesten, and R. Benedictus, *The relation between the strain energy release in fatigue and quasi-static crack growth*, Eng Fract Mech **145**, 86 (2015).
- [69] F. Lahuerta and R. P. L. Nijssen, *Energy dissipation in thermoset composites in mode I fatigue*, Mechanics of Advanced Materials and Structures, 00 (2015).
- [70] J. A. Pascoe, R. C. Alderliesten, and R. Benedictus, *Towards understanding fatigue disbond growth via cyclic strain energy*, Procedia Materials Science **3 (ECF-20)**, 610 (2014).
- [71] J. A. Pascoe, R. C. Alderliesten, and R. Benedictus, *On the relationship between disbond growth and the release of strain energy*, Eng Fract Mech **133**, 1 (2015).
- [72] J. Rice, *An examination of the fracture mechanics energy balance from the point of view of continuum mechanics*, in *Proceedings of the International Conference on Fracture*, edited by T. Yokobori, T. Kawasaki, and J. Swedlow (Japanese Society for Strength and Fracture of Materials, 1965) pp. 309–340.
- [73] J. Rice, *Mechanics of crack tip deformation and extension by fatigue*, in *Fatigue Crack Propagation ASTM STP 415* (American Society for the Testing of Materials, 1967) p. 247.

- [74] J. Weertman, *Rate of growth of fatigue cracks as calculated from the theory of infinitesimal dislocations distributed on a plane*, in *Proceedings of the First International Conference on Fracture*, edited by T. Yokobori, T. Kawasaki, and J. Swedlow (Japanese Society for Strength and Fracture of Materials, 1965) pp. 153–164.
- [75] J. Weertman, *Theory of fatigue crack growth based on a BCS crack theory with work hardening*, *Int J Fract* **9**, 125 (1973).
- [76] N. W. Klingbeil, *A total dissipated energy theory of fatigue crack growth in ductile solids*, *Int J Fatigue* **25**, 117 (2003).
- [77] S. R. Bodner, D. L. Davidson, and J. Lankford, *A description of fatigue crack growth in terms of plastic work*, *Eng Fract Mech* **17**, 189 (1983).
- [78] N. Klingbeil, J. Daily, and C. Baudendistel, *A dissipated energy approach to fatigue crack growth in ductile solids and layered materials*, in *Key Eng Mater*, Vol. 378-379 (2008) pp. 385–404.
- [79] N. Ranganathan, F. Chalon, and S. Meo, *Some aspects of the energy based approach to fatigue crack propagation*, *Int J Fatigue* **30**, 1921 (2008).
- [80] K. V. Smith, *Application of the dissipated energy criterion to predict fatigue crack growth of type 304 stainless steel following a tensile overload*, *Eng Fract Mech* **78**, 3183 (2011).
- [81] D. Cojocaru and A. M. Karlsson, *An object-oriented approach for modeling and simulation of crack growth in cyclically loaded structures*, *Advances in Engineering Software* **39**, 995 (2008).
- [82] D. Cojocaru and A. M. Karlsson, *Assessing plastically dissipated energy as a condition for fatigue crack growth*, *Int J Fatigue* **31**, 1154 (2009).
- [83] P. G. Nittur, A. M. Karlsson, and L. A. Carlsson, *Numerical evaluation of Paris-regime crack growth rate based on plastically dissipated energy*, *Eng Fract Mech* **124–125**, 155 (2014).



# 3

## METHODOLOGY

*With wonderful deathless ditties  
We build up the world's great cities.*

Arthur O'Shaughnessy - *Ode*

*The conceptual model of crack growth put forward in this thesis is that crack growth rate is the result of interaction between an amount of available energy and the amount of energy required per unit of crack growth. Alternatively these concepts can be interpreted as a crack driving force and a crack growth resistance. Crucially, both the available and the required energy may depend on the applied load. Evidence for that statement will be presented in later chapters.*

*This chapter presents the theoretical argument for the proposed conceptual model and defines a number of terms related to the strain energy that are used throughout this thesis. This chapter also discusses the specimens and test set-up, and presents the methods used for data analysis.*

### 3.1. CONCEPTUAL MODEL OF CRACK GROWTH

**B**EFORE setting out the theoretical framework that underlies this thesis, let us reflect for a moment on the difference between FCG and the models of quasi-static crack growth proposed by Griffith [1] and Irwin and Kies [2]. The key feature of these models, especially in the formulation of equation 2.4, is that they formulate a *stability criterion*. That is to say, these models explain when a crack will start to grow when there is no further external energy input. Any understanding of FCG on the other hand must explain not only when a crack will start to grow, but also when it will *stop*. After all, during a single fatigue cycle the crack will only advance by a finite amount. Thus any model of FCG must be able to explain why the crack advance will halt again, and preferably also how far the crack will advance during a single cycle.

From the first law of thermodynamics it follows that a finite amount of crack extension implies a finite amount of energy available for crack growth during one cycle. This ‘packet’ of available energy is consumed by the mechanisms that result in crack growth. This could be actual decohesion mechanisms, but also any dissipative processes that are inextricably linked to the crack growth, even if they do not themselves advance the crack. An example would be the plastic deformation near the crack tip. Even if this deformation does not serve to advance the crack tip, it is impossible to create crack growth without also generating this plasticity. Thus the energy dissipated in this plastic deformation should be considered part of the energy necessary to advance the crack.

Again invoking the first law of thermodynamics; the amount of crack growth generated in one cycle follows from the total amount of energy dissipated and the amount of energy that needs to be dissipated per unit of crack growth, i.e., assuming unit width:

$$\frac{da}{dN} = \frac{da}{dU} \frac{dU}{dN} \quad (3.1)$$

This equation is very similar to the equation proposed by Bodner et al [3] (eqn 2.29), but then generalised to take account of *all* energy dissipation, not just plastic dissipation.

In equation 3.1,  $dU/dN$  represents the total amount of energy dissipated during a single cycle. Thus  $dU/dN$  is equal to the amount of energy that was available for crack growth in that cycle. The factor  $da/dU$  represents the amount of crack growth per unit of dissipated energy. The inverse value  $dU/da$ , the amount of energy dissipation required per unit of crack growth, can be thought of as representing the resistance to crack growth.

Looking at the models discussed in Chapter 2, it is clear that those models generally attempt to relate the crack growth rate to only *one* parameter, usually interpreted as being some measure of the driving force. However by equation 3.1 it should be clear that there are two parameters that are important: how much energy is dissipated in total, and how much energy dissipation is required per unit of crack growth.

From this follows the conceptual model of crack growth used in this thesis, as shown in figure 3.1. According to this model, the crack growth rate is determined by the interaction between either the driving force or the energy available for crack growth on the one hand, and the resistance or energy required per unit of crack growth on the other hand. Crucially, the available energy and the required energy *both* depend on the applied load. Evidence for this statement will be provided in Chapter 4.

Summarising the above: a full explanation of FCG must not only explain how to find



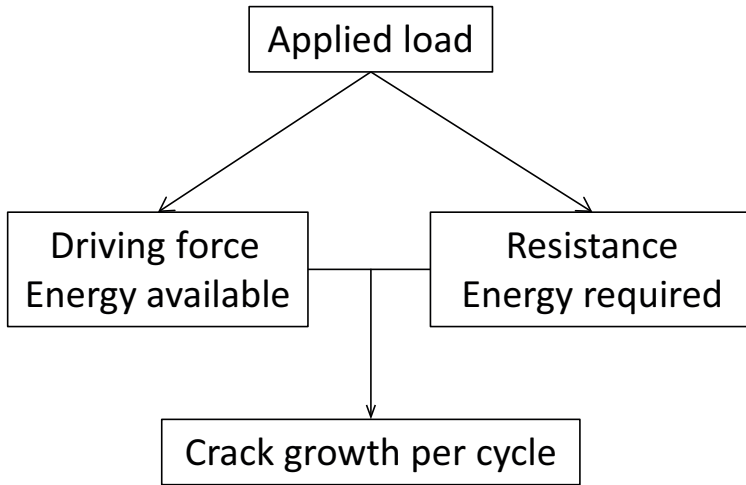


Figure 3.1: Conceptual model of FCG used in this thesis. Crack growth arises through the interaction of a driving force and a resistance to that force. Both the driving force and the resistance are influenced by the applied load

the crack growth rate based on a comparison of the driving force and the resistance. It must also explain how the driving force and the resistance depend on the applied load.

In the following chapters evidence will be presented supporting the conceptual framework sketched in figure 3.1. This will mainly be done by characterising the relationship between crack growth rate and energy dissipation. The remainder of this chapter will be devoted to an explanation of the general methodology used for the experiments and data analysis.

### 3.2. DEFINITION OF TERMS RELATED TO THE STRAIN ENERGY

CONSIDER a linear elastic material subjected to a fatigue load under displacement control. The force-displacement diagram for such a material is shown in figure 3.2. The area under this diagram is the work done on the specimen. Under the assumption of linear elasticity this is equal to the strain energy stored in the specimen. During the first load cycle the displacement is increased from  $d_0$  to  $d_{\min}$ , storing an amount of strain energy, which will be referred to as the monotonic energy,  $U_{\text{mono}}$ . During subsequent cycling a further amount of energy is added as the displacement is increased from  $d_{\min}$  to  $d_{\max}$ . If no energy dissipation takes place, this energy is returned to the loading device again as the specimen is unloaded from  $d_{\max}$  back to  $d_{\min}$ . This energy is referred to as the cyclic energy or cyclic work,  $U_{\text{cyc}}$ .

Under displacement control, if no energy dissipation occurs, the total amount of energy in the system  $U_{\text{tot}} = U_{\text{cyc}} + U_{\text{mono}}$  would remain constant. If crack growth occurs however, the specimen compliance  $C = d/p$  will increase and strain energy will be released from the system. Figure 3.3 shows how the total energy evolves over the course of a fatigue crack growth test on two specimens.

By fitting a suitable function and then taking the derivative (or a different suitable

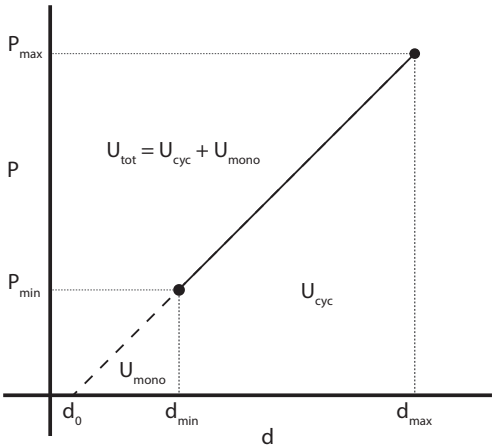


Figure 3.2: Theoretical force displacement diagram for a fatigue load cycle on linear elastic material under displacement control. Note that in general the force-displacement line does not pass through the origin.

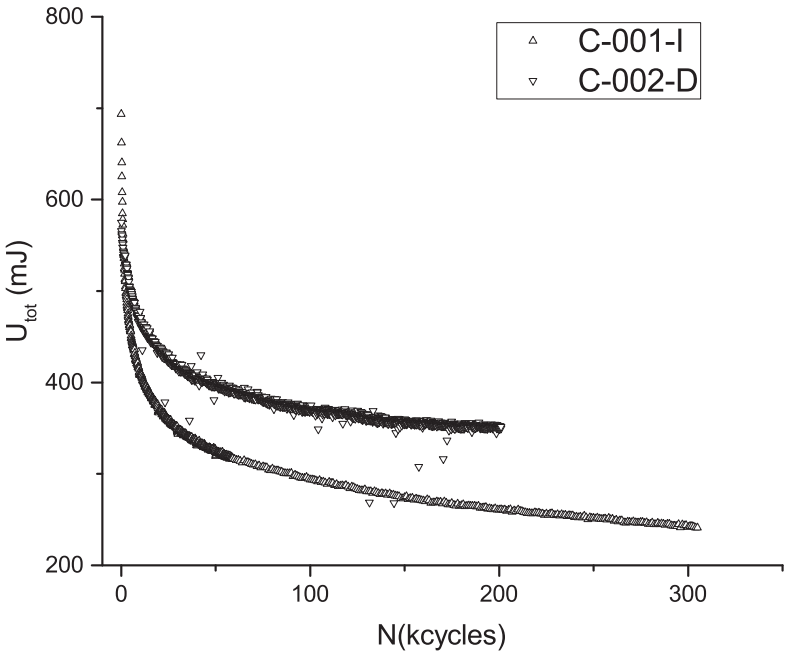


Figure 3.3: Total energy versus number of cycles for two specimens, each subjected to a different load cycle. For an explanation of the nomenclature see section 3.3, and for raw data see [4]

procedure) one can then obtain the change in energy per cycle  $dU/dN$ . The value of  $dU/dN$  for a given cycle is assumed to be equal to the energy dissipation in that cycle.

Rearranging equation 3.1 one obtains

$$\frac{dU}{dN} = G^* \frac{da}{dN} w \quad (3.2)$$

$$G^* = \frac{1}{w} \frac{dU/dN}{da/dN} = \frac{dU}{dA} \quad (3.3)$$

Here  $w$  is the specimen width and  $G^*$  is the amount of energy dissipated per unit of crack growth (in terms of fracture surface area).  $G^*$  appears to be identical to  $G = dU/da$  (with a suitable correction for the specimen width). However, it should be emphasised that  $G$  is a derivative, i.e. it applies for an infinitesimal increment of crack growth, and therefore applies at each instant of time. On the other hand,  $G^*$  is determined by the division of two parameters that have a time-resolution of one cycle. Therefore  $G^*$  represents the *average* energy dissipation per unit of crack growth in one cycle.  $G^*$  can thus be thought of as an ‘average SERR’. However,  $G^*$  is in general *not* equal to the mean value of  $G$ .

In case the specimen is loaded under force control, rather than displacement control, it is also possible to determine  $dU/dN$ . However in that case one has to take account of the work done by the constant force when the compliance increased. This can for example be done using the procedure outlined in [5]. This research focused on the displacement control load case, as this makes the experiments and data analysis easier to perform.

### 3.3. SPECIMEN DESCRIPTION

**T**HIS section gives a description of the general configuration of the specimens used in this research. Modified configurations were used to investigate the influence of bond line thickness and temperature. Details on these modifications will be given in the relevant chapters.

The specimens used in this research were coded according to the scheme: ‘letter’-‘3 digit number’-‘letter or Roman numeral’, e.g. ‘C-001-I’. The first letter refers to the specimen series and the number refers to the number of the specimen within that series. Due to the length of the specimens it was possible to conduct multiple fatigue tests on the same specimen. The last letter or Roman numeral is used to distinguish between these tests. Table 3.1 gives an overview of the test series discussed in this thesis.

The basic specimen geometry used in this research was the double cantilever beam (DCB) configuration. No standard exists for FCG in an adhesive joint, so the test set-up used in this thesis was based on ASTM standard D-5528 [6] and the work of Bürger [7]. Batches of specimens were produced by bonding two 6 mm thick aluminium Al 2024-T3 plates with Cytec FM94 K.03AD FILM 915 epoxy adhesive (FM94 for short). This adhesive film contains a polyester knit carrier. However, previous research has shown that this carrier does not significantly affect the disbond growth rate [7, Appendix A]. The aluminium was pre-treated with chromic acid anodisation (CAA). For series A through E bonding was conducted immediately after anodising. For the other specimens BR-127 primer was applied after CAA, and the aluminium was stored for some time before further processing.

Table 3.1: The different test series and the purpose of the tests.

Series	Test purpose
A	Quasi-static crack growth
B	Fatigue crack growth
C	Fatigue crack growth
D	Quasi-static and fatigue crack growth
E	Fatigue crack growth
G	Effect of bond line thickness
H	Effect of bond line thickness
T	Effect of temperature
AE	Acoustic emission / crack growth in a single cycle

Bonding was performed by placing a sheet of FM94 film between the two aluminium plates. A teflon (series A through E) or polyester (series G & H) tape was applied to a portion of each of the plates in order to prevent adhesion and create a pre-crack. The adhesive was cured in an autoclave in accordance with the manufacturer's specifications, i.e.: 1 hour at 120 °C and 6 bar (0.6 MPa) pressure. After curing, the plates were cut into strips, which were then milled to the final dimensions. Threaded holes were drilled into the specimens in order to allow attachment of the loading blocks. The nominal specimen width was 25 mm (see also figure 3.4). The actual specimen dimensions can be found in [8].

Diluted type-writer correction fluid (in essence, white paint) was applied to the side of the specimens in order to enhance visibility of the crack. A strip of paper graduated in 1 mm increments was fixed to the side of the specimen in order to provide a length scale for the crack length measurements.

For test series T and AE, specimens were used that were manufactured during the research project of Bürger [7], who used the same manufacturing process as described for this thesis. However as Bürger used longer specimens, a band saw was used to reduce the specimen length.

### 3.4. TEST SET-UP

THIS section describes the basic test set-up used throughout this research. Modifications to investigate specific factors are discussed in the relevant chapters.

Fatigue tests were performed on an MTS 10 kN hydraulic fatigue testing machine. Tests were conducted under displacement control at a fixed frequency of 5 Hz. The applied force and displacement at the minimum and maximum of the cycle were recorded by the fatigue machine every 100 cycles.

The crack length was measured by means of a camera aimed at the side of the specimen, as shown in figure 3.5. At the start of the test (when crack growth was relatively fast) pictures were taken every 100 cycles. After crack growth was deemed to have slowed sufficiently (typically after about 10 kcycles) the frequency of photography was reduced

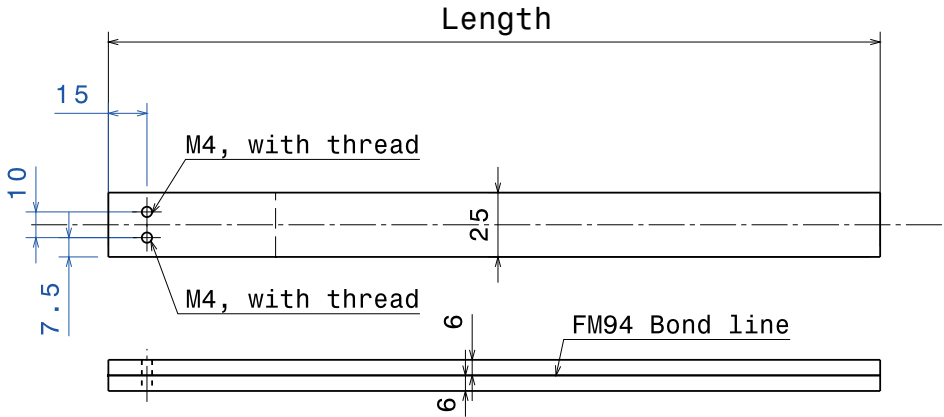


Figure 3.4: Nominal specimen dimensions in millimetres. Nominal specimen length was 300 mm for series A through E and 270 mm for series G & H. See [8] for the actual specimen dimensions.

to 1 photograph every 1000 cycles. Photographs were taken while the specimen was held open at maximum displacement. The image resolution was on the order of 20 pixels/mm, the exact value depending on the exact distance between the specimen and the camera, and on which camera equipment was available.

Quasi-static tests were performed on a 20 kN Zwick tensile test machine. Again force and displacement were recorded by the test machine and crack length was measured by means of a camera. Tensile tests were also conducted under displacement control, with a constant loading rate of 1 mm/min.

In accordance with ASTM D5528 [6] the crack length was defined as the straight line distance between the load line and the crack tip, as shown in figure 3.6, where the load line is assumed to be coincident with the centreline of the bolt holes. The displacement used in all calculations is the grip-to-grip displacement measured by the testing machines, which is assumed to be equal to the displacement  $d$  used in the ASTM standard, and shown in figure 3.6. This assumption basically means that the loading block attachment is assumed to be infinitely stiff, which is of course not the case in reality. However any displacement occurring in the loading blocks is thought to be negligible compared to the deformation of the arms of the specimen.

### 3.5. SELECTION OF APPLIED LOADS

**B**EFORE each fatigue test the specimens were loaded quasi-statically in order to properly initiate a crack in the specimen. This also allowed determination of the critical displacement  $d_c$  at which the force reaches a maximum. For the fatigue tests a maximum displacement  $d_{\max}$  was arbitrarily chosen as 0.9-0.95 times  $d_c$ . Then  $d_{\min}$  was selected

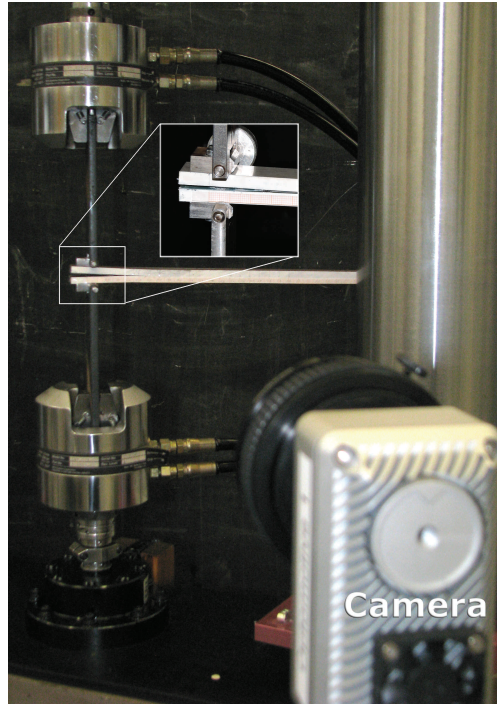


Figure 3.5: Test set-up, showing the specimen in the fatigue machine, as well as the camera position. The inset figure shows a close-up of the loading block attachment.

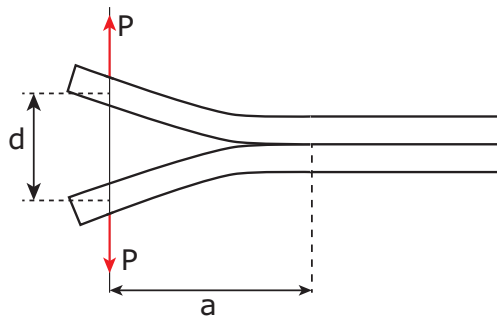


Figure 3.6: Definition of crack length and displacement

in order to obtain the desired value of  $R$ .

As the force-displacement curves did not pass exactly through the origin, the displacement ratio did not exactly equal the obtained force ratios, i.e:

$$R_d = \frac{d_{\min}}{d_{\max}} \neq \frac{P_{\min}}{P_{\max}} = R_p \quad (3.4)$$

During the first set of fatigue tests (series B and C) the objective was to obtain certain values of  $\Delta G$  and  $G_{\max}$  with respect to  $G_c$ . This resulted in  $R_p$ -ratios of 0.036 (test B-001-II), 0.29 (test C-001-I), 0.61 (test C-002-D and B-002-II) and 0.86 (test B-002-I). During subsequent tests  $R_d$  values were chosen equal to these  $R_p$  values in order to determine the desired  $d_{\min}$ . The selected  $R_d$  and obtained  $R_p$  values are shown in appendix A.

### 3.6. DATA ANALYSIS

**D**URING the experiments force, displacement, and crack length were recorded. This section describes how this data was processed in order to find the crack growth rate, the SERR, and the energy dissipation.

#### 3.6.1. CRACK GROWTH RATE

An image recognition algorithm was used to extract the crack length from the photographs taken during the test. This resulted in about 200-500 crack length measurements per test, depending on the number of applied cycles and the arbitrary choice of when to reduce the frequency of photography from 1 photograph every 100 cycles, to 1 photograph every 1000 cycles.

The measured crack length was matched with the number of cycles at which the photograph was taken. Then a continuous function was fit through the data, using the Matlab *cftool* toolbox [9]. Depending on the specimen a two or three parameter power-law was found to give the best fit, i.e:

$$a = \alpha N^\beta \quad \text{or} \quad a = \alpha N^\beta + \gamma \quad (3.5)$$

where  $\alpha$ ,  $\beta$ , and  $\gamma$  are curve-fit parameters. For the full list of generated functions, see appendix A.

The crack growth rate  $da/dN$  was found by taking the derivative of the obtained fitting functions.

#### 3.6.2. STRAIN ENERGY RELEASE RATE

ASTM standard D5528 presents four methods for calculation of  $G$  for a DCB test: pure beam theory, modified beam theory (MBT), compliance calibration (CC) and modified compliance calibration (MCC) [6]. It is known that pure beam theory overestimates  $G$  as it incorrectly treats the two arms of the specimen as perfectly built-in beams [6]. To select between the other three methods, all three methods were used to compute  $G$  values for quasi-static crack growth tests performed on specimen series A. As the computed  $G$  values showed little difference (see [4]), the CC method was selected based on its ease of use.

In the CC method,  $G$  is given by [6]:

$$G = \frac{nPd}{2wa} \quad (3.6)$$

where  $w$  is the specimen width, and  $n$  is a calibration parameter, equal to the slope of a linear fit through  $\log C$  versus  $\log a$ . The  $n$  values used were calculated for each specimen individually, and are shown in appendix A.

The test machine recorded displacement and force at the minimum and maximum of the cycle, as shown by the black dots in figure 3.2. The compliance was calculated by assuming linear behaviour between these two points, i.e.

$$C = \frac{d_{\max} - d_{\min}}{P_{\max} - P_{\min}} \quad (3.7)$$

As force and displacement were measured with a greater frequency than crack length, for the crack length needed in equation 3.6 the values given by the fitting functions (equation 3.5) were used.

Apart from  $G_{\max}$  crack growth rate was also correlated to  $(\Delta\sqrt{G})^2$ , defined as:

$$(\Delta\sqrt{G})^2 = (\sqrt{G_{\max}} - \sqrt{G_{\min}})^2 \quad (3.8)$$

Note that the Irwin equivalence (equation 2.5) implies that  $(\Delta\sqrt{G})^2$  is equivalent to  $\Delta K$ .

### 3.6.3. ENERGY DISSIPATION

For the calculation of the strain energy and energy dissipation values, it is important to note that the force-displacement line in general does not pass through the origin. This is particularly true if one extrapolates the linear behaviour between  $(P_{\max}, d_{\max})$  and  $(P_{\min}, d_{\min})$ . Rather, the force-displacement line will cross the displacement-axis (i.e.  $P = 0$ ) at a non-zero displacement  $d_0$ . This needs to be corrected for when calculating the energy values.

Consequently the following equations were used to determine the energy values for the fatigue tests:

$$d_0 = \frac{d_{\min} - CP_{\min}}{C} \quad (3.9)$$

$$U_{mono} = \frac{1}{2} P_{\min} (d_{\min} - d_0) \quad (3.10)$$

$$U_{cyc} = \frac{1}{2} (P_{\max} - P_{\min}) (d_{\max} - d_{\min}) + P_{\min} (d_{\max} - d_{\min}) \quad (3.11)$$

$$U_{tot} = U_{mono} + U_{cyc} \quad (3.12)$$

With  $C$  as defined by equation 3.7. Note that as  $d_0$  is non-zero:

$$U_{tot} \neq \frac{1}{2} P_{\max} d_{\max} \quad (3.13)$$

To determine the energy dissipation, continuous functions were fit for  $U_{cyc}$  and  $U_{tot}$  versus  $N$ , according to:

$$U = \alpha N^\beta \quad \text{or} \quad U = \alpha N^\beta + \gamma \quad (3.14)$$



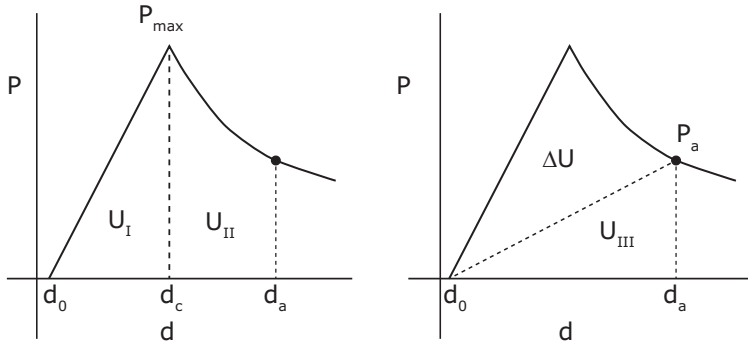


Figure 3.7: Method used to find the energy dissipation as a function of crack length  $\Delta U(a)$ , during the quasi-static tests.  $\Delta U(a) = U_I + U_{II} - U_{III}$ .

The energy dissipation was then obtained by taking the derivative of the curve fits. The obtained fit functions are shown in appendix A.

For the quasi-static tests the energy dissipation was calculated following the method illustrated in figure 3.7, where  $P_a$  and  $d_a$  are the force and displacement at a crack length of  $a$ . Between  $d_0$  and  $d_c$  the  $P$ - $d$  curve was linear, so calculation of the area  $U_I$  was straightforward. For  $d > d_c$  a polynomial function was fit to model the  $P$ - $d$  curve and then integrated to find  $U_{II}$ .  $U_I + U_{II}$  represents the total amount of work performed on the specimen. The remaining strain energy in the specimen,  $U_{III}$ , was calculated by assuming linear elastic behaviour of the specimen. Thus the dissipated energy as a function of crack length,  $\Delta U(a)$ , is given by:

$$U_I = \frac{1}{2} P_{\max} (d_c - d_0) \quad (3.15)$$

$$U_{II} = \int_{d_c}^{d_a} P dd \quad (3.16)$$

$$U_{III} = \frac{1}{2} P_a (d_a - d_0) \quad (3.17)$$

$$\Delta U(a) = U_I + U_{II} - U_{III} \quad (3.18)$$

## REFERENCES

- [1] A. A. Griffith, *The phenomena of rupture and flow in solids*, Philosophical Transactions of the Royal Society of London Series A, Containing Papers of a Mathematical or Physical Character **221**, 163 (1921).
- [2] G. R. Irwin and J. Kies, *Critical energy rate analysis of fracture strength*, Welding Journal - Research Supplement **33**, 193s (1954).
- [3] S. R. Bodner, D. L. Davidson, and J. Lankford, *A description of fatigue crack growth in terms of plastic work*, Eng Fract Mech **17**, 189 (1983).
- [4] J. A. Pascoe, R. C. Alderliesten, and R. Benedictus, *Damage tolerance of adhe-*

- sive bonds - dataset I*, (2013), available via: <http://dx.doi.org/10.4121/uuid:a2997418-682b-46f5-a988-ba0c88d7350e>.
- [5] J. A. Pascoe, R. C. Alderliesten, and R. Benedictus, *On the relationship between disbond growth and the release of strain energy*, Eng Fract Mech **133**, 1 (2015).
  - [6] ASTM Standard D 5528/ D 5528-01, *Standard test method for mode I interlaminar fracture toughness of unidirectional fiber-reinforced polymer matrix composites*, (2007), ASTM International, West Conshohocken, PA, USA.
  - [7] D. Bürger, *Mixed-mode Fatigue Disbond on Metallic Bonded Joints*, Phd thesis, Delft University of Technology (2015), <http://dx.doi.org/10.4233/uuid:ec4dbcd6-052d-4009-bf9e-cdcbf4614174>.
  - [8] J. A. Pascoe, R. C. Alderliesten, and R. Benedictus, *Damage tolerance of adhesive bonds - datasets*, (2014), collection of datasets, available at: <http://dx.doi.org/10.4121/uuid:c43549b8-606e-4540-b75e-235b1e29f81d>.
  - [9] The MathWorks Inc, *MATLAB and Curve Fitting Toolbox Release 2012b*, (2012).

# 4

## ENERGY DISSIPATION DURING FATIGUE CRACK GROWTH

*Real investigation is not the reception of a transcendental vision, a process of thought beyond the power of an ordinary mortal. The prayer of the scientist might well be, “Lord, show us the obvious.”*

Cecilia Payne-Gaposchkin, *So you want to do research?*

*Fatigue tests were performed at room temperature on specimens with a standard adhesive thickness. It was demonstrated that LEFM approaches that rely on only 1 parameter are inadequate to fully model the data. Rather than modelling the crack driving force directly, it is proposed to use energy dissipation to characterise the crack growth behaviour.*

*It is shown that the crack growth rate correlates very strongly to the energy dissipation per cycle  $dU/dN$ . The energy dissipation per unit of crack growth,  $G^*$ , which can be interpreted as the resistance to crack growth, is not constant. It is shown that  $G^*$  correlates linearly to  $G_{\max}$ , with higher  $G_{\max}$  resulting in higher  $G^*$ . At a fixed  $G^*$ , the total energy dissipation per cycle is strongly correlated to  $(\Delta\sqrt{G})^2$ ,  $\Delta G$ ,  $U_{\text{cyc}}$  and  $U_{\text{tot}}$ .*

*Quasi-static crack growth is investigated and compared to fatigue crack growth. It is found that during quasi-static crack growth, the resistance  $G^*$  is higher than during fatigue crack growth. These results indicate that different mechanisms are active during quasi-static crack growth and fatigue crack growth.*

*Fractographic images are presented to further support the results that were found.*

### 4.1. INTRODUCTION

THE first stage of the thesis research was to investigate energy dissipation during fatigue crack growth experiments. In particular the goal was to examine the relationship between the energy dissipation and the crack growth rate.

In total, 11 fatigue crack growth experiments were performed that provided valid results for standard adhesive thickness tested at room temperature. These results will be discussed in detail in this chapter, and then used as a baseline to examine the effects of adhesive thickness and temperature in the next two chapters.

For easier presentation, the data has been grouped into 4 sets:  $R = 0.036, 0.29, 0.61$ , and  $0.86$ . The actual obtained  $R_d$  and  $R_p$  values are shown in table A.1. The full data is available from 4TU.ResearchData [2].

## 4

### 4.2. LEFM APPROACH

THE standard LEFM approaches to fatigue crack growth were discussed in Chapter 2. They generally use some form of the SERR as a similitude parameter. Figures 4.1 and 4.2 show the data from this research plotted according to the LEFM methodology, using  $G_{\max}$ ,  $(\Delta\sqrt{G})^2$  (as defined in equation 3.8), and  $\Delta G = G_{\max} - G_{\min}$ , as the similitude parameters.

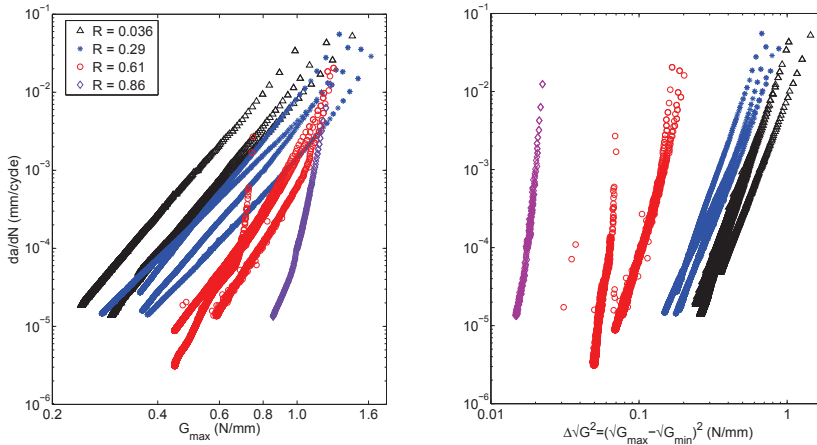


Figure 4.1: Crack growth rate as a function of  $G_{\max}$  or  $(\Delta\sqrt{G})^2$ . A clear  $R$ -ratio dependence is visible. [1]

There is a clear dependence on the  $R$ -ratio when using  $G_{\max}$  and  $(\Delta\sqrt{G})^2$  as a similitude parameter. For a given  $G_{\max}$  an increase in  $R$  gives a *decrease* in  $da/dN$ , whereas for a given  $(\Delta\sqrt{G})^2$  an increase in  $R$  gives an *increased*  $da/dN$ . This is consistent with the results reported in literature.

When using  $\Delta G$ , an  $R$ -ratio effect is still visible, but no consistent trend is apparent. Compared to  $R = 0.036$ , the results for  $R = 0.29$  appear to be slightly shifted to the right, but the  $R = 0.61$  results more or less overlap with 2 of the 3 curves for  $R = 0.036$ . The only clear effect is for  $R = 0.86$ , where the curve is clearly shifted to the left (i.e. higher

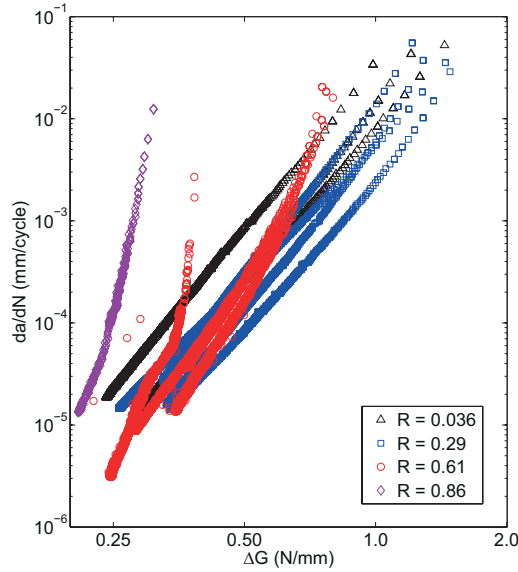


Figure 4.2: Crack growth rate as a function of  $\Delta G = G_{\max} - G_{\min}$ . There is no clear  $R$ -ratio effect, except for  $R = 0.86$ .

crack growth rate for the same  $\Delta G$ ). That a change in  $R$ -ratio produces a smaller effect when using  $\Delta G$  as a similitude parameter than when using  $(\Delta\sqrt{G})^2$  is to be expected. With some algebra (see Appendix B) it can be shown that changing  $R$ , while keeping  $\Delta G$  constant, produces a smaller change in mean load than changing  $R$  while keeping  $(\Delta\sqrt{G})^2$  constant.

What is not clear is why the  $R$ -ratio effect seen in figure 4.2 is not-monotonically increasing or decreasing, and does not match what has been reported in literature [3, 4]. Increasing  $R$  always increases the mean load. One might think this would lead to an increase in the crack growth rate [3], which here only appears to happen for  $R = 0.86$ . In contrast to this reasoning, and the experiments in this research, in literature it is usually reported that an increase of  $R$  for constant  $\Delta G$  leads to a reduction in crack growth rate [3, 4]. With the results of this thesis that will be presented below the behaviour reported in literature can be explained. This will be done in section 4.4.5.

Recently Jones et al. [3] have suggested that the  $R$ -ratio behaviour seen here is anomalous for the case where  $G_{\max}$  is used as a similitude parameter, and that therefore  $(\Delta\sqrt{G})^2$  should be regarded as the correct similitude parameter. Furthermore they suggest that  $(\Delta\sqrt{G})^2$  should be interpreted as the crack driving force<sup>1</sup>. Jones et al. claim that the  $G_{\max}$  behaviour is anomalous, because it implies that an increasing mean stress results in a lower crack growth rate. On the other hand, when using  $(\Delta\sqrt{G})^2$ , an increasing mean stress results in an increased crack growth rate, which matches what has been established for FCG in metals when using  $\Delta K$  as similitude parameter.

<sup>1</sup>Jones et al. actually use  $\Delta\sqrt{G} = \sqrt{G_{\max}} - \sqrt{G_{\min}}$  but this does not change the argument presented here

These statements are worth examining in more detail, because they make explicit a number of views that implicitly underlie much of the literature. First of all it should be noted that the similarity of the  $R$ -effect seen when using  $(\Delta\sqrt{G})^2$  in adhesives and when using  $\Delta K$  in metals is not surprising. By equation 2.5  $\Delta\sqrt{G}$  and  $\Delta K$  are equivalent. Therefore, using the equivalence of the  $R$ -ratio behaviour to justify selecting  $(\Delta\sqrt{G})^2$  as a similitude parameter is tautological. If one accepts that  $\Delta K$  is the appropriate similitude parameter, then by extension so is<sup>2</sup>  $(\Delta\sqrt{G})^2$ .

This leaves three questions: (1) is the  $G_{\max}$  behaviour indeed anomalous? (2) do these results justify the selection of  $(\Delta\sqrt{G})^2$  as similitude parameter? and, (3) should  $(\Delta\sqrt{G})^2$  be interpreted as a crack driving force?

## 4

#### 4.2.1. $R$ -RATIO EFFECT WITH $G_{\max}$ AS SIMILITUDE PARAMETER

If one regards selecting  $G_{\max}$  as a similitude parameter as being equivalent to interpreting it as a crack driving force, then the conclusion that increasing the mean stress (through an increased  $R$ -ratio) leads to a reduction in crack growth rate is indeed puzzling. However, as discussed in section 2.3 and illustrated in figure 2.1,  $G_{\max}$  by itself does not, and can not, uniquely define a load cycle. It is true that increasing  $R$  while keeping  $G_{\max}$  constant implies an increase of the mean stress. *However it also implies a decrease of the load range*, i.e.  $\Delta G$  or  $(\Delta\sqrt{G})^2$ .

That crack growth depends not only on the maximum load, but also on the load range, is well established, with lines of evidence going back to the work of Paris [5–7] and Wöhler [8]. It is also the assumption behind the selection of  $\Delta K$  and  $(\Delta\sqrt{G})^2$  as similitude parameters by Jones et al. Based on this established relationship between load range and crack growth rate, a decrease in crack growth rate for a decrease in load range is exactly what would be expected. Therefore, the  $R$ -ratio effect seen in figure 4.1 and elsewhere for  $G_{\max}$  is not anomalous. *Rather, it is a correct reflection of the fact that different combinations of  $G_{\max}$  and  $R$  define different load cycles.*

In the literature the  $R$ -ratio effect is often implicitly regarded as a material effect, which modifies the fundamental relationship between the crack driving force (interpreted to be e.g. either  $G_{\max}$  or  $(\Delta\sqrt{G})^2$ ) and the crack growth rate. Although there is indeed evidence that  $R$  affects the material behaviour [9], the argument above shows that a different  $R$  also implies a different applied load. Therefore the results shown in figure 4.1 should not be understood as showing solely material behaviour, as the curves for different  $R$ -ratios correspond to different applied load cycles.

#### 4.2.2. SUITABILITY OF $(\Delta\sqrt{G})^2$ AS A SIMILITUDE PARAMETER

Given that the  $R$ -ratio behaviour shown in figure 4.1 is in accordance with what one would expect, the next question is whether these results justify the selection of  $(\Delta\sqrt{G})^2$  as similitude parameter. To answer this question it is good to recall what the purpose of a similitude parameter is. A similitude parameter is a value that can be calculated for a given structure. It can then be used to compare two different structures in order

<sup>2</sup>Strictly speaking it is  $\Delta\sqrt{G}$  that is equivalent to  $\Delta K$ , but since a power-law fit is used, if  $\Delta K$  is appropriate, then both  $\Delta\sqrt{G}$  and  $(\Delta\sqrt{G})^2$  can be used, as long as the exponent is adjusted appropriately.

to predict some kind of behaviour; e.g. the crack growth rate. In particular, it can be used to compare a full-scale operational structure with a test specimen, with the idea that the same value of the similitude parameter in both the full-scale structure and the test specimen, will result in the same crack growth rate. Thus the main requirement of a similitude parameter is *consistency*. *The same value of the similitude parameter should always result in the same behaviour.*

Figure 4.1 therefore shows that strictly speaking *neither*  $G_{\max}$  nor  $(\Delta\sqrt{G})^2$  is suitable as similitude parameter. In both cases one needs to have some way of accounting for the  $R$ -ratio. To obtain the same crack growth rate, one must not only have the same  $G_{\max}$  or  $(\Delta\sqrt{G})^2$ , but also the same  $R$ . A variety of methods that take the  $R$ -ratio into account (explicitly or implicitly) were discussed in section 2.3. The key feature of all these models is that they do not rely on a single similitude parameter. Instead they require *at least two* parameters.

Indeed, although Jones et al. [3] only refer to  $\Delta\sqrt{G}$  as a similitude parameter, inspecting the equation they propose, it is quickly apparent that it depends not only on  $\Delta\sqrt{G}$ , but also upon  $G_{\max}$ , and also contains a parameter that is a function of  $R$  (viz.  $\Delta\sqrt{G_{th}}$ ). In essence then, the ‘Hartman-Schijve’ equation proposed by Jones et al. contains *three* similitude parameters, or perhaps a ‘three-part’ similitude parameter. After all, the crack growth rate follows by combining  $G_{\max}$ ,  $\Delta\sqrt{G}$ , and  $\Delta\sqrt{G_{th}}$ , according to equation 2.22.

In the literature it is common practice to select only one similitude parameter and then regard one or more parameters as modifying the fundamental relationship between the similitude parameter and  $da/dN$ . By the argument presented in this section it would seem to be more appropriate to regard all these parameters together as either joint similitude parameters, or as components of an overarching similitude parameter. E.g. if one employs the Hartman-Schijve equation proposed by Jones et al. ([3], equation 2.22), the similitude parameter is not  $\Delta\sqrt{G}$ , but rather

$$\text{Similitude parameter} = \frac{\Delta\sqrt{G} - \Delta\sqrt{G_{th}}}{\sqrt{1 - \frac{\sqrt{G_{\max}}}{\sqrt{A}}}} \quad (4.1)$$

The conclusion of the above is that regardless of which parameter(s) exactly get designated as ‘similitude parameter’, a prediction model for fatigue crack growth will need to take into account more than a single parameter. Whether implicitly or explicitly, both the range and the mean (or equivalently, maximum) of the applied load need to be taken into account. This can be done in various ways, as discussed in section 2.3, and with enough experimental data and proper curve fitting, all these different approaches can provide good predictions. However, as discussed in Chapter 1, a good prediction does not imply understanding of the underlying physics. This leads to the third question: should  $(\Delta\sqrt{G})^2$  be interpreted as the crack driving force?

#### 4.2.3. INTERPRETATION OF $(\Delta\sqrt{G})^2$ AS CRACK DRIVING FORCE

In [3] Jones et al. declare  $\Delta\sqrt{G}$  to be the crack driving force, on the basis that it is capable of predicting the crack growth rate when employed as a similitude parameter. In section 2.6 it was mentioned that Ochensberger and Kolednik [10, 11] regarded  $\Delta\sqrt{J}$  as the crack

driving force<sup>3</sup>, for much the same reason. Thus the objections raised in sections 2.5 and 2.6 remain relevant.

Mathematically it is impossible for  $(\Delta\sqrt{G})^2$  to uniquely define a load cycle. In fact, there are an infinite number of possible load cycles with the same  $(\Delta\sqrt{G})^2$ . Unless the crack driving force really only depends on the range of the load, and not on the absolute minimum and maximum values reached, it therefore seems unreasonable to regard  $(\Delta\sqrt{G})^2$  as representative of the driving force. The  $R$ -ratio effect seen in figure 4.1 shows that the crack growth rate does in fact depend on the absolute values reached, and not solely on the range.

Thus, although  $(\Delta\sqrt{G})^2$  may be a suitable similitude parameter for crack growth predictions, as long as one also takes the  $R$ -ratio in to account, it cannot be regarded as the crack driving force. The requirement of a similitude parameter is primarily consistency, not physical relevance. Of course that a certain parameter is capable of consistently predicting material behaviour suggests it does have some physical relevance. However, the mere fact that a certain parameter can make a good similitude parameter, does not prove a particular physical interpretation of that parameter.

Quite apart from the question of how to quantify the crack driving force, there is another issue with the current approaches to predicting FCG based on a driving force.

#### 4.2.4. ISSUES WITH CURRENT DRIVING FORCE APPROACHES

Any driving force based approach faces the question why crack growth during a single cycle is finite. Current approaches (e.g. [3, 11]) attempt to relate a driving force directly to the crack growth rate, assuming a constant driving force value for each cycle. However if the driving force is a constant value such as  $(\Delta\sqrt{G})^2$ , then why is the amount of crack growth during a single cycle not infinite?

To model this using a driving force based approach one would need to model the driving force dependence on time. One would also need to model the resistance to this driving force. Taken together this would then give the crack growth velocity dependence on time within a single cycle, which could then be integrated to give the total amount of crack growth during the cycle.

A more simple way of taking these factors into account would seem to be to relate the crack growth rate to energy in the system. After all, during a single fatigue cycle, only a finite amount of work is performed on the system.

### 4.3. CORRELATION BETWEEN ENERGY DISSIPATION AND CRACK GROWTH RATE

FIGURE 4.3 shows the crack growth rate,  $da/dN$ , plotted against the amount of energy dissipated per cycle,  $dU/dN$ . The energy dissipation is shown both in terms of cyclic energy  $U_{cyc}$  and in terms of total energy  $U_{tot}$ . It can be seen that in both cases there is a

<sup>3</sup>Note that  $\Delta\sqrt{J}$  and  $\Delta\sqrt{G}$  are equivalent if the amount of plasticity is sufficiently small.



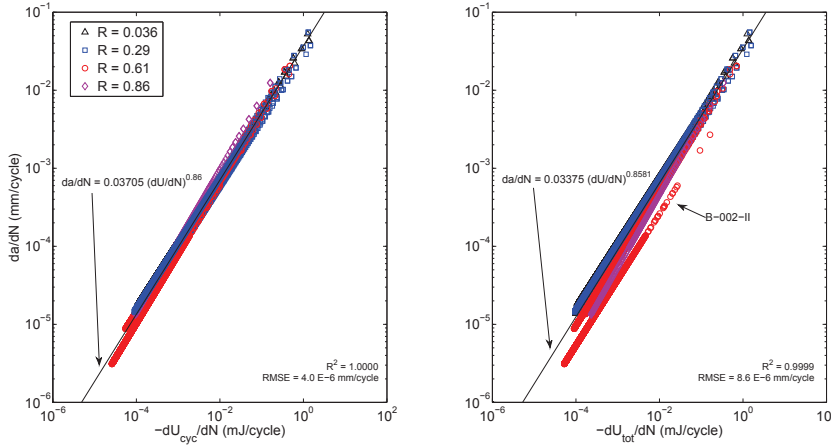


Figure 4.3: Crack growth rate as a function of energy dissipation per cycle. Energy dissipation is shown based on both  $U_{cyc}$  (left panel) and  $U_{tot}$  (right panel), as defined in Chapter 3. The value of the fit parameters  $\alpha$  and  $\beta$ , as defined in equation 4.2 are also given, as well as the coefficient of determination and the root mean square error of the fits.

very strong correlation, which can be captured by the model:

$$\frac{da}{dN} = \alpha \left( \frac{dU}{dN} \right)^\beta \quad (4.2)$$

where  $\alpha$  and  $\beta$  are curve fit parameters.

It is clear that both  $U_{cyc}$  and  $U_{tot}$  show a very strong correlation between energy dissipation and crack growth rate. For  $U_{tot}$  the correlation is slightly weaker, and in particular the line for experiment B-002-II ( $R = 0.61$ ) appears to be an outlier.

Nevertheless, if the compliance changes, it follows from the resulting change in the force-displacement line that not only  $U_{cyc}$  must change, but also  $U_{mono}$ . Therefore, based on the physics,  $U_{tot}$  seems to be the most appropriate parameter to examine, rather than  $U_{cyc}$ . Thus unless it is explicitly indicated otherwise, any mention of  $dU/dN$  from this point onwards refers to  $dU/dN$  based on  $U_{tot}$ .

Comparing figures 4.1 and 4.3 it is immediately apparent that the  $R$ -ratio effect is greatly reduced when plotting  $da/dN$  against  $dU/dN$ . Nevertheless, a small  $R$ -ratio effect is still present. Note that figure 4.3 is comparing the measured energy dissipation due to crack growth with the crack growth rate, rather than comparing a measure of the load cycle to the crack growth rate. Thus the  $R$ -ratio effect in this case is solely due to the material behaviour, and not due to the ‘hidden’ changes of the load cycle that are partly responsible for the  $R$ -ratio effect seen in figure 4.1. The effect of  $R$ -ratio on energy dissipation will be discussed in more detail in the next section.

Besides the  $R$ -ratio effect, another interesting feature of figure 4.3 is that the correlation between  $da/dN$  and  $dU/dN$  is non-linear, having in fact an exponent of approximately 0.86. This means that the amount of energy dissipated per unit of crack growth is not constant. If the energy dissipation is increased by a factor of 2, the crack growth rate will

only increase by a factor of approximately 1.81. In other words, crack growth at high crack growth rates requires more energy per unit of crack growth. One could thus say that crack growth at high rates is less efficient than crack growth at low rates. This has also been observed for fatigue driven delamination in CFRP [12].

To understand these observations, the framework suggested by Broberg [13–16] may be helpful. Broberg postulates the existence of three regions around the crack tip that are involved in the crack growth process, as shown in figure 4.4. The first region Broberg defines is the ‘end-region’ around the crack-tip. The defining characteristic of this region is that it is autonomous, i.e. it does not depend on the crack length or the far-field applied load. In other words, the properties of the end-region are material properties. The end-region is also the smallest region that can still be regarded as a continuum. Therefore its size depends on the type of material. In perfectly brittle materials it is equal to the inter-atomic distance, but it is of the order of the distance between inclusions in materials that have dimple type fracture [16]. Surrounding this end-region is a plastic region, in which plastic deformation occurs. Surrounding that is an elastic region, in which all deformation is elastic.

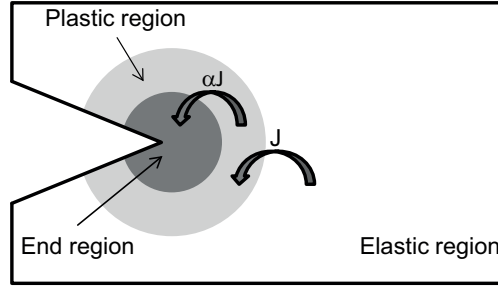


Figure 4.4: Schematic representation of the various regions surrounding the crack tip and energy flows between them in the Broberg model.

Broberg postulates that crack growth occurs when the amount of energy flowing to the end-region,  $\Phi$ , reaches a critical value. Although Broberg does not discuss this, in the framework proposed in this thesis, the finite amount of crack growth within a single cycle, can be explained by the amount of energy flowing to the end-region also being finite. In a perfectly brittle material the amount of energy flowing to the end-zone is given by the  $J$ -integral, i.e.  $\Phi = J$ . However, in a material that is capable of plastic deformation, the plastic region will absorb energy. In such a material  $J$  does not define the amount of energy flowing to the end-zone, but only describes the amount of energy flowing to the plastic zone. The amount of energy flowing to the end-zone is then given by:

$$\Phi = \alpha J \quad (4.3)$$

$$0 < \alpha < 1 \quad (4.4)$$

where the ratio  $\alpha$  depends on the properties of the plastic zone. Note that this is somewhat similar to the distinction Simha et al. draw between  $J_{tip}$  and  $J_{far}$ , as defined in equation 2.26 [17, 18].

LEFM rests upon the assumption that the SIF, the SERR, and/or the  $J$ -integral can be used to describe the conditions at the crack-tip. Per the above, this implies the assumption that  $\alpha$  is constant, because if  $\alpha$  is not constant, then the same value of  $J$  (and thus by extension  $G$  or  $K$ ) in two different cases does not imply the same amount of energy reaching the crack tip.

Broberg [16] cites the work of Andersson (summarised in [19]) as evidence that  $\alpha$  is not necessarily constant. Figure 4.3 provides further evidence for this proposition, as it shows that the amount of energy dissipated per unit of crack growth was not constant during the current experiments.

Even if one does not accept all the details of Broberg's model, it does seem reasonable that there is a small region around the crack tip, of which the properties are solely governed by the material. For example, material decohesion must ultimately involve breaking of molecular bonds. The amount of energy required for this is a function of the bond strength, which is a material property. The same goes for the surface energy, although it must be pointed out that at microscopic scales the fracture surface is not flat. The crack surface that is usually measured is the projection onto a flat plane of the actual crack surface, and thus changes in roughness might cause large differences in the ratio of actual to projected fracture surface. If this is not taken into account, it could give the impression that the surface energy is not constant.

Thus there are two possible explanations for the change in energy dissipation per unit of crack growth seen in figure 4.3. The first is that the ratio of actual fracture surface to projected fracture surface is not constant. To be consistent with the results seen in figure 4.3, the amount of actual fracture surface per unit of projected area would have to increase as the crack growth rate increases, in other words, the crack surface should become more rough.

The second possible explanation is that the amount of energy dissipation in the region surrounding the crack tip is not constant. I.e. in Broberg's terms: that  $\alpha$  is variable. According to this hypothesis, at higher crack growth rates (which imply greater loading) more energy dissipative mechanisms (e.g. plastic deformation) are activated around the crack tip. Although these mechanisms do not directly contribute to crack growth, they are strongly linked to it, so that crack growth without activating these mechanisms is not possible. Thus more energy is dissipated per unit of crack advance.

Purely from the geometry of the force-displacement curve it follows that for a linear elastic material at a higher maximum load, the amount of energy released by an increment of crack growth will also be higher. This is illustrated in figure 4.5. In other words, at higher load,  $G$  and  $J$  are higher. If one assumes the same increment of crack growth always results in the same amount of energy dissipation in the end region, the only possible way to have the same  $da$  at a higher  $J$ , is for the plastic region to absorb more energy, i.e. for  $\alpha$  to be higher. The assumption that a certain increment of crack growth always requires the same amount of energy dissipation in the end region follows from Broberg's definition of the end region as autonomous. It still needs to be confirmed experimentally.

Of course it is very well possible that both of the above hypotheses are correct, and that the increase of energy dissipation per unit crack growth is driven both by an increase in actual surface area and by an increase of dissipative mechanisms near the crack tip.

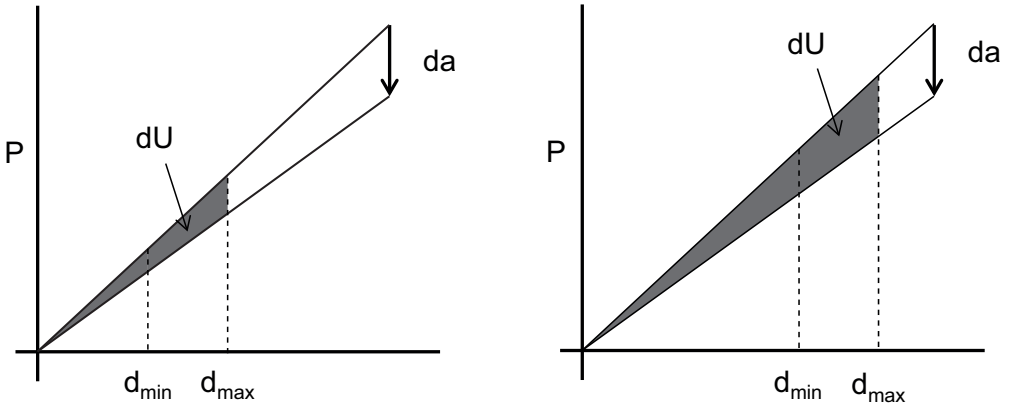


Figure 4.5: Schematic illustration of the point that at higher maximum load the same increment of crack growth  $da$  will result in a higher increment of energy release  $dU$ .

#### 4.4. COMPARISON TO THE CONCEPTUAL MODEL

IN section 3.1 a conceptual model of FCG was introduced, in which the amount of crack growth is determined by the balance of the amount of energy available for crack growth, and the amount of energy that is required. Of course the first law of thermodynamics demands that these two values are equal.

Thus the measured energy dissipation  $dU/dN$  can be interpreted both as the total amount of energy that was available for crack growth in a given cycle, and as the amount of energy required for the amount of crack growth that took place in that cycle. If two cycles had the same amount of energy dissipation, but a different crack growth rate, the amount of energy dissipated per unit of crack growth is necessarily different. The amount of energy dissipated per unit of crack growth can be calculated from the experimental data according to equation 3.3. Since this  $G^*$  value determines how much crack growth can occur for a given amount of available energy, it can be interpreted as the material's crack growth resistance.

Thus for the purposes of this thesis, crack growth resistance will be defined as:

The amount of energy dissipated per unit of crack growth,  $G^*$ .

and the total amount of energy required for crack growth in a given cycle will be defined as:

The total amount of energy dissipated in a given cycle,  $dU/dN = G^* \cdot da/dN \cdot w$ .

with  $w$  the specimen width. Invoking the first law of thermodynamics, the amount of energy available for crack growth will be assumed to be equal to the amount of energy required.

In section 3.1 it was postulated that both the crack growth resistance, and the amount of available energy, may depend on the applied load cycle. This dependence will be examined in the following sections.

#### 4.4.1. CRACK GROWTH RESISTANCE

As mentioned above, the fact that the fit (equation 4.2) has an exponent that does not equal 1, implies that the energy dissipation per unit of crack growth,  $G^*$ , is not constant. Furthermore, it was mentioned that there seems to be a small  $R$ -ratio effect visible in the  $dU/dN$  vs  $da/dN$  graphs in figure 4.3. To gain more insight into these factors, it is instructive to examine the amount of energy dissipation for a fixed  $da/dN$  value. This is done in figures 4.6 and 4.7, which show the amount of energy needed to create  $10^{-4}$  mm/cycle crack growth in each specimen, as a function of  $G_{\max}$ ,  $(\Delta\sqrt{G})^2$ , and  $\Delta G$ .

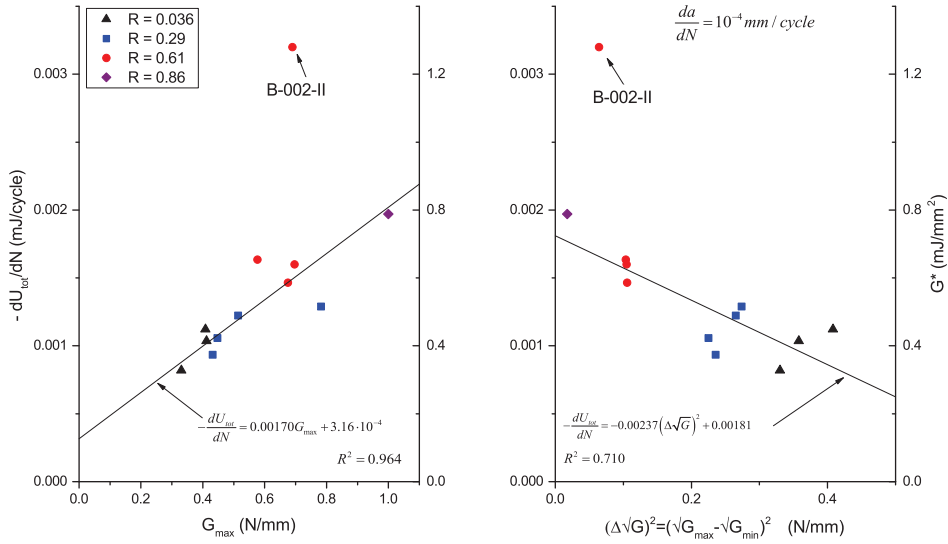


Figure 4.6: Energy dissipation at a crack growth rate of  $10^{-4}$  mm/cycle as a function of  $G_{\max}$  (left panel) and  $(\Delta\sqrt{G})^2$  (right panel). Linear fits through the data points are also shown. The data for experiment B-002-II was excluded from these fits as an outlier. As all data points in this figure correspond to the same  $da/dN$  value, an approximation of  $G^*$  is also shown, obtained by dividing the axis values by  $25 \cdot 10^{-4}$  (i.e.  $da/dN$  times the nominal specimen width) [1].

It is important to note that because figure 4.6 was constructed for a single  $da/dN$  value, the  $G_{\max}$  and  $(\Delta\sqrt{G})^2$  values are *not independent*. That is to say: a higher  $G_{\max}$  value implies a lower  $(\Delta\sqrt{G})^2$  value and vice versa.

There is a large range of  $G_{\max}$  values (from 0.33 to 1.0 N/mm) that all result in the same crack growth rate of  $10^{-4}$  mm/cycle. Similarly there is a large range of  $(\Delta\sqrt{G})^2$  values (from 0.018 to 0.40 N/mm) and  $\Delta G$  values (from 0.25 to 0.52 N/mm) that nevertheless all resulted in the same crack growth rate. This further highlights the point that one cannot base a prediction of crack growth rate on only one parameter. Given the lack of a clear correlation between  $dU/dN$  and  $\Delta G$ , the best combination of parameters seems to be  $G_{\max}$  and  $(\Delta\sqrt{G})^2$ .

Another interesting point is that there is a large difference between the minimum and maximum amount of energy dissipation required to obtain the same crack growth

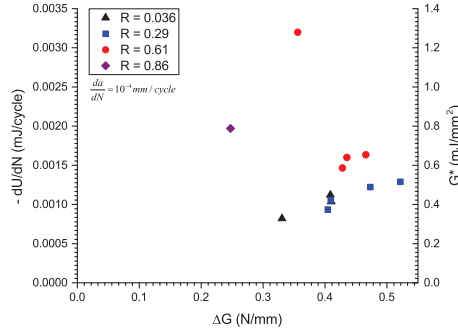


Figure 4.7: Energy dissipation at a crack growth rate of  $10^{-4}$  mm/cycle as a function of  $\Delta G$ . An approximation of  $G^*$  is also shown, obtained by dividing the axis values by  $25 \cdot 10^{-4}$  (i.e.  $da/dN$  times the nominal specimen width).

increment of  $10^{-4}$  mm. Indeed the maximum measured energy dissipation value is a factor of 2.4 higher than the minimum measured value.

It is clear that the amount of energy required for crack growth increases for higher  $G_{\max}$  values, or correspondingly for higher  $R$  values, and decreases for higher  $(\Delta\sqrt{G})^2$  values. For  $\Delta G$  there is no clear pattern. The correlation between  $dU/dN$  and  $G_{\max}$  appears to be stronger than that between  $dU/dN$  and  $(\Delta\sqrt{G})^2$ . Thus with reference to the conceptual model, it seems that a higher value of  $G_{\max}$  results in a higher value of the crack growth resistance.

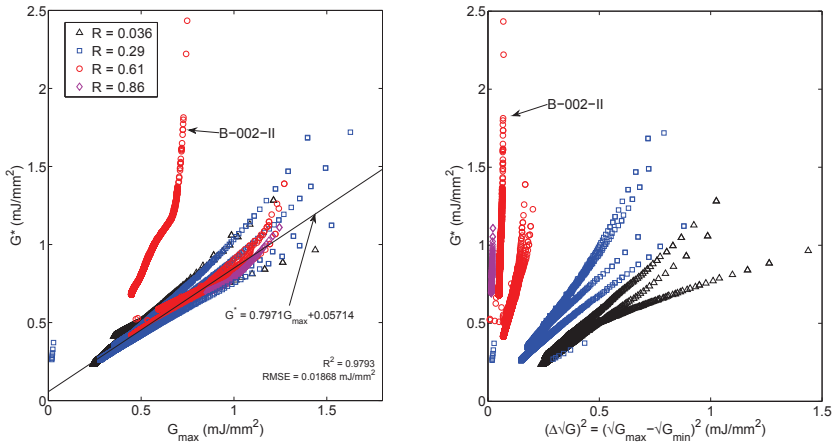


Figure 4.8:  $G^*$  as a function of  $G_{\max}$  (left panel) and  $(\Delta\sqrt{G})^2$  (right panel). A linear fit for  $G^*$  as a function of  $G_{\max}$  is also shown. The data for experiment B-002-II ( $R=0.61$ ) was excluded from this fit as an outlier.

This is made even more clear in figures 4.8 and 4.9, which show  $G^*$  as a function of

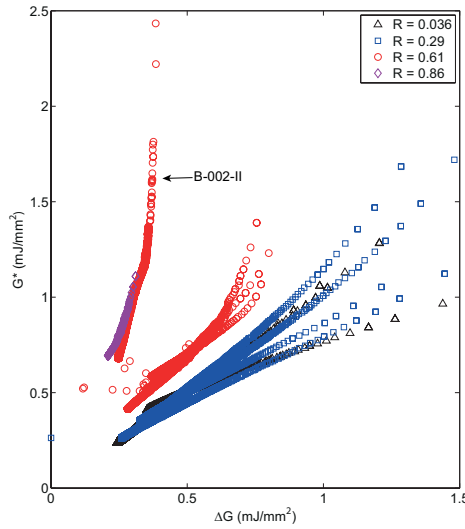


Figure 4.9:  $G^*$  as function of  $\Delta G$ .

$G_{\max}$ ,  $(\Delta\sqrt{G})^2$ , and  $\Delta G$ . Note that in figure 4.8, the  $G_{\max}$  and  $(\Delta\sqrt{G})^2$  values *are* independent, which explains why  $G^*$  increases both for increasing  $G_{\max}$  and increasing  $(\Delta\sqrt{G})^2$ , unlike in figure 4.6.

Regarding the data from experiment B-002-II as an outlier, there is a clear linear relationship between  $G^*$  and  $G_{\max}$ , independent of  $R$ -ratio. In contrast, while a higher  $(\Delta\sqrt{G})^2$  and  $\Delta G$  do lead to a higher  $G^*$ , this relationship clearly depends on the  $R$ -ratio. This implies that the material behaviour is driven by the relationship between  $G^*$  and  $G_{\max}$ . There only appears to be a relationship between  $G^*$  and  $(\Delta\sqrt{G})^2$  or  $\Delta G$  because for a given  $R$ -ratio a higher  $(\Delta\sqrt{G})^2$  or  $\Delta G$  also implies a higher  $G_{\max}$ .

The present results can not fully explain why there is a relationship between  $G^*$  and  $G_{\max}$ , however a hypothesis can be attempted. Figure 4.5 shows that a given crack growth increment at a higher maximum load (i.e. higher  $G_{\max}$ ) will result in a larger release of strain energy. The question is, since  $da$  remains the same, how is this extra strain energy dissipated?

It is known that  $G_{\max}$  is correlated to the amount of plasticity surrounding the crack tip. A greater amount of plastic deformation would result in more energy dissipation without necessarily causing crack extension. Therefore a logical hypothesis would seem to be that a higher  $G_{\max}$  leads more plastic deformation, and that this in turn increases the material's resistance to crack growth (i.e.  $G^*$ ).

An interesting feature of the linear relation between  $G^*$  and  $G_{\max}$  is that it does not pass through the origin. Instead for  $G_{\max} = 0$ ,  $G^* = 0.05714$  mJ/mm<sup>2</sup>. This provides a theoretical minimum for the energy required per unit of crack growth in order for the crack to grow. As  $G_{\max}$  increases, so does the amount of energy dissipation required per unit of crack growth. The value of  $G^*$  for  $G_{\max} = 0$  can therefore be regarded as a theoretical minimum value, as it is impossible to create crack growth without dissipating

at least that amount of energy per unit of crack growth. Of course, since crack growth cannot occur for  $G_{\max} = 0$  the actual threshold value is most likely larger.

Although it's tempting to think of this minimum value as the energy purely required for material de-cohesion, it should be noted that the surface energy for a general epoxy is several orders of magnitude lower than the value found here. Typical values for epoxies lie in the range of  $40 - 50 \cdot 10^{-6}$  mJ/mm<sup>2</sup> [20]. The extra energy dissipation here is likely caused by some combination of the ratio of actual to projected surface not being equal to 1, and by damage processes occurring around the crack tip even at very low loads.

It should also be noted that the minimum value discussed here is of course a purely theoretical limit. To actually achieve crack growth with only 0.05714 mJ/mm<sup>2</sup> energy dissipation, one would have to create crack growth with  $G = 0$ , which is not possible in practice. It should also be kept in mind that this minimum value of  $G^*$  applies a threshold to the energy requirement; if not enough energy is supplied, no crack growth will occur. However this does *not* directly translate to a threshold on the applied load. For that the relationship between applied load and available energy needs to be clarified first.

The procedure of extrapolating the  $G^*$  vs  $G_{\max}$  relationship to  $G_{\max} = 0$  can produce a (very) conservative lower bound limit of  $G^*$ . Perhaps in future this can then be translated to a load threshold, if needed for design purposes. This value is likely too conservative for most engineering applications however, as in practice threshold is often defined as the load level that will produce a crack growth rate below some limit (e.g.  $10^{-6}$  mm/cycle), which can be treated as an absence of crack growth over the operational life-time of the structure. This is distinct from the load level that physically produces no crack growth at all.

#### 4.4.2. AVAILABLE ENERGY

The relationship found in figure 4.8 allows one to calculate the resistance to crack growth for a given load cycle, i.e. how much energy must be dissipated per unit of crack growth. The total amount of crack growth that will then occur in that load cycle is governed by the total amount of energy that is available in that cycle. This is demonstrated in figures 4.10 and 4.11, which show the total energy dissipation per cycle  $dU/dN$ , i.e. the total amount of energy available for crack growth, for a fixed value of  $G^*$ . Since  $G^*$  was the same in each case, it follows by the definition given in equation 3.3 that each value of  $dU/dN$  in figures 4.10 and 4.11 corresponds to a unique value of  $da/dN$ . In other words, although the resistance to crack growth ( $G^*$ ) is the same in each case, the crack growth rate is different.

The question then becomes, what determines the amount of energy available in each case? Although the physical mechanisms are not clear, figure 4.10 does show clearly that the amount of energy available is strongly correlated to  $(\Delta\sqrt{G})^2$  (of if one prefers,  $\Delta\sqrt{G}$ ) and/or  $\Delta G$ , and is not correlated with  $G_{\max}$ .

Recently Alderliesten [21, 22] has recommended the use of the cyclic energy  $U_{cyc}$  as the basis for similitude. In that light, it is interesting to redraw figure 4.10 in terms of  $U_{cyc}$  and  $U_{tot}$ . This is done in figure 4.12.

This figure makes it clear that the amount of energy available is quite strongly correlated to  $U_{cyc}$  and somewhat less to  $U_{tot}$ . Figures 4.10 through 4.11 show four possible



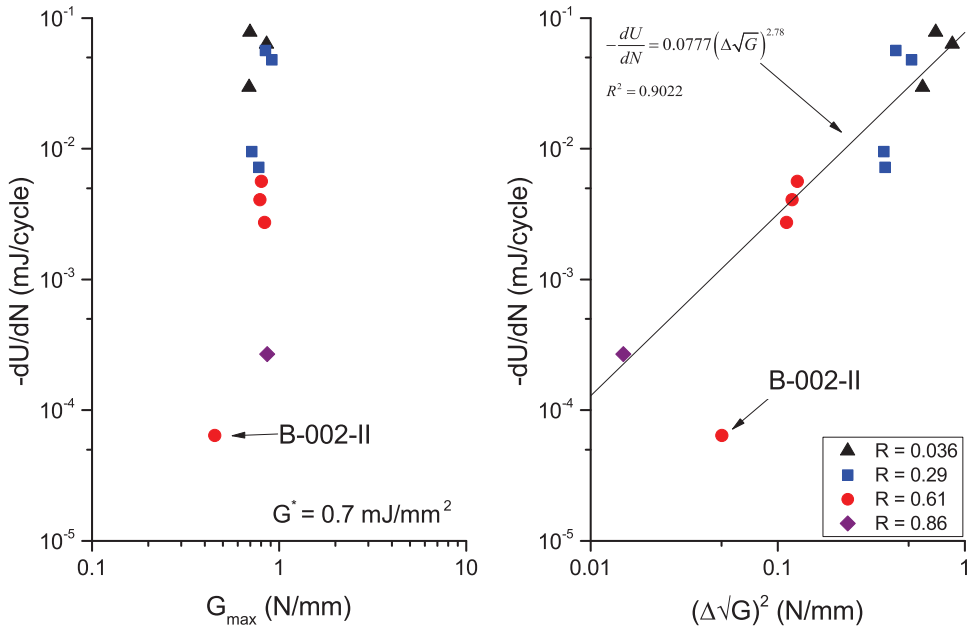


Figure 4.10:  $dU/dN$  as a function of  $G_{\max}$  (left panel) and  $(\Delta\sqrt{G})^2$  (right panel) for a fixed value of  $G^* = 0.7 \text{ mJ/mm}^2$ . The right panel also shows a power-law curve fit. To produce this fit, B-002-II was excluded as an outlier. Note that since  $G^*$  is fixed, each value of  $dU/dN$  corresponds directly to a single  $da/dN$  value.

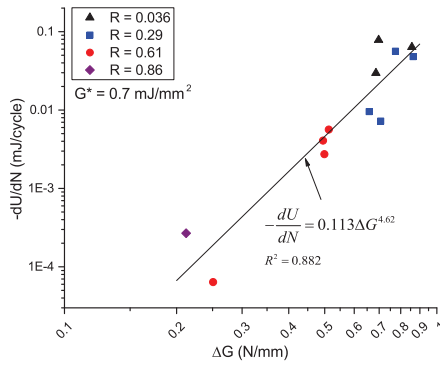


Figure 4.11:  $dU/dN$  as a function of  $\Delta G$  for a fixed value of  $G^* = 0.7 \text{ mJ/mm}^2$ . A power-law fit through the data points is also shown. Note that since  $G^*$  is fixed, each value of  $dU/dN$  corresponds directly to a single  $da/dN$  value.

parameters that are correlated to the amount of available energy:  $(\Delta\sqrt{G})^2$ ,  $\Delta G$ ,  $U_{cyc}$  and  $U_{tot}$ . Based on the data there is no reason to prefer any of them over the others, at least

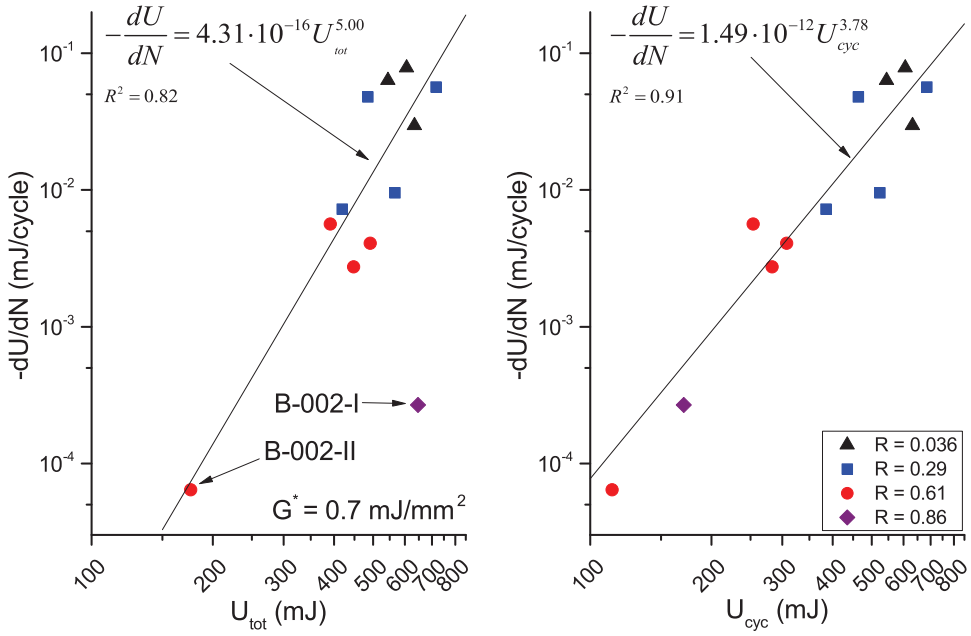


Figure 4.12:  $dU/dN$  as a function of  $U_{tot}$  (left panel) and  $U_{cyc}$  (right panel) for a fixed value of  $G^* = 0.7 \text{ mJ/mm}^2$ . Power-law curve fits are also shown for both cases. For the curve fit as a function of  $U_{tot}$  the data for experiment B-002-I was excluded as an outlier.

when looking for a fixed value of  $G^*$ . The correlation between  $dU/dN$  and  $U_{tot}$  is somewhat lower than for the other parameters, but the difference does not seem large enough to justify any firm conclusions.

Regardless of which similitude parameter is selected, in all cases  $da/dN$  is a power-law function of the selected parameter, with an exponent greater than 1. This means that if  $U_{cyc}$  (or  $\Delta G$ ,  $(\Delta\sqrt{G})^2$ , or  $U_{tot}$ ) is increased, while  $G^*$  is kept fixed, not only is there more work being performed on the specimen, but the fraction of that work that is dissipated also increases. A schematic example of this point using arbitrary units is shown in figure 4.13.

Imagine that for a given  $G^*$  value, a  $U_{cyc}$  of 100 units would result in a dissipation of 10 units of energy, i.e. 10% of  $U_{cyc}$ . If  $U_{cyc}$  is then increased to 200 units, (assuming the exponent found in figure 4.12 is still valid) the dissipation will increase by a factor of  $2^{3.78}$ , to 137 units. This is equal to 69% of the new  $U_{cyc}$  value. Although the units in this case are not representative, the example hopefully makes the point clear: if  $G^*$  is kept fixed, the fraction of the applied work that is dissipated increases if the applied work itself is increased.

No explanation for this observation could be found during the present research. Modelling of the micro-mechanics of crack growth, or some kind of multi-scale approach, may shed more light onto this matter.

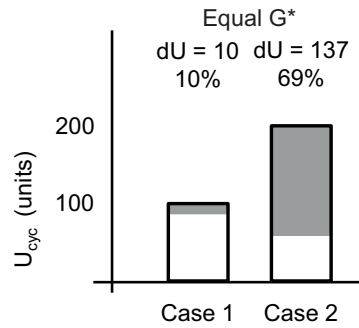


Figure 4.13: Schematic illustration using arbitrary units that at a fixed  $G^*$  the fraction of cyclic work that is dissipated increases if the amount of cyclic work is increased.  $U_{cyc}$  is increased by a factor of 2, and therefore  $dU$  is increased by a factor of  $2^{3.78}$

#### 4.4.3. EXISTENCE OF A FATIGUE THRESHOLD

Figure 4.12 also has some implications for the concept of a fatigue threshold. One might imagine the existence of a certain load level (the fatigue threshold) below which no crack growth occurs. This would imply that only the portion of the load cycle that is above the threshold matters. However, figure 4.12 contradicts this hypothesis. Since figure 4.12 shows data for a fixed  $G^*$  value, and  $G^*$  is related to  $G_{max}$ , this implies that  $G_{max}$  must be the same.

Since  $G_{max}$  is the same, a larger  $U_{cyc}$  can only be created by a reduction in minimum load (hence in figure 4.12 the  $R$ -ratio is lower for higher  $U_{cyc}$ ). If a threshold exists, then at some point the minimum load would be reduced below the threshold level, as shown in figure 4.14. As illustrated in the figure, if only the portion of the load cycle above the threshold value matters for crack growth, then a further reduction of the minimum load (increase of  $U_{cyc}$ ), should not lead to an increase of the amount of available energy.

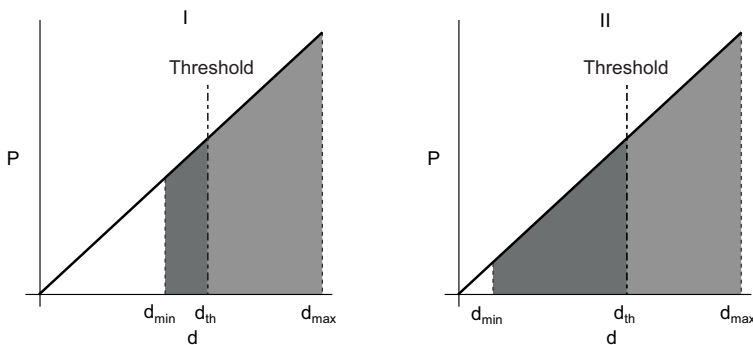


Figure 4.14: Schematic illustration of the implication of figures 4.12 and 4.13 for the concept of a fatigue threshold. If a threshold exists, one would expect that cases I and II would both lead to the same amount of energy available for crack growth, whereas figure 4.12 shows that the amount of energy available is in fact different.

However, figure 4.12 clearly shows that increasing  $U_{cyc}$  always leads to an increase in

the amount of available energy ( $dU/dN$ ), even if the minimum load is reduced all the way to zero. This leaves three possibilities concerning the fatigue threshold.

The first possibility is that there is no threshold at all, which seems impossible based on physical principles. At the very least, the amount of energy required to break a single molecular bond should form a threshold value, even if such a threshold is mainly of theoretical and academic interest.

A second possibility is that a threshold exists, but is very small, so that the effect shown in figure 4.14 would only be visible when comparing two different cycles with minimum loads close to zero in both cases. In section 4.4.1 it was found that the minimum energy required per  $\text{mm}^2$  of crack growth is on the order of 0.06 mJ. However, the smallest possible crack growth increment is much smaller than  $1 \text{ mm}^2$ . If one assumes that the smallest crack growth increment is on the order of the inter-atomic distance in the material, then the minimum amount of required energy, and therefore the threshold, would be very small indeed. For all practical purposes this situation would probably be equivalent to there not being any threshold at all.

The third possibility is that a threshold does exist, but it only applies to the maximum load. If the load never exceeds the threshold, no crack growth occurs. However, if the threshold is exceeded during at least part of the load cycle, then the entire load cycle is relevant to the amount of crack growth. An analogy could be the case of friction: once a certain threshold (the static friction) is overcome and an object is moving, the amount of friction reduces; there is a static and a kinetic friction. In the same way it is possible that there is a 'static' and a 'kinetic' threshold for crack growth. Once the load exceeds the 'static' threshold, crack growth will continue for as long as the load is above a lower 'kinetic' threshold. Although this would match with the findings shown in figure 4.12, it is unclear what underlying physical mechanisms could cause this.

#### 4.4.4. EMPIRICAL PREDICTION APPROACH BASED ON CURRENT FINDINGS

The previous sections have shown that both the crack growth resistance, and the amount of energy available for crack growth, depend on the applied load. The crack growth resistance  $G^*$  can be written as a linear function of  $G_{\max}$ . In contrast, for a fixed  $G^*$  the energy dissipation, and thus also the crack growth rate, can be written as a power-law function of  $(\Delta\sqrt{G})^2$ ,  $\Delta G$ ,  $U_{cyc}$ , or  $U_{tot}$ . In the following,  $(\Delta\sqrt{G})^2$  will be used as an example, but the same procedure can be applied based on  $\Delta G$ ,  $U_{cyc}$ , or  $U_{tot}$ . The relationship between  $(\Delta\sqrt{G})^2$  and  $da/dN$  can be written symbolically as:

$$\frac{da}{dN} = \xi (\Delta\sqrt{G})^\psi \quad (4.5)$$

where  $\xi$  and  $\psi$  are curve fit parameters.

Strictly speaking equation 4.5 is written in terms of  $\Delta\sqrt{G}$ , rather than  $(\Delta\sqrt{G})^2$ , however this merely changes the numerical value of  $\psi$ , which is determined by curve fitting in any case.

The parameters  $\xi$  and  $\psi$  are not constant, but vary with  $G^*$ . Thus by fitting a power-law function through the  $da/dN$  vs  $(\Delta\sqrt{G})^2$  data at different fixed values of  $G^*$ , different values of  $\xi$  and  $\psi$  are obtained. This is shown in figure 4.15.

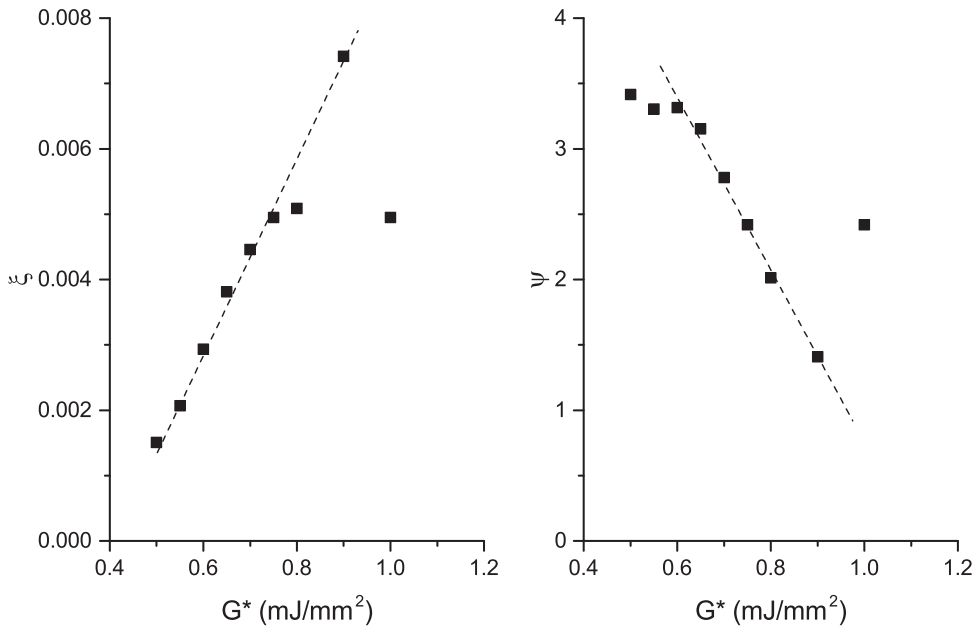


Figure 4.15: Fit parameters  $\xi$  (left panel) and  $\psi$  (right panel) as a function of  $G^*$ . The dashed lines are guides to the eye. The data for experiment B-002-II was excluded as an outlier during the curve fitting procedure used to find  $\xi$  and  $\psi$ .

Before interpreting this figure, the caveat should be noted that each of the experiments discussed in this chapter covered a different range of  $G^*$  values, as can be seen in figure 4.8. Thus in figure 4.15 for each value of  $G^*$  a different set of specimen data was used to find the  $\xi$  and  $\psi$  values. This makes any conclusions somewhat tentative until a more thorough statistical analysis can be done to verify the validity and statistical significance of the determined  $\xi$  and  $\psi$  values. This is also why the dashed lines drawn in figure 4.15 are merely guides to the eye, and not linear fits.

Nevertheless figure 4.15 suggests that there is a relationship between  $G^*$  and both  $\xi$  and  $\psi$ , and in particular, that there exists a linear relationship over a large range of  $G^*$  values. Figure 4.15 also suggests that there is a certain value of  $G^*$  for which  $\psi$  becomes equal to 1. This would imply that at that  $G^*$  value there is a linear relationship between  $da/dN$  and  $\Delta\sqrt{G}$ . However, given that  $G^*$  is continuously changing over the course of a fatigue test, and given the uncertainties regarding the validity of the determined  $\psi$  values, it would seem to be premature to attach any significance to this  $G^*$  value.

With the relationships shown in figure 4.15 it is possible to create an empirical prediction method as follows. First one finds  $G^*$  as a function of  $G_{\max}$  (using e.g. a relationship such as shown in figure 4.8). Then the values of  $\xi$  and  $\psi$  are determined for this value of  $G^*$ . With  $\xi$  and  $\psi$ ,  $da/dN$  can then be determined as a function of  $\Delta\sqrt{G}$ . The

mathematical formulation is thus:

$$G^* = \alpha G_{\max} + \beta \quad (4.6)$$

$$\xi = \kappa_1 G^* + \lambda_1 \quad (4.7)$$

$$\psi = \kappa_2 G^* + \lambda_2 \quad (4.8)$$

$$\frac{da}{dN} = \xi (\Delta\sqrt{G})^\psi \quad (4.9)$$

where  $\alpha$ ,  $\beta$ ,  $\kappa_1$ ,  $\kappa_2$ ,  $\lambda_1$ , and  $\lambda_2$  are curve fit parameters. These equations can be combined to form:

$$\frac{da}{dN} = \kappa_1 \alpha G_{\max} (\Delta\sqrt{G})^{\kappa_2(\alpha G_{\max} + \beta) + \lambda_2} + (\kappa_1 \beta + \lambda_1) (\Delta\sqrt{G})^{\kappa_2(\alpha G_{\max} + \beta) + \lambda_2} \quad (4.10)$$

By implementing equations 4.6 through 4.9 in an iterative procedure the crack growth can be predicted. However, before applying this procedure to a real case, more experimental data and statistical analysis is needed to confirm the validity of the relationships between  $\xi$  and  $G^*$ , and  $\psi$  and  $G^*$ .

As discussed in Chapter 2, previous two-parameter approaches to crack growth have relied either on multiplication of  $G_{\max}$  and  $\Delta\sqrt{G}$ , or on superposition, e.g. [23]:

$$\frac{da}{dN} = C G_{\max}^\gamma (\Delta\sqrt{G})^{1-\gamma} \quad (4.11)$$

or [24]:

$$\frac{da}{dN} = C_1 G_{\max}^{n_1} + C_2 (\Delta\sqrt{G})^{n_2} \quad (4.12)$$

The most important difference between these methods and the approach proposed here, is that in the present approach  $G_{\max}$  is included in the exponent of the power-law relationship. In other words, the previous methods assume a constant relationship between the loading parameters and the crack growth rate; whereas in the present model the relationship is itself a function of the applied load.

However, as with the models already available in literature, the present approach is once again empirical and largely phenomenological. The method does explicitly include both  $G_{\max}$  and  $\Delta\sqrt{G}$ , which can be interpreted as representing the crack growth resistance and the available energy. However, the link to the underlying physics is tenuous at best. In particular, there is no satisfactory explanation for the form of equations 4.5 and 4.10. Why the relationship between  $da/dN$  and  $\Delta\sqrt{G}$  should depend on  $G^*$  in the manner that was found is also not clear. Consequently the method presented in this section should be regarded as a suggested direction for further development, rather than a fully developed prediction approach.

#### 4.4.5. EXPLANATION OF THE $R$ -RATIO EFFECT WHEN USING $\Delta G$ AS A SIMILITUDE PARAMETER

Previously it was mentioned that the  $R$ -ratio effect reported in literature when plotting  $da/dN$  against  $\Delta G$  is somewhat puzzling. As recently pointed out by Jones et al. [3], increasing the  $R$  ratio for a fixed  $\Delta G$  implies an increase of the mean stress. Thus one

would expect an increase in crack growth rate. However, with the data presented in the previous sections, the  $R$ -ratio effect seen when using  $\Delta G$  as a similitude parameter can be explained.

With some algebra (see Appendix B) one can show that if  $\Delta G$  is kept constant, and  $R$  is increased, then  $G_{\max}$  will increase, while  $U_{cyc}$  remains constant. This implies that the resistance  $G^*$  also increases, while the applied work remains constant. In fact, the relationships shown in figure 4.15 show that for increasing  $G^*$ , a given  $U_{cyc}$  will even result in a lower amount of energy available for crack growth.

Thus keeping  $\Delta G$  constant while increasing  $R$ , results in an increase in the crack growth resistance, and a reduction in the energy available for crack growth. It is then no surprise that the crack growth rate will be lower, and the data presented in [3] does in fact make sense.

## 4.5. CRACK GROWTH UNDER QUASI-STATIC LOADING

**C**RACK growth under quasi-static loading is usually treated differently to crack growth under fatigue loading. Under quasi-static load crack growth is usually only assumed to occur if  $G$  exceeds  $G_c$ , whereas under fatigue loading crack growth occurs for  $G_{\max}$  values well below  $G_c$ . This difference in the treatment of crack growth under quasi-static and fatigue loading is somewhat curious. After all, the material cannot see into the future, so any crack growth that occurs during the loading portion of a single fatigue cycle should also occur during quasi-static loading. Any differences between fatigue and quasi-static loading must either be caused by mechanisms that are only triggered for high values of  $G$  (i.e. approaching  $G_c$ ), or by hysteresis during the unloading portion of the fatigue cycle.

Measuring the strain energy dissipation allows a straight-forward comparison between quasi-static and fatigue driven crack growth. This was recently shown by Amaral et al. [12]. They found that for mode I delamination in a CFRP laminate, crack growth under quasi-static loading required more energy per unit of crack growth than under fatigue loading.

In this section data is presented for 5 specimens tested under quasi-static loading (series A in [2]) with an applied displacement rate of 1 mm/min, as described in section 3.4. Figure 4.16 shows the measured SERR as a function of crack length for these specimens. There is an initial peak value, which is most likely caused by needing to initiate a cohesive crack in the adhesive layer, starting from the tape that was placed between the adhesive layer and the adherents as a crack starter. This is shown schematically in figure 4.17. After about 50 mm of crack growth a steady-state condition is reached, where  $G$  remains constant until the crack nears the end of the specimen (i.e.  $a > 270$  mm).

The energy dissipation  $\Delta U$  during the quasi-static tests was calculated according to the method described in section 3.6.3. Figure 4.18 shows the total energy dissipation and the associated crack extension ( $a - a_0$ ) that was measured during the tests, where  $a_0$  is the crack length at the maximum force. There is a linear relationship between ( $a - a_0$ ) and  $\Delta U$ , which implies that the energy dissipation per unit of crack growth was constant during the test. This also suggests that the active mechanisms during quasi-static crack growth are in a kind of 'steady-state' condition. E.g. under quasi-static load the amount of extra plastic deformation caused by an increment of crack growth at a short

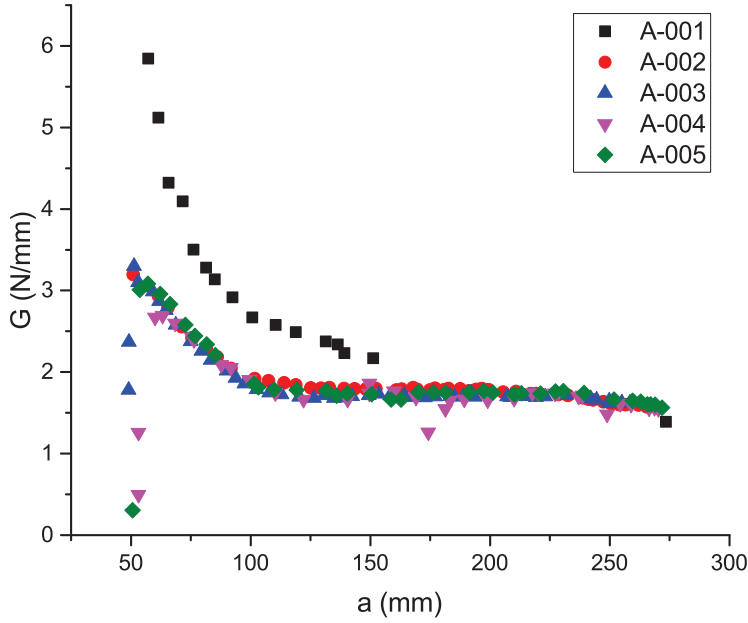


Figure 4.16: SERR as a function of crack length for the quasi-static loading experiments on the series A specimens. The specimens were tested under displacement control with a displacement rate of 1 mm/min. The initial peak value is caused by needing to initiate the cohesive crack in the adhesive layer. The total specimen length was 300 mm, but the crack length is measured from the load application points, which were about 15 mm from the specimen edge. Thus the end of the specimen corresponds to a crack length of about 285 mm.

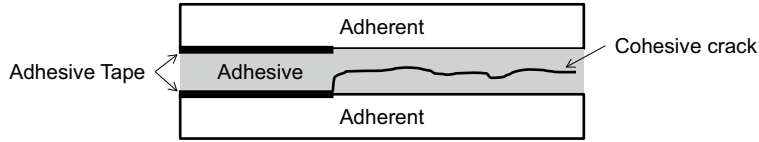


Figure 4.17: Schematic illustration of the cohesive crack initiating from the adhesive tape used as a crack-starter. The figure is not to scale.

crack length is equal to the amount of extra plastic deformation caused by an increment of crack growth at a long crack length. Thus the amount of energy dissipation due to plasticity is the same in both cases.

Another noteworthy feature is that the fit of the  $(a - a_0)$  vs  $\Delta U$  data does not pass through the origin. This can be examined more intuitively by fitting the inverse relationship, i.e.  $\Delta U$  as a function of  $(a - a_0)$ , with a first-order polynomial. This gives:

$$\Delta U = 45.53(a - a_0) + 184.2 \quad (4.13)$$

with an  $R^2$  value of 0.9965 and a root mean square error (RMSE) of 180.1 mJ.

The Matlab *cftool* [25] gives the 95% confidence bounds of the second term in equation 4.13 as 133.6 mJ and 234.8 mJ, so even when taking the scatter bands into account, the  $\Delta U$  vs  $(a - a_0)$  line does not pass through the origin. This implies that even without



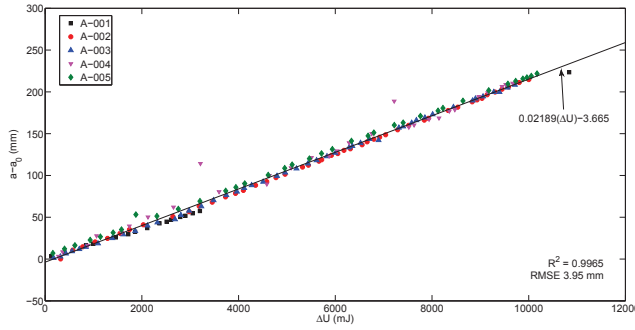


Figure 4.18: Energy dissipation  $\Delta U$  and total crack extension ( $a - a_0$ ) for the quasi-static tests. A linear (first-order polynomial) fit through the data points is also shown.

crack extension there is still energy dissipation. A possible explanation is that the energy dissipation value represents an energy threshold. According to this interpretation, in order to be able to grow the crack under quasi-static conditions (for the present geometry and loading), at least 184 mJ of energy would need to be supplied (taking the mean value for the last term in equation 4.13). If this threshold is not exceeded then there would be no crack growth, or at least not using all the mechanisms that are active during quasi-static growth.

Given that fatigue crack growth was observed to occur for energy dissipation values far below even 1 mJ (see figure 4.3), it seems unlikely that the value of 184 mJ represents a crack growth threshold. A linear fit through the origin gives:

$$\Delta U = 46.57 (a - a_0) \quad (4.14)$$

with  $R^2 = 0.9916$  and  $RMSE = 279.8$  mJ.

It therefore seems premature to conclude there is indeed a threshold for quasi-static crack growth. To resolve this question more data is needed, focussing especially on energy dissipation during short crack growth (i.e. on the order of 0-5 mm) under quasi-static loading. A further recommendation would be to conduct these experiments starting from a sharp cohesive crack in the material.

In figure 4.19 the energy dissipation under quasi-static load is compared with the data from the fatigue tests. The crack growth data for quasi-static crack growth falls slightly above the extrapolation of the fatigue data. This matches the results presented by Amaral et al. [12], if one uses a power-law extrapolation of the fatigue data of Amaral et al., rather than the linear fit that was used in the cited paper.

Another interesting comparison between quasi-static and fatigue crack growth is to examine the  $G_{\max}$  versus  $G^*$  behaviour, which is shown in figure 4.20. For the quasi-static tests,  $G^*$  was calculated as:

$$G_{quasi-static}^* = \frac{\Delta U}{w(a - a_0)} \quad (4.15)$$

For quasi-static growth most of the data points are clustered in the range of  $G_{\max} = 1.6 - 1.8$  N/mm, with some more data points at higher  $G_{\max}$  values. It is clear that for

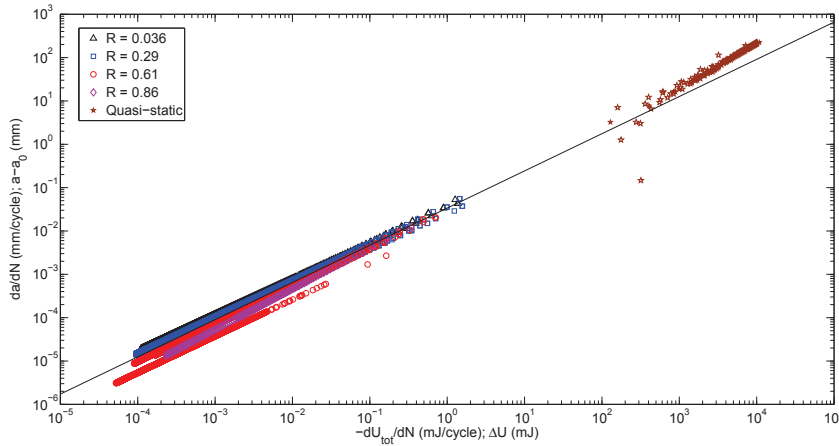


Figure 4.19: Crack growth ( $da/dN$  for the fatigue tests,  $(a - a_0)$  for the quasi-static tests) as a function of energy dissipation ( $dU/dN$  for the fatigue tests,  $\Delta U$  for the quasi-static tests). The solid line is the fit through the fatigue test data, as shown in figure 4.3, so excluding the data for specimen B-002-II.

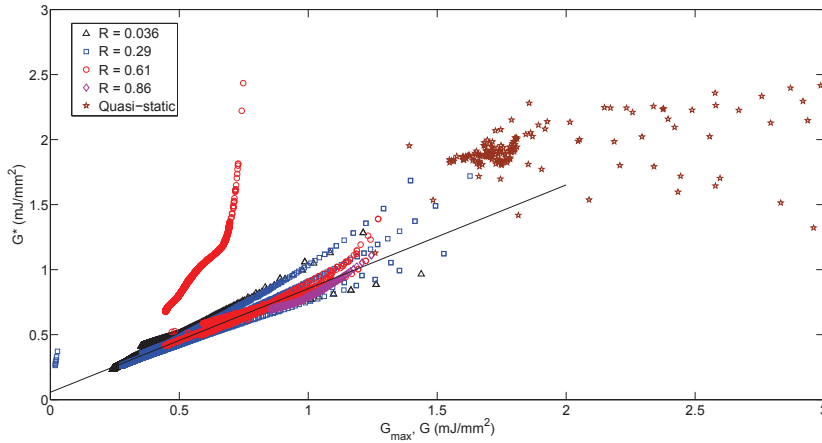


Figure 4.20:  $G^*$  versus  $G_{\max}$  (fatigue) and  $G$  (quasi-static).

quasi-static crack growth the relationship between  $G_{\max}$  and  $G^*$  that was found for fatigue no longer applies. Instead the main cluster of  $G^*$  values for quasi-static growth is higher than what would be expected based on the fatigue behaviour. This suggests that under quasi-static crack growth indeed other dissipative mechanisms are activated, presumably after some  $G$  value threshold is exceeded. As a result the resistance to crack growth under quasi-static loading is higher than under fatigue loading. One could also state that fatigue crack growth is a more efficient process than quasi-static crack growth.

To further investigate the cross-over between fatigue and quasi-static crack growth behaviour more data is needed for the fast fatigue crack growth (i.e.  $da/dN = 0.01 - 1$

mm/cycle) regime. This would fill in the gap in the data between  $G = 1 - 1.5$  N/mm that is visible in figure 4.20. To gather this data the experimental procedure used in this thesis could be applied, starting at a sufficiently high  $G_{\max}$  value (i.e.  $0.9-0.95 G_{\max}$ ). Crack length, force, and displacement should then be measured as frequently as possible for the first 1000-2000 cycles. Preferably there should be a measurement every cycle, rather than every 100 cycles was done here. The curvature of some of the curves in figure 4.20 suggests that there may be a gradual transition between quasi-static and fatigue behaviour, rather than a sharp jump.

Another difference between the fatigue and quasi-static data in figure 4.20 is that there is a clear linear trend for the fatigue data, whereas there is no clear trend for the quasi-static data. The quasi-static data seems to fall within a scatter band that widens as  $G$  increases. Given the definitions of  $G$  and  $G^*$  employed in this thesis one would expect  $G$  and  $G^*$  to be equal for quasi-static growth. Why that is not the case here for the high  $G$  values is unclear, although it may be related to the high  $G$  values corresponding to the initiation of the cohesive crack from the adhesive tape.

In conclusion, the presented data suggests that in quasi-static growth different dissipative mechanisms are active than in fatigue crack growth<sup>4</sup>. This is shown by  $G^*$  being higher for a given value of  $G_{\max}$  than would be expected based on the fatigue behaviour.

## 4.6. FRACTOGRAPHY

**F**RACTOGRAPHY was performed on the specimens in order to gain more insight into the relationships found in the previous section, in particular the relationship between  $G_{\max}$  and  $G^*$ .

After the fatigue tests had been performed, quasi-static loading was applied to completely separate the two arms of all the series E specimens, as well as specimen C-001 and B-002. In all cases adhesive residue was present on both fracture surfaces, indicating crack growth occurred through cohesive failure in the adhesive. Figure 4.21 shows a photograph of the fracture surfaces of the lower arms of the series E specimens. Both fatigue crack growth areas can be clearly identified on each specimen, as can the crack growth caused by the quasi-static loading.

The crack fronts are curved, with the crack length in the middle of the specimen being longer than at the sides (at least at the end of each fatigue test). This has some implications for the calculations discussed in the previous section, as the computation of  $G^*$  implicitly assumes a straight crack front. If the crack front is curved, there will be a greater increase of crack area for the same increase of crack length at the side of the specimen. Thus the true value of  $G^*$  will be lower than the one computed with the assumption of a straight crack front.

Looking at figure 4.21, all specimens appear to have a similar crack front curvature, so it may be assumed that the error in the  $G^*$  computation was more or less the same in all specimens. Nevertheless, differences in the curvature may account for some of the scatter seen in the results. In this thesis the crack growth behaviour was investigated using only one specimen geometry. If tests are being performed in order to support the design

<sup>4</sup>Of course some or all of the mechanisms active during FCG are most likely also still active during quasi-static growth.

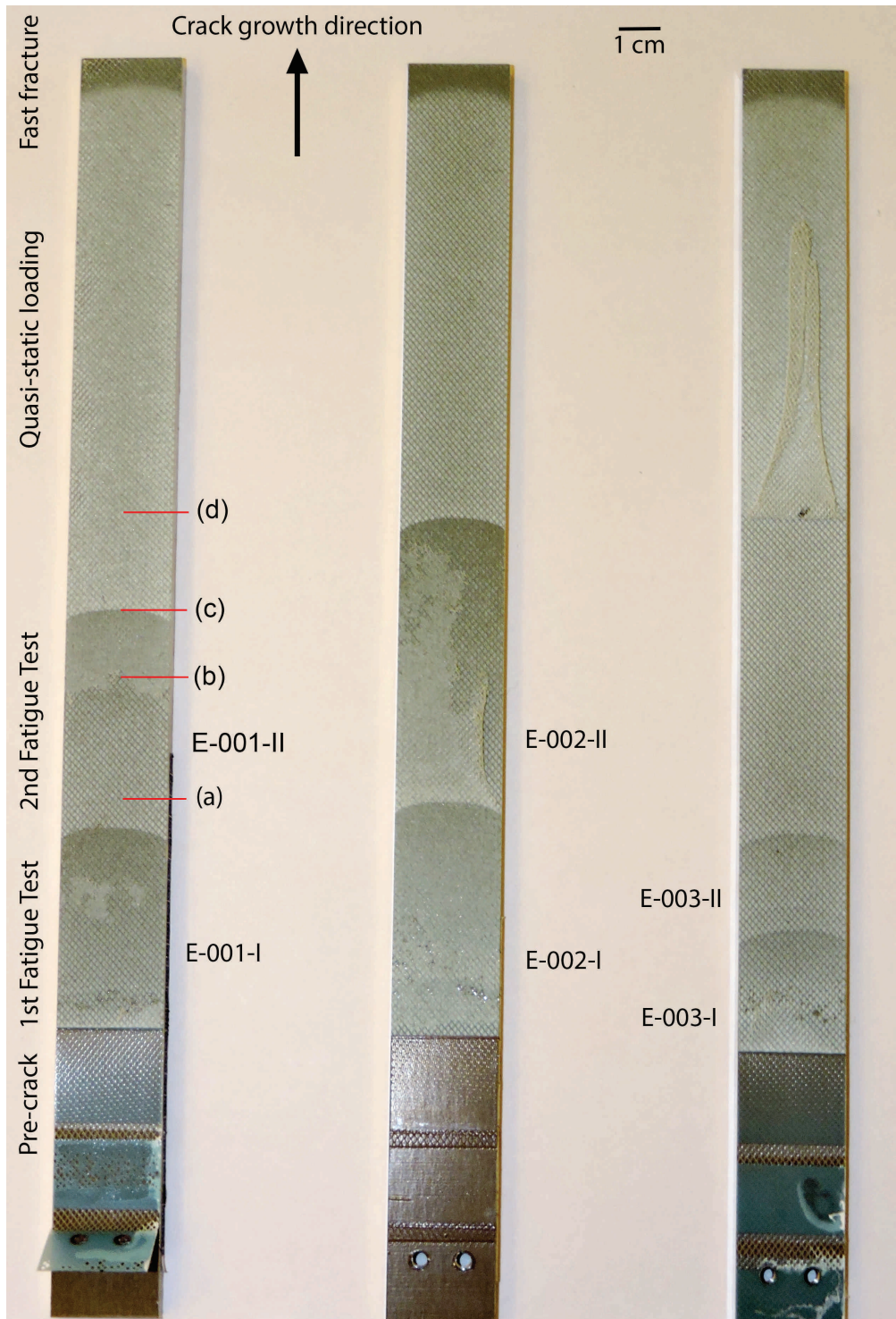


Figure 4.21: Macroscopic view of the fracture surfaces for the lower halves of the series E specimens. Two fatigue tests were performed on each specimen. The associated crack growth areas have been labelled in the figure. After completion of the second fatigue test, quasi-static loading was applied to separate the specimens, resulting in a large area of stable crack growth and a small area of unstable fast fracture. The approximate location of the magnified views shown in figure 4.22 is indicated by the letters in parentheses. The crack growth direction was from the bottom of the picture to the top.

of an actual structure the error introduced by failing to take account of the curvature may be more significant. The amount of crack front curvature in a laboratory specimen will likely be different than in a real structure with a different geometry. Note that the assumption of a straight crack front introduces errors not only into the calculation of  $G^*$ , but also into the calculation of  $G$  [26, 27].

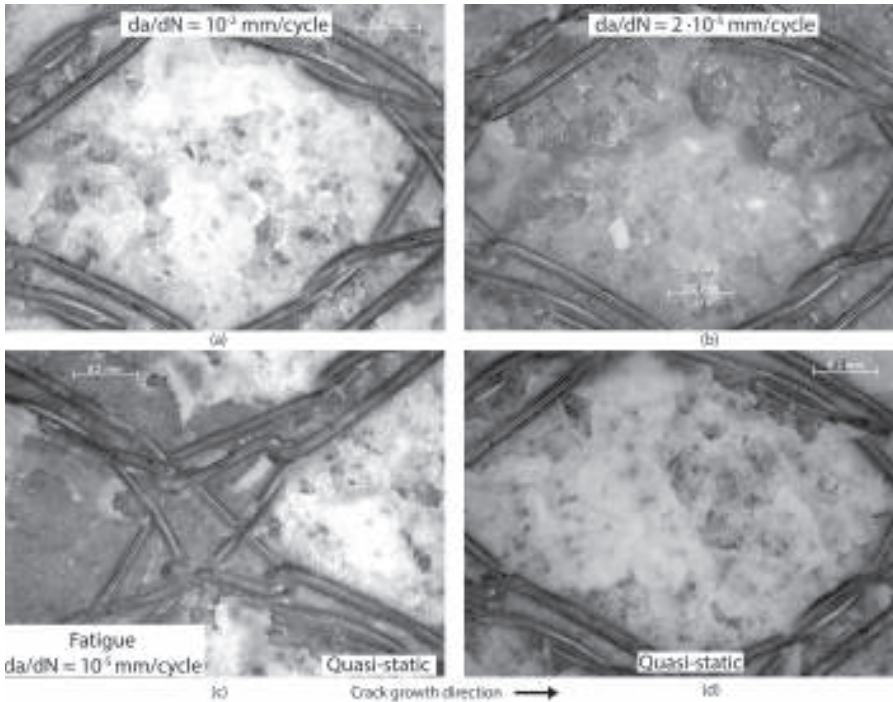


Figure 4.22: Microscopic view of the fracture surface of the upper arm of specimen E-001. The images shown were taken at 4 different locations, corresponding to different crack growth rates and types. Panel (a) shows a fracture surface corresponding to fatigue crack growth at approximately  $10^{-2}$  mm/cycle; panel (b) shows FCG at approximately  $2 \cdot 10^{-5}$  mm/cycle; panel (c) shows the boundary between FCG (at about  $10^{-5}$  mm/cycle) and growth due to quasi-static loading, and panel (d) shows crack growth under quasi-static loading. The approximate location of these images with respect to the entire specimen is shown in figure 4.21. The visible ‘cables’ are the fibres of the adhesive carrier. The contrast of these images has been enhanced, and an unsharp mask filter has been applied.

Figure 4.22 shows a microscopic view of the fracture surfaces on the upper arm of specimen E-001. Based on the location at which the pictures were taken they can each be related approximately to a crack growth rate. The difference between low rate fatigue (i.e.  $da/dN \approx 10^{-5}$  mm/cycle, panels (b) and (c)) and quasi-static crack growth (panel(d)) is clearly visible. At high crack growth rates (panel (a)) the fracture surface looks quite similar to the quasi-static surface (panel (d)). This supports the hypothesis that the transition between FCG and quasi-static crack growth behaviour as  $G$  is increased is a gradual one, as was suggested in the previous section.

The high-rate fatigue and quasi-static surfaces have a lighter colour than the low rate fatigue surfaces. Comparing the low-rate surface and the quasi-static surface in panel



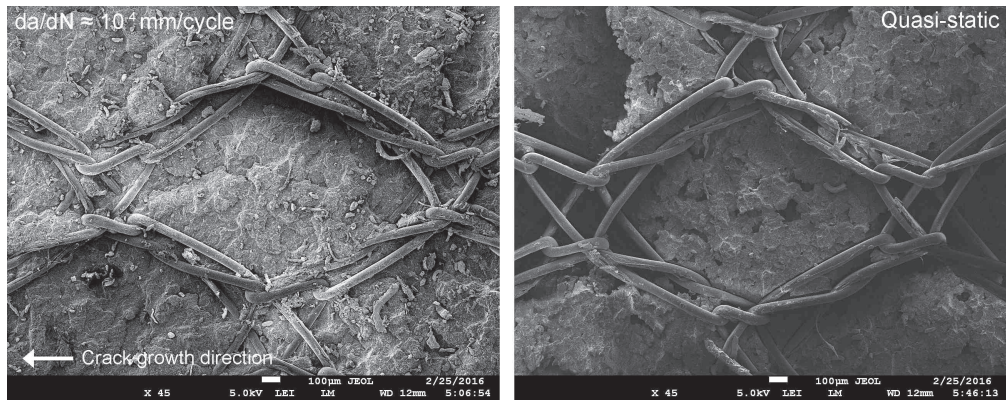


Figure 4.23: SEM image of the fracture surface on the upper arm of specimen E-002 at a magnification of 45X. The left panel corresponds to fatigue crack growth at approximately  $10^{-4}$  mm/cycle, and the right panel corresponds to quasi-static crack growth. The crack growth direction was from right to left. The ‘cables’ visible in the images are the fibres of the adhesive carrier. The contrast of these images has been enhanced and an unsharp mask filter has been applied.

(c), the quasi-static surface is more ‘fluffy’, whereas the fatigue surface is more flat. This difference in surface texture can also be seen when comparing panel (a) and panel (b), albeit not as clearly. This suggests that under high-rate fatigue and especially under quasi-static loading there is more plastic deformation than for low rate FCG. This would require more energy dissipation per unit of crack growth, which matches the observation that  $G^*$  is higher for high-rate FCG than for low-rate FCG. Amaral et al. have reported similar observations for mode I delamination in CFRP [12].

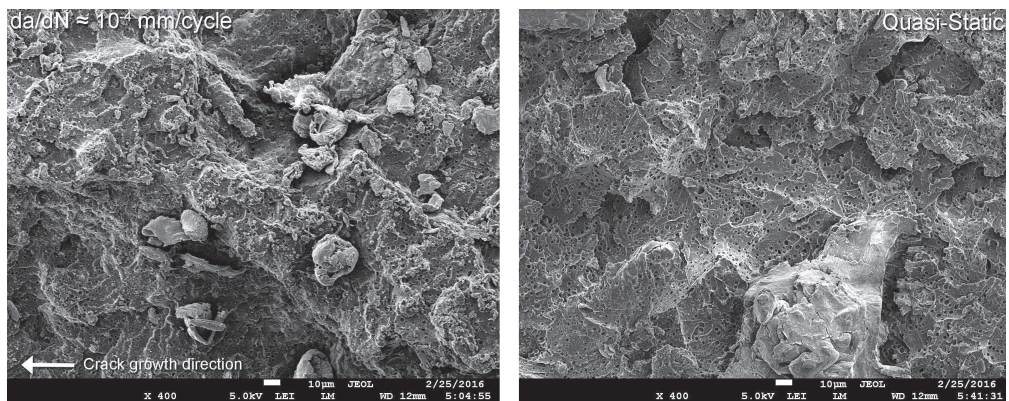


Figure 4.24: SEM image of the fracture surface on the upper arm of specimen E-002 at a magnification of 400X. The left panel corresponds to fatigue crack growth at approximately  $10^{-4}$  mm/cycle, and the right panel corresponds to quasi-static crack growth. The crack growth direction was from right to left. There are many hemispherical imprints visible, which most likely represent areas of adhesive that surrounded toughening particles. The contrast of these images has been enhanced, and an unsharp mask filter has been applied.

Figure 4.23 shows scanning electron microscope (SEM) images of the fracture surface

on the upper arm of specimen E-002. Again the difference between quasi-static and fatigue growth is quite clear. The fatigue surface appears to be flatter, whereas the quasi-static surface is rougher, showing more gaps and height differences. However, at higher magnification the differences between quasi-static and fatigue crack growth disappear, as can be seen in figure 4.24.

At this magnification there are no longer obvious differences between the fatigue and quasi-static crack surfaces themselves. However the fatigue surface does appear to be covered in more debris than the quasi-static surface, perhaps caused by the formation of rollers, or other processes caused by rubbing of the fracture surfaces.

## 4.7. CONCLUSION

The results presented in this section show that the total energy dissipation in a fatigue cycle is very strongly correlated to the crack growth rate in that cycle. This has also been reported for CFRP [12, 28] and aluminium [29]. The concept of crack growth resistance was introduced, which was defined as the amount of energy dissipation per unit of crack growth,  $G^*$ . It was shown that this can readily be calculated from the experimental data, and that  $G^*$  is not constant over the course of a fatigue test.

The conceptual model introduced in Chapter 3 states that the amount of crack growth in a cycle follows from the total amount of available energy, and the amount of energy required per unit of crack growth. In this chapter it was shown that the required energy per unit of crack growth is strongly correlated to  $G_{\max}$ , whereas the available energy is correlated to  $(\Delta\sqrt{G})^2$ ,  $\Delta G$ ,  $U_{\text{tot}}$ , and/or  $U_{\text{cyc}}$ . Fractography suggests that the relationship between  $G_{\max}$  and  $G^*$  may be partially explained by an increase of the amount of plastic deformation around the crack tip. However, more research is required to explain these relationships between the available and required energies and the applied load.

The difference between quasi-static and fatigue crack growth was also examined. The results suggest that under quasi-static loading additional mechanisms are active compared to fatigue loading, and this is also reflected in the different fracture surfaces that are obtained. Under quasi-static loading  $G^*$  is higher than under fatigue loading, which means that the resistance to quasi-static crack growth is higher than the resistance to fatigue crack growth.

## REFERENCES

- [1] J. A. Pascoe, R. C. Alderliesten, and R. Benedictus, *Characterising resistance to fatigue crack growth in adhesive bonds by measuring release of strain energy*, *Procedia Structural Integrity* **2** (ECF 21), 80 (2016).
- [2] J. A. Pascoe, R. C. Alderliesten, and R. Benedictus, *Damage tolerance of adhesive bonds - datasets*, (2014), collection of datasets, available at: <http://dx.doi.org/10.4121/uuid:c43549b8-606e-4540-b75e-235b1e29f81d>.
- [3] R. Jones, A. J. Kinloch, and W. Hu, *Cyclic-fatigue crack growth in composite and adhesively-bonded structures: The FAA slow crack growth approach to certification and the problem of similitude*, *Int J Fatigue* **88**, 10 (2016).

- [4] C. Rans, R. C. Alderliesten, and R. Benedictus, *Misinterpreting the results: How similitude can improve our understanding of fatigue delamination growth*, *Compos Sci Technol* **71**, 230 (2011).
- [5] P. Paris, M. Gomez, and W. Anderson, *A rational analytic theory of fatigue*, *The Trend in Engineering* **13**, 9 (1961).
- [6] P. Paris, *The fracture mechanics approach to fatigue*, in *10th Sagamore Army Materials Research Conference* (Syracuse University Press, 1964) pp. 107–132.
- [7] P. Paris and F. Erdogan, *A critical analysis of crack propagation laws*, *J Basic Eng* **85**, 528 (1963).
- [8] A. Wöhler, *Ueber die Festigkeits-Versuche mit Eisen und Stahl*. *Zeitschrift für Bauwesen* **XX**, 73 (1870).
- [9] L. Yao, R. C. Alderliesten, and R. Benedictus, *Interpreting the stress ratio effect on delamination growth in composite laminates using the concept of fatigue fracture toughness*, *Composites Part A* **78**, 135 (2015).
- [10] W. Ochensberger and O. Kolednik, *A new basis for the application of the J-integral for cyclically loaded cracks in elastic-plastic materials*, *Int J Fract* **189**, 77 (2014).
- [11] W. Ochensberger and O. Kolednik, *Physically appropriate characterization of fatigue crack propagation rate in elastic-plastic materials using the J-integral concept*, *Int J Fract* **192**, 25 (2015).
- [12] L. Amaral, L. Yao, R. Alderliesten, and R. Benedictus, *The relation between the strain energy release in fatigue and quasi-static crack growth*, *Eng Fract Mech* **145**, 86 (2015).
- [13] K. B. Broberg, *Critical review of some theories in fracture mechanics*, *Int J Fract* **4**, 11 (1968).
- [14] K. B. Broberg, *Crack-growth criteria and non-linear fracture mechanics*, *J Mech Phys Solids* **19**, 407 (1971).
- [15] K. B. Broberg, *Discussion of initial and subsequent crack growth*, *Eng Fract Mech* **5**, 1031 (1973).
- [16] K. B. Broberg, *On stable crack growth*, *J Mech Phys Solids* **23**, 215 (1975).
- [17] N. K. Simha, F. D. Fischer, O. Kolednik, and C. R. Chen, *Inhomogeneity effects on the crack driving force in elastic and elastic-plastic materials*, *J Mech Phys Solids* **51**, 209 (2003).
- [18] N. K. Simha, F. D. Fischer, G. X. Shan, C. R. Chen, and O. Kolednik, *J-integral and crack driving force in elastic-plastic materials*, *J Mech Phys Solids* **56**, 2876 (2008).
- [19] H. Andersson, *The steadily growing, elastic-plastic crack tip in a finite element treatment*, *Int J Fract* **9**, 231 (1973).



- [20] Anonymous, *Surface Energy Data for Epoxies and epoxy resins*, Tech. Rep. (Diversified Enterprises, 2009) [http://www.accudynetest.com/polymer\\_surface\\_data/epoxy.pdf](http://www.accudynetest.com/polymer_surface_data/epoxy.pdf) Downloaded on 29 March 2016.
- [21] R. C. Alderliesten, *The explanation of stress ratio effect and crack opening corrections for fatigue crack growth in metallic materials*, Advanced Materials Research **891-892**, 289 (2014).
- [22] R. C. Alderliesten, *How proper similitude can improve our understanding of crack closure and plasticity in fatigue*, Int J Fatigue **82, Part 2**, 263 (2016).
- [23] M. Hojo, K. Tanaka, C. G. Gustafson, and R. Hayashi, *Effect of stress ratio on near-threshold propagation of delamination fatigue cracks in unidirectional CFRP*, Compos Sci Technol **29**, 273 (1987).
- [24] R. Khan, *Delamination Growth in Composites under Fatigue Loading*, Phd thesis, Delft University of Technology (2013), <http://doi.org/10.4233/uuid:dbd8025c-c660-452b-8b0b-391c8ad3a89f>.
- [25] The MathWorks Inc, *MATLAB and Curve Fitting Toolbox Release 2012b*, (2012).
- [26] B. Davidson, *An analytical investigation of delamination front curvature in double cantilever beam specimens*, J Compos Mater **24**, 1124 (1990).
- [27] Z. Jiang, S. Wan, Z. Zhong, S. Li, and K. Shen, *Effect of curved delamination front on mode-I fracture toughness of adhesively bonded joints*, Eng Fract Mech **138**, 73 (2015).
- [28] L. Yao, R. C. Alderliesten, M. Zhao, and R. Benedictus, *Discussion on the use of the strain energy release rate for fatigue delamination characterization*, Composites Part A **66**, 65 (2014).
- [29] D. Pasman, *Fatigue crack growth in solid round metallic bars with a shoulder fillet* (Delft University of Technology, Delft, 2015) MSc thesis.



# 5

## EFFECT OF THICKNESS

*Young man, the games we play are lessons we learn. The assumptions we make, things we ignore and things we change make us what we become.*

Terry Pratchett, *Dodger*

*In the previous chapter it was shown that the energy dissipation per unit of crack growth was not constant, but was strongly correlated to the  $G_{\max}$  value. It was hypothesised that this was due to  $G_{\max}$  describing the amount of plasticity at the crack tip. In order to test this hypothesis specimens with varying adhesive thicknesses were prepared, in order to obtain different amounts of plasticity for the same far-field loading.*

*Post-hoc numerical analysis by Zavatta [1] showed that the amount of plasticity generated did in fact not change for the range of thicknesses studied. This fits with the observation that the  $G^*$  vs  $G_{\max}$  relationship was not affected by adhesive thickness. However, the relationship between  $dU/dN$  and  $U_{cyc}$  was strongly affected by the adhesive thickness.*

*These results indicate that the adhesive thickness does not influence the material resistance to crack growth (in terms of energy dissipation per unit of crack growth at a given load), but does influence the amount of energy available for a given applied load cycle.*

---

The experimental work was carried out by N. Zavatta, as a part of his MSc thesis under the author's supervision [1]

## 5.1. INTRODUCTION

THE results in the previous chapter show that the energy required per unit of crack growth is not constant. A higher crack growth rate is correlated with a higher  $G^*$ , as is a higher  $G_{\max}$ . It was thought that these observations could perhaps be (partially) explained by differing amounts of plasticity around the crack tip.

In order to investigate this further it was decided to perform fatigue tests on specimens with different bond-line thicknesses. By varying the adhesive thickness, the constraint on the crack tip is modified, allowing different plastic zones to be created for the same far-field loading condition.

The effect of adhesive layer thickness has been investigated in a number of previous studies [2–11]. In general, it was concluded that greater adhesive thickness results in less constraint. This then results in larger plastic deformations and consequently lower crack growth rates. An exception was the work of Chai [4] who investigated the brittle epoxies Namco 2808 and Hercules 3502, and the tough thermoplastic PEEK (polyether ether ketone). The brittle epoxies exhibited an increased fracture toughness for increasing thickness. However in the case of PEEK the fracture toughness first decreased with increasing thickness, up to a thickness of 0.038 mm. At thicknesses above this value the fracture toughness again increased for increasing thickness. The changes in fracture toughness corresponded to changes in the fracture surface, implying that the failure mechanisms were not constant, although there was cohesive failure in all cases.

Another work that is of interest is that of Wilson [11]. Wilson investigated the effect of the thickness of adhesive layers added between the glass-fibre pre-preg and aluminium layers in a Glare fibre metal laminate (FML). Laminates were made with different adhesive thicknesses and the growth rate of delaminations between the glass-fibre / adhesive and metal layers was measured. The conclusion of this work was that addition of a thin adhesive layer (0.06 mm) resulted in a large reduction of the delamination growth. Application of thicker layers resulted in a further reduction of the delamination growth rate, but to a much lesser extent. Increasing the adhesive thickness from 0.24 mm to 0.36 mm produced no further reduction of the delamination growth rate (although in both cases the growth rate was far below the value for standard Glare). Wilson suggested this was due to the initial addition of an adhesive layer moving the locus of failure from the metal – pre-preg interface, to the stronger pre-preg – adhesive interface. Further increasing the thickness then slightly strengthened the pre-preg – adhesive interface, but the effect on the crack growth rate was much smaller than the initial shift of failure locus.

Compared to the literature, except for the works of Chai [4] and Wilson [11], the results discussed in this chapter deal with lower thicknesses (here up to about 0.3 mm, whereas literature reports on thicknesses up to several millimetres). Although Wilson also investigated FM-94 epoxy, Wilson examined mode II loading, whereas the present research only examined the effect of mode I loading.

## 5.2. SPECIMENS AND TEST SET-UP

IN order to manufacture specimens with varying thicknesses the manufacturing procedure described in chapter 3 needed to be adjusted. Results of three different types of specimens are compared in this chapter.

Type I specimens contained 1 layer of adhesive film, these are the series A through E specimens discussed in the previous chapter, and manufactured according to the procedure in chapter 3. Type II specimens contained 2 layers of adhesive film. These are the series G specimens. They were manufactured following the procedure of chapter 3, but two layers of adhesive film were placed between the aluminium plates, rather than just one layer of film. Thus the type II specimens also contained two carrier mats (one per layer). The type III specimens were coded series H and contained ‘1.5 layers’ of adhesive. This was achieved by placing one layer of adhesive film with carrier between the aluminium plates, and then adding strips of FM94-U-06 carrier-less adhesive film over approximately half the mating surface area, as shown in figure 5.1.

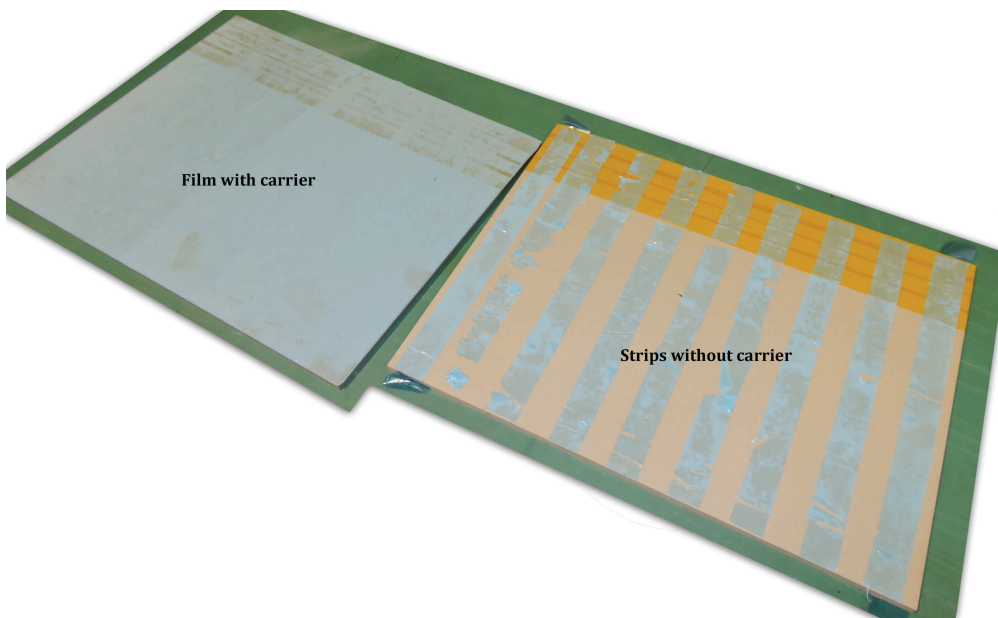


Figure 5.1: Manufacturing of the ‘1.5 layer’ specimens. The plate on the left is entirely covered by a sheet of epoxy film, the plate on the right is covered with strips of adhesive over approximately half its surface area. The plates were then placed on top of each other, with the adhesive in the middle of the resulting stack.

During curing the adhesive without carrier flows, resulting in a bond-line thickness somewhere between that of the type I and type II specimens. Due to the lack of a carrier the thickness cannot be accurately controlled. However, the main point of this series of experiments was to try to relate any differences in crack growth to the adhesive thickness. Since the adhesive thickness was measured for each specimen individually, it was thought that small variations in the adhesive thickness from specimen to specimen would not affect the ability to find a relationship between adhesive thickness and crack growth behaviour.

After manufacturing the adhesive thickness of each specimen was measured using an optical microscope aimed at the side of the specimen. The measured thickness values are shown in table 5.1. For the standard thickness specimens (i.e. type I / series A-E) only two thickness measurements were available, giving a mean thickness value of 0.08 mm.

Table 5.1: Adhesive thickness at the mid-point of the specimen, measured using an optical microscope aimed at the side of the specimen [1].

Specimen	Thickness (mm)
G-002 (2 adhesive layers)	$0.275 \pm 0.015$
G-006	$0.275 \pm 0.005$
G-008	$0.275 \pm 0.005$
G-009	$0.265 \pm 0.015$
G-010	$0.285 \pm 0.005$
H-002 (1.5 adhesive layers)	$0.195 \pm 0.005$
H-003	$0.135 \pm 0.005$
H-006	$0.220 \pm 0.010$
H-008	$0.210 \pm 0.010$

## 5

The fatigue tests were conducted according to the methodology described in chapter 3, at displacement ratios ( $R_d$ ) of 0.036, 0.29, 0.61, and 0.86. The resulting  $R_p$  values are reported in table A.2. Due to the low amount of crack growth for the specimens tested at  $R_d = 0.86$  (G-010-I and H-008-I) the crack growth rate could not be properly determined. Consequently, these experiments were excluded from further analysis.

The experimental data is available from 4TU.ResearchData [12].

### 5.3. RESULTS AND DISCUSSION

PLOTTING  $da/dN$  against  $G_{\max}$  in the traditional manner gives figure 5.2. The phenomenon that different  $da/dN$  vs  $G_{\max}$  curves are obtained for different  $R$ -ratios is also seen for the increased thickness specimens. For  $R = 0.036$  and  $R = 0.61$  the increased thickness specimens have a higher crack growth rate at a given  $G_{\max}$  than the standard thickness specimens. For  $R = 0.29$ , different behaviour is seen. The 1.5 layer specimen still has an increased crack growth rate compared to the standard thickness specimens. However the crack growth rate for the 2 layer specimen is lower than for the standard thickness specimen. Overall it seems safe to say that in general using an increased adhesive thickness will result in a faster crack growth rate, but this effect may be counteracted by material scatter.

In his study of the thickness effect on delamination growth Wilson [11] found an asymptotic decrease of the crack growth rate for an increasing thickness. In the present work however, no particular relationship between adhesive thickness and crack growth rate could be found. At  $R = 0.036$  the relationship between thickness and crack growth rate is monotonic, but for  $R = 0.29$  the crack growth rate for the 2 layer specimen is lower than for the 1.5 layer specimen. At  $R = 0.61$  one 2 layer specimen showed a faster crack growth rate than the 1.5 layer specimen, whereas the other showed a slower crack growth rate. Therefore before a quantitative relationship between the thickness and the crack growth rate can be found, more experiments need to be done in order to understand the amount of scatter in the results.

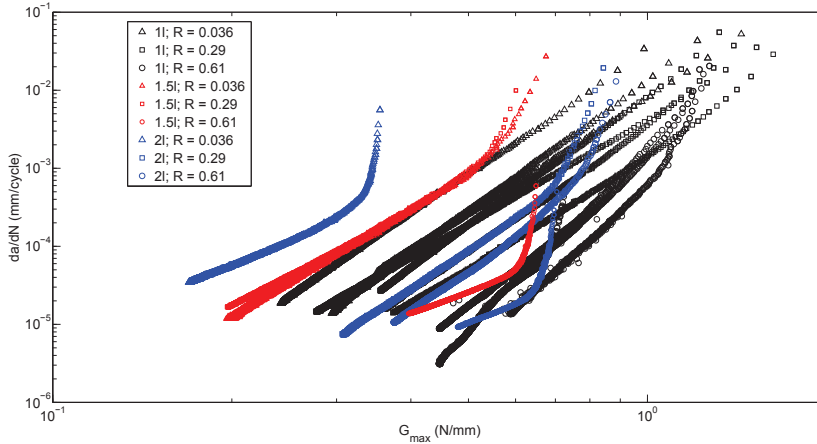


Figure 5.2: Crack growth rate as a function of maximum SERR. The correlation between  $G_{\max}$  and  $da/dN$  is for different  $R$  ratios and also for different thicknesses.

Another striking difference between the present results and those of Wilson, is that the present results show an increase of the crack growth rate for an increasing thickness, whereas Wilson found a decrease. As Wilson tested the same material over a similar range of thicknesses, the most likely explanation of the difference in crack growth behaviour is the difference in loading mode. Wilson tested crack growth under mode II loading, whereas in this thesis only mode I loading was investigated. Further micro-mechanical analysis is required to explain why different loading modes result in different thickness effects.

In the literature it is usually reported that even under mode I the crack growth rate is slower for greater adhesive thickness. The most likely explanation for this difference is the range of thicknesses examined. The maximum thickness here was smaller than 0.3 mm, whereas in the literature thicknesses on the order of several millimetres are examined. Indeed, as will be discussed below in greater detail, numerical modelling suggests that for the range of adhesive thicknesses examined here, the plastic zone size does not change. In the literature changes in plastic zone size due to different amounts of constraint are usually identified as the mechanism causing an effect of thickness on crack growth rate. That the plastic zone size here does not seem to change, may therefore explain why the effect of the thickness on the growth rate was different.

The crack growth rate as a function of energy dissipation is shown in figure 5.3. As before the curves collapse into a narrow band, with 4 exceptions: B-002-II (1 adhesive layer;  $R = 0.61$ ), H-006-I (1.5 layers;  $R = 0.61$ ), G-006-III (2 layers;  $R = 0.036$ ), and G-008-I (2 layers;  $R = 0.61$ ). Whereas for experiment B-002-II the slope of the  $da/dN$  versus  $dU/dN$  line seems to match that of the bulk of the data, the lines for H-006-I, G-006-III and G-008-I are both rotated and translated with respect to the rest of the data. H-006-I and G-008-I in particular show a large difference compared to the other data, having a crack growth rate that is up to two orders of magnitude lower than that of the other specimens at the high end of the  $dU/dN$  range.

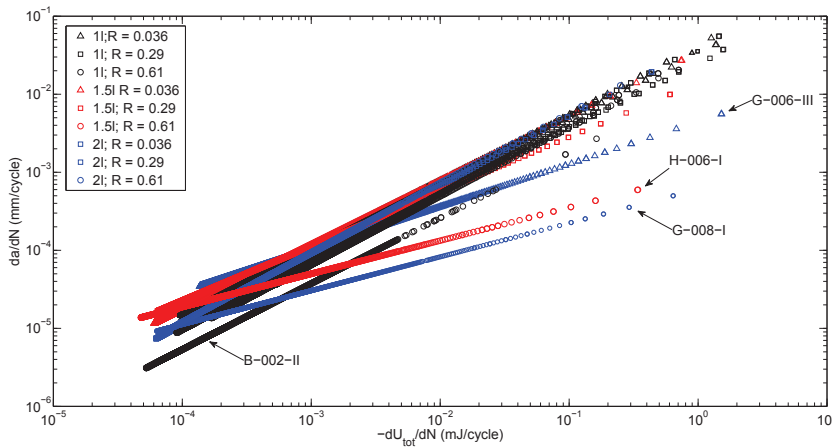


Figure 5.3: Crack growth rate as a function of strain energy dissipation.

5

This anomaly can potentially be explained by the observed crack growth behaviour. For both H-006-I and G-008-I secondary cracks were observed to be growing along the adhesive / adherend interface, as shown in figure 5.4. The secondary cracks start from downward kinks in the main crack and then progress towards and along the adhesive / adherend interface, as shown schematically in figure 5.5. The growth of these cracks will cause energy dissipation, without contributing to the advance of the main crack. Thus the secondary cracks can perhaps explain the much higher rates of energy dissipation per unit of crack growth seen for specimens H-006-I and G-008-I.

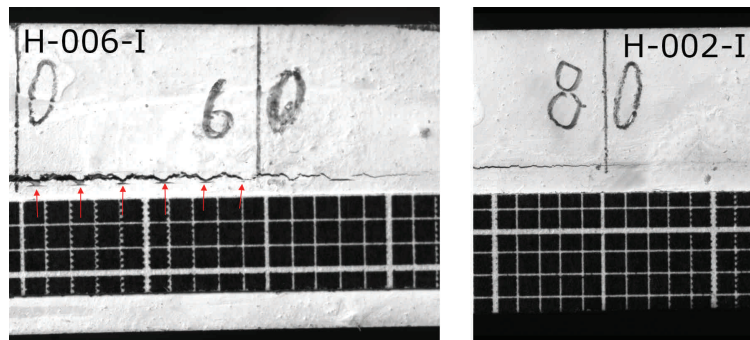


Figure 5.4: Photographs showing secondary cracks (during experiment H-006-I, left panel) and normal crack growth (during experiment H-002-I, right panel). The arrows mark the location of the secondary cracks. Note that secondary crack growth only appears to have occurred during the early (high rate) crack growth. Figure 5.5 shows how 'secondary crack' has been defined in this case.

However, the crack growth rates for these two specimens are up to two orders of magnitude below the other data for a given  $dU/dN$  value. Based on the photographs such as shown in figure 5.4, it seems the secondary cracks create at most an amount of fracture surface equal to that of the main crack. Thus the large difference in crack growth rates



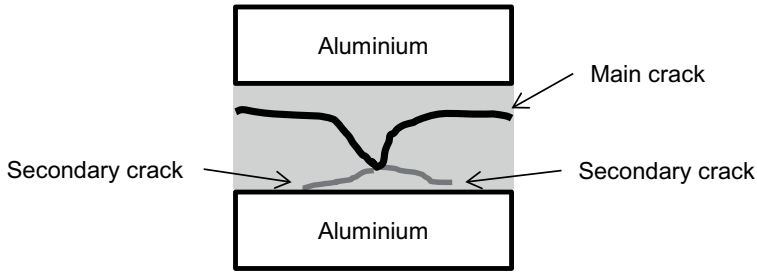


Figure 5.5: Schematic representation of the main and secondary cracks visible in figure 5.4. The figure is not to scale.

seen for specimens H-006-I and G-008-I, compared to the average behaviour, can only be explained by the secondary cracks if these also cause an additional shielding effect. Beyond merely changing the amount of fracture surface corresponding to a given  $da/dN$ , the secondary cracks must also cause an increase in the energy dissipation per unit of actual crack surface, in order to create the effect that is seen.

For experiments B-002-II and G-006-III the reason for the anomalous behaviour is unclear. No secondary crack growth was seen for these specimens. However it should be noted that the difference in crack growth rates between these specimens and the average behaviour is much smaller than for H-006-I and G-008-I. This is particularly true for experiment B-002-II, which has the same slope as most of the other experiments, but is translated towards lower crack growth rates for a given energy dissipation.

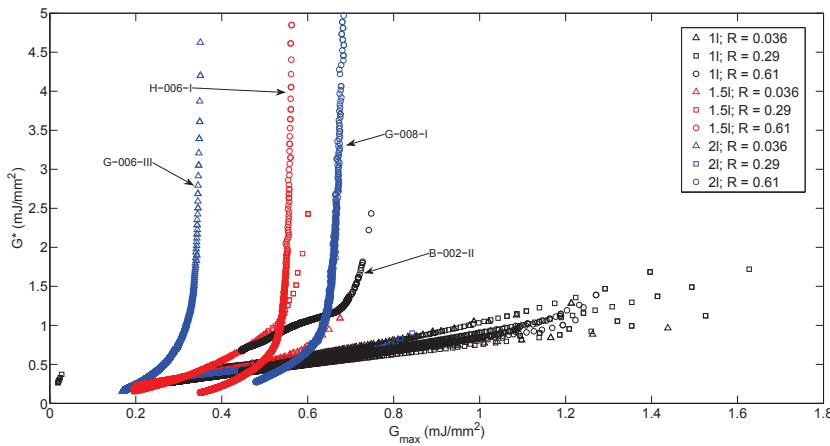


Figure 5.6:  $G^*$  as a function of  $G_{\max}$ . Note that the curves for H-006-I, G-006-III, and G-008-I continue beyond the maximum y-axis value shown. The graphs that were noted as outliers in figure 5.3 are also outliers here.

Figure 5.3 does not show any particular effect of thickness. However some differences can be seen if one considers  $G^*$  as a function of  $G_{\max}$ . This is shown in figure 5.6. It can be seen that the increased thickness curves (red & blue) continue down to

lower  $G_{\max}$  values than the 1 adhesive layer specimen curves (black). From this figure it is clear that the adhesive thickness as such does not modify the correlation between  $G^*$  and  $G_{\max}$ , unless new mechanisms such as secondary crack growth are activated. However, if such mechanisms are activated, then the correlation changes drastically. This leads to the conclusion that any correlation between  $G^*$  and  $G_{\max}$  that is established is only valid as long as no new dissipative mechanisms are activated. In other words, the adhesive thickness does not affect the resistance to crack growth, unless new dissipative mechanisms are activated. In practical situations, if an energy based approach is being relied upon, it is therefore necessary to check whether the dissipative mechanisms remain the same or not.

This conclusion is further reinforced by figure 5.7, which shows energy dissipation as a function of  $G_{\max}$  for a fixed crack growth rate of  $10^{-4}$  mm/cycle. The results for the increased thickness specimens fall along the linear trend of the 1 adhesive layer results.

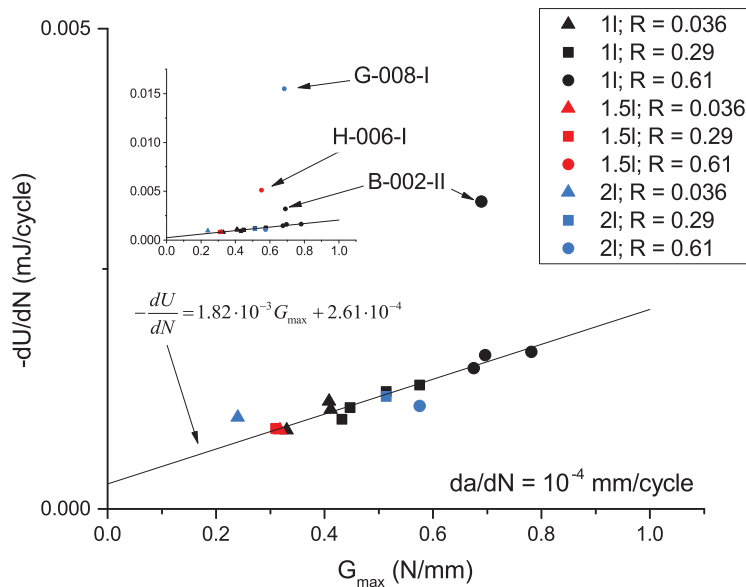


Figure 5.7: Energy dissipation as a function of  $G_{\max}$  for  $10^{-4}$  mm/cycle. The solid line shows a linear fit through the 1 adhesive layer specimen results, excluding experiment B-002-II.

Again the experiments noted before as outliers form an exception to the rule. Especially for H-006-I (1.5 layers,  $R=0.61$ ) and G-008-I (2 layers,  $R = 0.61$ ) far more energy is required to produce  $10^{-4}$  mm crack growth than for the other specimens. However although the energy required is much higher than for the other specimens, the applied load (in terms of  $G_{\max}$  and  $R$ ) is roughly the same, or perhaps slightly lower than for the specimens that do follow the normal trend. This implies that although the load was the same, more energy was released in this case.

This can be seen even more clearly in figure 5.8, which shows  $dU/dN$  as a function of  $U_{cyc}$ . It is clear that the 1.5 and 2 adhesive layer specimens follow a different trend than the 1 layer specimens. For a given cyclic work value, the amount of energy dissipated by

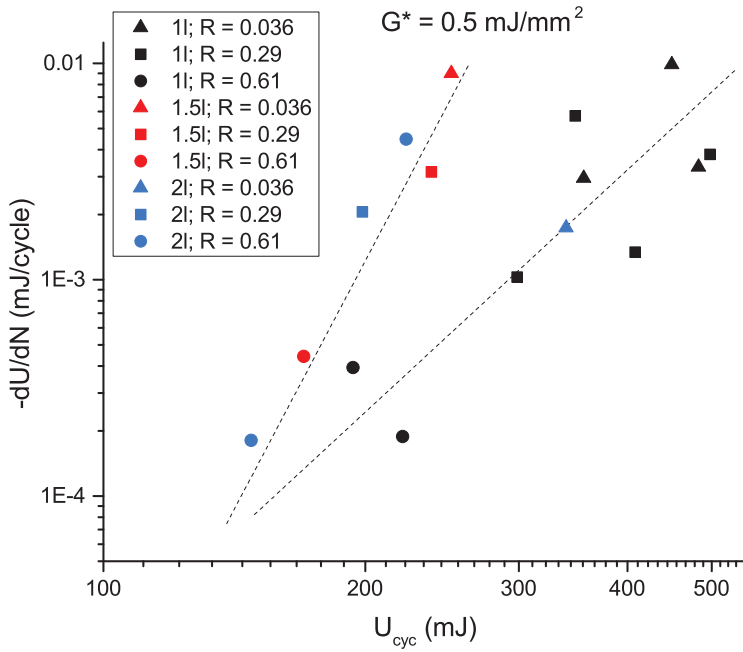


Figure 5.8: Energy dissipation as a function of  $U_{cyc}$  for  $G^* = 0.5 \text{ mJ/mm}^2$ . The dashed lines are guides to the eye, indicating the different behaviour of the 1 adhesive layer specimens compared to the 1.5 and 2 adhesive layer specimens.

the increased thickness specimens is far higher than for the 1 layer specimens. As  $G^*$  is the same for all data points in figure 5.8, this also corresponds to a much higher crack growth rate.

From figures 5.6 and 5.8 one can thus conclude that as long as no new dissipative mechanisms are activated, the adhesive thickness does not influence the relationship between  $G^*$  and  $G_{max}$ , but does change the relationship between  $dU/dN$  and  $U_{cyc}$ . In other words, the adhesive thickness does not affect the crack growth resistance, but does affect the amount of energy available for crack growth, for a given load cycle. Comparing a ‘thin’ and a ‘thick’ specimen, the same  $G_{max}$  value will lead to the same  $G^*$  value in both cases. However, for a given  $G^*$  the amount of energy available for a given  $U_{cyc}$  will be higher for a thick specimen and thus the crack growth rate will also be higher. The thickness is not affecting the material resistance, but is affecting the relationship between the far-field applied load and the crack driving force.

As discussed in chapter 4 the exact mechanisms determining the relationship between available and required energy on the one hand and the applied load on the other are unclear. However it seems likely that the stress distribution and plastic deformation at the crack tip play a role. The effect of adhesive thickness on the crack-tip stress distribution and plastic zone were investigated numerically by Zavatta [1].

Zavatta employed FEM and cohesive zone modelling to create a 2D model of the DCB specimens. In Zavatta’s model the two arms of the DCB specimen are joined via a cohesive zone. In each arm, the aluminium and adhesive are modelled separately. The model

was meshed using quadrangular elements. The mesh elements used in the adhesive layers were smaller than those used in the aluminium layers, and thus surface-based tie constraints were used to join the various parts of the model together. For further details on the model, the reader is referred to [1].

A quasi-static test was simulated, with displacement increasing up to a final value of 15 mm. This was done for two adhesive thicknesses, corresponding to 1.5 and 2 adhesive layers. The  $G_c$  used in the numerical simulations was tuned so that the final crack length obtained during the numerical simulation matched the crack length that was obtained experimentally during a quasi-static test. This meant that a value of  $G_c = 2.5$  N/mm was used for the simulations, rather than the value of  $G_c = 1.7$  N/mm which had been determined experimentally.

Zavatta reported on the stress field around the crack tip after the final crack length had been obtained, as well as the plastic energy dissipation. He found that an increase in thickness led to a slight reduction in the stress at the crack-tip. The plastic zone length remained the same, but due to the greater thickness the total plastic zone volume was increased. Due to combination of an increase in plastic zone volume, but a decrease in the amount of plastic strain within that volume, the amount of energy dissipated by plasticity did not depend on the adhesive thickness.

These results are somewhat difficult to reconcile with the experimental results. Per figure 5.8 one would expect more energy dissipation for an increased thickness. However there are two important caveats concerning Zavatta's results. First of all Zavatta's calculations were performed for the case of crack growth under quasi-static loading, so it is not entirely clear to what extent these results apply to FCG. Secondly Zavatta only modelled the 1.5 layer and 2 layer adhesive thicknesses. It can be seen in figure 5.8 that the difference between the 1.5 and 2 layer specimens mutually, in terms of  $dU/dN$  vs  $U_{cyc}$  behaviour, is much smaller than the difference between the increased thickness specimens and the regular specimens. The 1.5 and 2 layer specimen data appears to fall along the same trend line, whereas the standard thickness data clearly follows a different trend.

The fact that a  $G_c$  of 2.5 N/mm was required in the model to match the experimental crack length at the right force and displacement, whereas the experimentally determined  $G_c$  value was only 1.7 N/mm, also implies that the model does not fully capture all the applicable physical mechanisms.

The decrease of crack growth rate for increasing adhesive thickness reported in literature is ascribed to greater amounts of plasticity for greater thickness. However Zavatta's results here show that increasing the thickness from that of the 1.5 layer specimens to that of the 2 layer specimens has only a negligible effect on the amount of plastic energy dissipation. This explains the similarity in the 1.5 and 2 layer results seen in figure 5.8. However, it does not explain why the increased thickness specimens had a higher crack growth rate than the standard thickness specimens, despite what would be expected based on the literature.

It would seem that the results seen here differ from those in literature due to the much lower thicknesses examined here. It is possible that at this range of thicknesses the constraint imposed by the aluminium arms limits any thickness effect. Therefore it is also to be expected that the behaviours described here apply only to a limited range of adhesive thickness. In the case of Wilson's experiments the thickness was in the same

range, but there was a shift of failure locus, which did not occur here.

## 5.4. CRACK GROWTH IN GLASS-FIBRE COMPOSITES

THE limiting case for adhesive thickness is a fibre reinforced polymer laminate. In that case there is no longer an adhesive layer, but at most a resin rich layer between two laminae. Thus interlaminar crack growth (i.e. delamination) in such a laminate makes an interesting case study to examine the effect of adhesive thickness. Two research projects on crack growth in GFRP laminates were therefore conducted under supervision of the author.

In both cases crack growth was examined in GFRP laminates consisting of S2 glass fibres with FM94 as the matrix material. De Jong and van den Hoogenband [13] investigated crack growth under quasi-static loading, and Al Amery [14] studied FCG. As the 'adhesive' was the same material studied for the rest of this thesis, any differences in behaviour can be considered to be due to geometrical effects, rather than material differences.

Two different lay-ups were tested, in both cases with the crack occurring in the mid-plane of the laminate. In the first laminate type the crack was between two 0° layers (referred to as 0//0), and in the second laminate type the crack was between a -45° and a +45° layer (referred to as -45//+45). The full lay-ups are given in [14].

### 5.4.1. QUASI-STATIC CRACK GROWTH

Quasi-static crack growth was examined by de Jong and van den Hoogenband [13]. Figure 5.9 shows the amount of crack growth versus the dissipated energy. It includes quasi-static and fatigue results for both the single adhesive layer adhesive bond specimens and the GFRP specimens. The fatigue data for the GFRP specimens was taken from the work of Al Amery [14] and is discussed in the next section.

When compared to the trend of the adhesive joint specimens, both the quasi-static data for the glass fibre specimens and the quasi-static data for the adhesive bond specimens fall below a linear extrapolation of the fatigue crack growth data. This indicates that under quasi-static there is more energy dissipation per unit of crack growth than under fatigue loading, as has previously been found for CFRP specimens [15].

### 5.4.2. FATIGUE CRACK GROWTH

Al Amery [14] performed fatigue tests at  $R_d = 0.01, 0.25$ , and  $0.75$ . Due to concerns regarding the validity of the  $R_d = 0.01$  result for the 0//0 specimen<sup>1</sup>, these results are excluded from the present analysis.

Figure 5.10 shows  $da/dN$  as a function of  $dU/dN$  for the 1 layer thickness adhesive specimens and both glass fibre specimen types. It is clear that the glass fibre specimens do not quite follow the same trend as the adhesive specimens. In a standard adhesive bond only cohesive failure of the epoxy occurs, whereas in the GFRP specimens there is also fibre-matrix debonding and ultimately fracture of bridging fibres that dissipates energy. These extra dissipative mechanisms may explain why the energy dissipation per unit crack growth is not the same for crack growth in GFRP.

<sup>1</sup>The obtained  $R_p$  value was -0.64

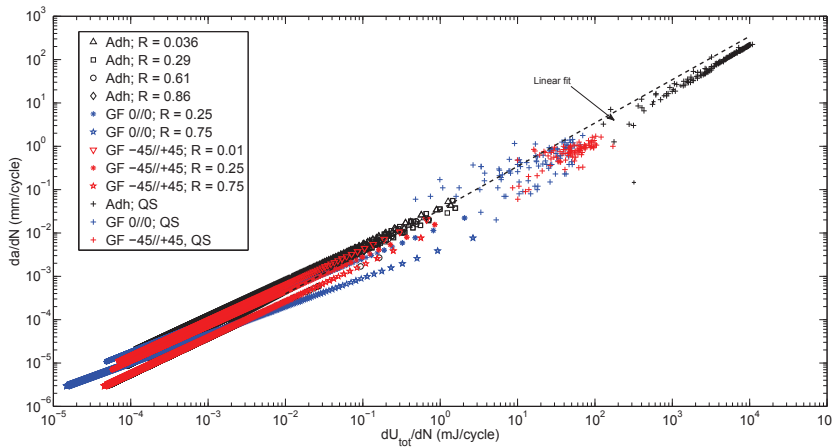


Figure 5.9: Crack growth as a function of energy dissipation for both fatigue and quasi-static loading. Results are shown for the regular adhesive bond specimens discussed in Chapter 4 (Adh), as well as the two glass fibre laminates (GF 0//0 and GF -45//+45). For the fatigue specimens  $da/dN$  and  $dU/dN$  are shown, whereas for the quasi-static specimen  $\Delta U$  and  $\Delta a$  are shown.  $\Delta U$  is the energy dissipated between two measurement points, computed according to the method described in section 3.6.3, and  $\Delta a$  is the crack growth increment between two measurement points. The dashed line is a linear fit through the adhesive bond specimen fatigue data.

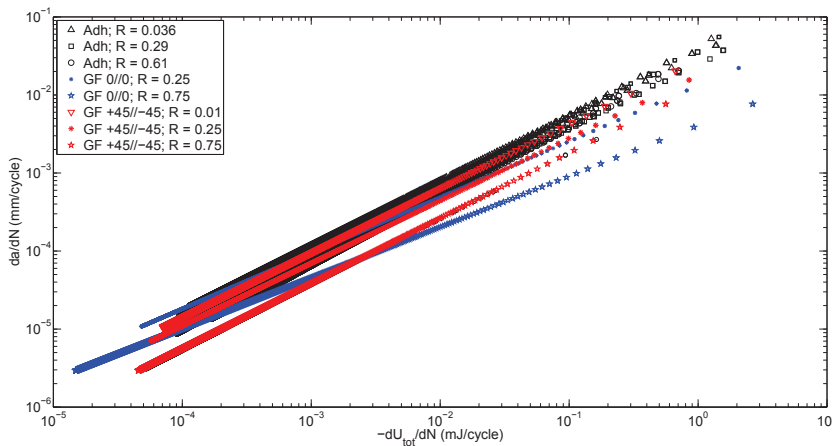


Figure 5.10: Crack growth rate as a function of energy dissipation for both the standard thickness adhesive specimens (Adh) and the glass fibre (GF) specimens.

Apart from the general trend being different, there is also a more pronounced  $R$ -ratio effect for the glass fibre specimens. There also seems to be a difference in energy dissipation between the 0//0 and -45//+45 specimens, although with only 1 specimen tested per test condition this conclusion is perhaps somewhat premature.

Once again it is interesting to examine the behaviour for a fixed crack growth rate,

and for a fixed  $G^*$  value, which is shown in figure 5.11 and figure 5.12 respectively.

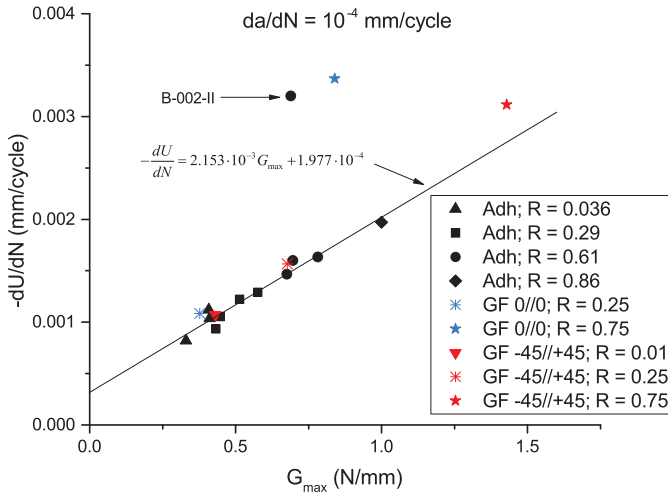


Figure 5.11: Energy dissipation as a function of  $G_{max}$  for the standard thickness adhesive specimens and the glass fibre specimens at a crack growth rate of  $10^{-4}$ . The line indicates a linear fit through the data for the standard thickness adhesive specimens, excluding the outlier B-002-II ( $R=0.61$ ).

The -45//+45 glass fibre specimens appear to follow roughly the same  $dU/dN$  vs  $G_{max}$  trend as the adhesive specimens, whereas the trend for the 0//0 specimens may be different. However the possibility that the  $R=0.75$  specimen is an outlier can not be discounted based on the limited amount of data available. The glass fibre data is shifted somewhat up along this trend, requiring a higher  $G_{max}$  to produce  $10^{-4}$  mm crack growth at a given  $R$  ratio. This matches the trend observed in the previous section of increasing adhesive thickness lowering the required  $G_{max}$  for crack growth.

In contrast to the  $G^*$  vs  $G_{max}$  trend, the  $dU/dN$  vs  $U_{cyc}$  trend is very different when comparing the adhesive bond to the GFRP specimens. It also appears that the 0//0 and -45//+45 specimens have mutually different behaviour; for the 0//0 specimens the energy dissipation for a given  $U_{cyc}$  was higher than for the -45//+45 specimens. Additionally the trends for the adhesively bonded specimens and the glass fibre specimens appear to intersect, but this can not be confirmed based on the available data.

Apart from the effect of thickness, the differences in  $dU/dN$  vs  $U_{cyc}$  behaviour may here also be at least partially attributed to fibre bridging. Yao et al [16] found that while fibre bridging affects the relationship between  $\Delta\sqrt{G}$  (and thus by extension,  $G_{max}$ ) and  $da/dN$ , it does not affect the relationship between  $dU/dN$  and  $da/dN$ . Thus the amount of energy that needs to be dissipated per unit of crack growth is not affected, but the amount of energy that is available for crack growth for a given load cycle is.

This matches with the results discussed here: the relationship between load and energy dissipation per unit of crack growth is not affected by the change from adhesive joint to composite laminate, but the relationship between load and total amount of en-

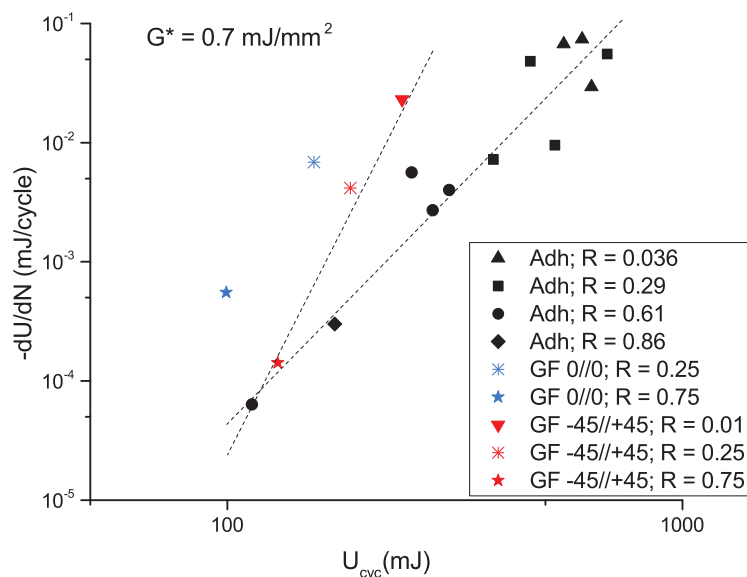


Figure 5.12: Energy dissipation as a function of  $U_{cyc}$  for the standard thickness adhesive specimens and the glass fibre specimens for  $G^* = 0.7 \text{ mJ/mm}^2$ . The dashed lines are guides to the eye, showing the different behaviour of the adhesive and glass fibre specimens.

ergy dissipation is.

## 5.5. CONCLUSION

IN summary, from the results presented in this section it can be concluded that changing the adhesive thickness does not affect the material resistance to crack growth. As long as no extra dissipative mechanisms are activated the energy dissipated per unit of crack growth for a given  $G_{max}$  remains the same. Originally it was thought that different adhesive thicknesses would result in different plastic zone sizes, and that therefore varying the adhesive thickness could be used to test the hypothesis that the  $G^*$  vs  $G_{max}$  relationship is governed by crack tip plasticity. However Zavatta's work shows that the plastic zone sizes were most likely not significantly different in this case. The observation that the  $G^*$  vs  $G_{max}$  relationship was not affected by the adhesive thickness this supports this proposition.

The amount of energy dissipated in a single cycle for a given  $U_{cyc}$  is higher for both increased adhesive thickness, and for the GFRP specimens. These results indicate that the adhesive thickness influences the amount of energy available for crack growth, thereby creating more or less crack growth for a given  $G^*$  value. In other words for a given far field load, adhesive thickness affects the amount of available energy, but not the material resistance to crack growth.



## REFERENCES

- [1] N. Zavatta, *Influence of adhesive thickness on adhesively bonded joints under fatigue loading*, (2015), MSc thesis, Università di Bologna, available from [http://amslaurea.unibo.it/9713/1/zavatta\\_nicola\\_tesi.pdf.pdf](http://amslaurea.unibo.it/9713/1/zavatta_nicola_tesi.pdf.pdf).
- [2] S. Azari, M. Papini, and J. K. Spelt, *Effect of adhesive thickness on fatigue and fracture of toughened epoxy joints – part I: Experiments*, Eng Fract Mech **78**, 153 (2011).
- [3] S. Azari, M. Papini, and J. K. Spelt, *Effect of adhesive thickness on fatigue and fracture of toughened epoxy joints – part II: Analysis and finite element modeling*, Eng Fract Mech **78**, 138 (2011).
- [4] H. Chai, *On the correlation between the mode I failure of adhesive joints and laminated composites*, Eng Fract Mech **24**, 413 (1986).
- [5] S. Krenk, J. Jönsson, and L. P. Hansen, *Fatigue analysis and testing of adhesive joints*, Eng Fract Mech **53**, 859 (1996).
- [6] M. M. Abou-Hamda, M. M. Megahed, and M. M. I. Hammouda, *Fatigue crack growth in double cantilever beam specimen with an adhesive layer*, Eng Fract Mech **60**, 605 (1998).
- [7] S. Mall and G. Ramamurthy, *Effect of bond thickness on fracture and fatigue strength of adhesively bonded composite joints*, Int J Adhes Adhes **9**, 33 (1989).
- [8] X. X. Xu, A. D. Crocombe, and P. A. Smith, *Fatigue crack growth rates in adhesive joints tested at different frequencies*, J Adhes **58**, 191 (1996).
- [9] D. W. Schmueser, *A fracture mechanics approach to characterizing cyclic debonding of varied thickness adhesive joints to electroprimed steel surfaces*, J Adhes **36**, 1 (1991).
- [10] R. Joseph, J. P. Bell, A. J. McEvily, and J. L. Liang, *Fatigue crack growth in epoxy/aluminum and epoxy/steel joints*, J Adhes **41**, 169 (1993).
- [11] G. Wilson, *Fatigue Crack Growth Prediction for generalized fiber metal laminates and hybrid materials*, Ph.D. thesis, Delft University of Technology (2013).
- [12] J. A. Pascoe, A. Al Amery, N. Zavatta, R. C. Alderliesten, and R. Benedictus, *Effect of bondline thickness on fatigue crack growth in FM 94*, (2016), dataset, available via <http://dx.doi.org/10.4121/uuid:1495c951-33e2-43ab-9f41-5ed3b57ba02f>.
- [13] J. de Jong and T. van den Hoogenband, *Verschil tussen quasi-statische scheurgroei en scheurgroei door vermoeiing in glasvezelcomposieten met verschillende interfaces.*, Tech. Rep. (Pre-University Leiden, 2015) in Dutch.
- [14] A. Al Amery, *Strain energy loss per crack growth rate experiment in glass fiber* (Hogeschool InHolland, 2015) BSc thesis.

- [15] L. Amaral, L. Yao, R. Alderliesten, and R. Benedictus, *The relation between the strain energy release in fatigue and quasi-static crack growth*, Eng Fract Mech **145**, 86 (2015).
- [16] L. Yao, R. C. Alderliesten, M. Zhao, and R. Benedictus, *Discussion on the use of the strain energy release rate for fatigue delamination characterization*, Composites Part A **66**, 65 (2014).

# 6

## EFFECT OF TEMPERATURE

*Rapidi vicinia solis  
mollit odoratas, pennarum vincula, ceras;*

*The vicinity of the sun  
softens the fragrant wax, the bond of the feathers;*

*Ovid - Metamorphoses*

*The effect of temperature on fatigue crack growth behaviour was studied by performing a number of crack growth tests at 80 °C. The test procedure was otherwise identical to that described in Chapter 3, allowing the results to be compared to the room temperature data described in Chapter 4.*

*The results showed that at 80 °C the crack growth rate increased. For two of the three specimens tested (corresponding to 4 out of 6 experiments) the failure mode was adhesive failure, rather than cohesive failure, which explains why differences were noted in the crack growth behaviour.*

*For a given load cycle the resistance to crack growth (energy dissipated per unit crack growth, i.e.  $G^*$ ) was higher, but this was outweighed by the increase in energy available ( $dU/dN$  for a given  $(\Delta\sqrt{G})^2$  and  $G^*$ ). As a result, for a given load cycle, the crack growth rate was faster at 80 °C than at room temperature. The reason for the increase in available energy is unclear. Further research into the micro-mechanics of crack growth is necessary to determine why it occurs.*

## 6.1. INTRODUCTION

THE previous chapter described an attempt to modify the amount of plasticity at the crack tip by changing the thickness of the adhesive layer. Another way of modifying the amount of plasticity is to modify the adhesive's yield strength by changing the test temperature. Thus a test campaign was carried out where 6 fatigue tests were performed at a temperature of 80 °C.

### 6.1.1. PREVIOUS WORK ON THE EFFECT OF TEMPERATURE

So far little work seems to have been done on the effect of temperature on FCG in adhesive bonds. The only investigations that could be found in the literature on this matter, were the works of Russell [1] and Ashcroft et al [2, 3].

Russell tested three epoxy adhesives (viz. FM-300K, FM-300 and EA-9321) at -50 °C, 20 °C, and 100 °C under mode II loading. He reported that the FCG rate increased for increasing temperature. Ashcroft and Shaw [3] performed tests at -50 °C, 20 °C, and 90 °C on CFRP specimens, bonded with a "proprietary modified epoxy" adhesive. They found a reduced crack growth rate at 90 °C. However they also found that the locus of failure changed at different temperatures. In particular, only at 90 °C did the failure occur in the adhesive layer.

The present author examined the effect of a reduced temperature on crack growth in an FM73 epoxy adhesive bond during his MSc thesis [4]. In that research it was found that the crack growth rate was lower at lower temperature.

Although no other work on the effect of temperature on FCG in adhesive bonds seems to have been done, there has been some research of this effect in FRPs [5–10] and FMLs [11, 12], as summarised in [13].

Chan and Wang [5] found that in an epoxy GFRP lower temperatures reduced the fracture toughness, and that higher temperatures reduced the exponent of a Paris-type power-law fit. Sjögren and Asp [6] reported an increased crack growth rate at higher temperature for a given  $G_{\max}$  value, as well as a reduced fatigue threshold value. It is interesting to note that the temperature effect disappeared if  $G_{\max}$  was divided by a  $G_c$  determined for the corresponding temperature. This suggests that changes in  $G_c$  are able to capture the effect of temperature.

In many cases non-monotonous behaviour is seen. In the results reported by Coronado et al [10] between -30 °C and 30 °C a higher temperature results in a longer initiation period, but a faster crack growth. However, at -60 °C the crack growth is faster than at -30 °C, and at 90 °C it is slower than at 50 °C. Coronado et al ascribed this to the matrix becoming more brittle at low temperatures and more ductile at high temperatures.

Rans et al [12] examined delamination growth in an FML. They found the growth rate at -40 °C was lower than at 70 °C, but higher than at room temperature.

Non-monotonous behaviour was also reported by Shindo et al [7–9]. They performed experiments at 4K, 77K, and room temperature. At 4 K the crack growth rate was lower than at room temperature, but higher than at 77K. Shindo et al suggested that at 4K freezing of the demolecular motion of the resin prevents stress relaxation, and that this explains the faster delamination growth rate at 4K.

So far the only quantitative model of the effect of temperature on fatigue crack growth (in adhesives and composites) is due to Burianek and Spearing [11]. They based their

model on a standard Paris-type relationship, but included an Arrhenius relationship as follows:

$$\frac{da}{dN} = Ce^{\left(\frac{-Q}{RT}\right)} (\Delta G)^n \quad (6.1)$$

where  $R$  is the ideal gas constant,  $T$  is the temperature and  $Q$  is an activation energy.

Burianek and Spearing selected an Arrhenius relationship based on its use to describe the temperature dependence of creep in metals. Why this would suggest its usefulness for fatigue crack growth in adhesives and composites was not explained.

Summarising the available literature it is clear that there is at present no quantitative understanding of the effect of temperature on crack growth. Furthermore, any effects of temperature are likely material dependent, even if the different materials are from the same material class.

### 6.1.2. EFFECT OF TEMPERATURE ON FM 94 MATERIAL PROPERTIES

It seems reasonable to assume that any changes in crack growth behaviour as a result of different temperature are related to changes in the mechanical properties of the material. Unfortunately there is not a lot of available data for the effect of temperature on FM 94, a point which has also hindered previous investigations [14]. The manufacturer's data-sheet [15] does not provide any stress-strain curves. Stress-strain curves have been published for FM 73 [16], which is a very similar adhesive. Unfortunately only shear stress - shear strain curves are available, and the methodology used to obtain the data is unclear. Qualitatively one can say that increasing the temperature reduces both the stiffness and the yield stress, while increasing the failure strain. This has also been reported by others in the literature [17, 18].

It seems reasonable to assume that FM 94 will behave in qualitatively the same manner, as it is a modification of the FM 73 adhesive. Thus at higher temperatures one would expect a larger amount of plasticity at the crack tip. However, due to the difficulty of generating sufficiently accurate experimental data to calibrate a constitutive model for a thin adhesive layer, this was not checked during this research.

## 6.2. EXPERIMENTAL SET-UP

THE increased temperature experiments were conducted using the experimental set-up described in Chapter 3. The only difference was the addition of a climate chamber enclosing the specimen and part of the fatigue machine. This necessitated the use of longer actuator arms on the fatigue machine. The test temperature was monitored with a thermocouple placed on the specimen surface.

The specimens used for the high temperature tests were from a batch of specimens originally manufactured by B rger [19]. In order to fit in the climate chamber the specimens had to be shortened, but otherwise they had the same nominal dimensions as the other specimens used for this thesis.

In total three specimens were tested at 80  C, with two tests being conducted on each specimen. Before each fatigue test the specimens were loaded quasi-statically at 1 mm/min until crack propagation was visually observed. The fatigue tests were performed under displacement control, with displacement ratios of  $R_d = 0.036$  (T-001), 0.29

(T-002), and 0.61 (T-003). The applied  $R_d$  ratios are shown in table 6.1, and the obtained  $R_p$  values are displayed in table A.3. Two tests were performed at each displacement ratio, with both tests performed on the same specimen.

Table 6.1: Applied  $R_d$  values for the 80 °C fatigue tests. The corresponding  $R_p$  values are shown in table A.3.

Specimen	$R_d$
T-001	0.036
T-002	0.29
T-003	0.61

Due to the short length of the specimens, during some of the experiments the cracks neared the end of the specimens. This invalidates the assumptions behind the DCB configuration (i.e. that the two arms may be treated as cantilever beams), and produced anomalous results (in particular, very fast crack growth). For this reason all the data for experiment T-001-II ( $R_d = 0.036$ ) and all data for  $N > 260$  kcycles for experiment T-002-II ( $R_d = 0.29$ ) were excluded from further analysis.

## 6

### 6.3. RESULTS

FIGURE 6.1 shows the crack growth rate as a function of  $G_{\max}$ . The data for the specimens tested at 80 °C is compared to the room temperature data discussed in Chapter 4. It is clear that at 80 °C crack growth is faster than at room temperature. In addition, there seems to be a stronger  $R$ -ratio effect for the high temperature specimens.

The data for  $R = 0.036$  and  $R = 0.29$  for the high temperature specimens is located far from both the data for the  $R = 0.61$  specimens at 80 °C, and the room temperature data. The 80 °C data for  $R = 0.61$  still indicates a higher crack growth rate at elevated temperature, for a given combination of  $G_{\max}$  and  $R$ . However, the difference with the room temperature growth rate is much smaller. This is most likely caused by the difference in the failure mechanisms. At 80 °C adhesive failure was found for the  $R = 0.036$  and 0.29 specimens, whereas cohesive failure was found for the  $R = 0.61$  specimens. Cohesive failure was also found for all the room temperature experiments. This will be discussed in more detail later.

Crack growth as a function of energy dissipation is shown in figure 6.2. For a given amount of energy dissipation, the crack growth rate is higher for the high temperature specimens.

This is also seen in figure 6.3, which shows the energy dissipation as a function of  $G_{\max}$  for a crack growth rate of  $10^{-4}$  mm/cycle. It is clear that at 80 °C crack growth occurs at lower  $G_{\max}$  values, and at correspondingly lower  $dU/dN$  values. The  $dU/dN$  vs  $G_{\max}$  data show a linear trend for both the 80 °C and room temperature specimens. However, the 80 °C results are all below the trend of the room temperature specimens. Thus a given  $G_{\max}$  value results in a lower crack growth resistance at higher temperatures. Extrapolation of the linear trends to  $G_{\max} = 0$  also suggests that minimum required energy for crack growth is lower at higher temperatures. Thus if there is a fatigue threshold (see

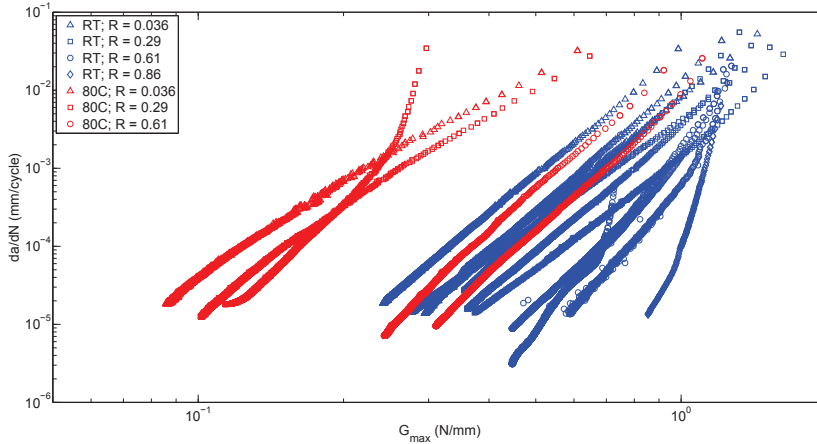


Figure 6.1: Crack growth rate as a function of  $G_{\max}$  for the room temperature (RT) specimens and the specimens tested at 80 °C (80C). The upward curvature seen for one of the 80C;  $R = 0.29$  specimens is thought to be caused by the crack nearing the end of the specimen.

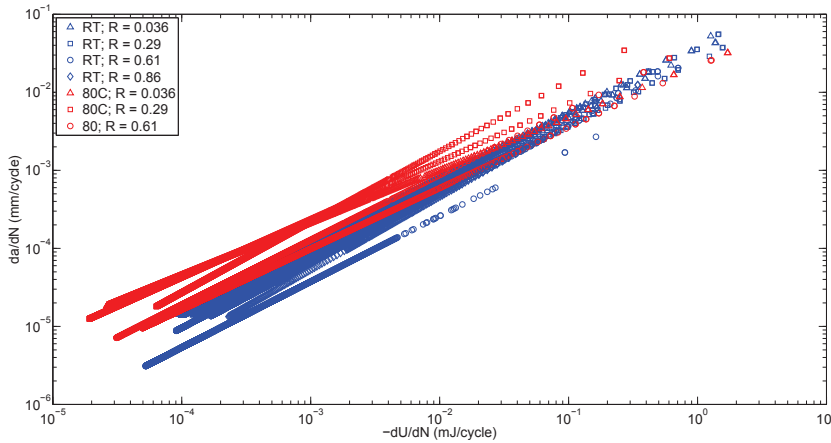


Figure 6.2: Crack growth rate as a function of  $dU/dN$  for the room temperature (RT) specimens and the specimens tested at 80 °C (80C).

the discussion in section 4.4.3) it is likely also lower.

However, these trends do not persist over the entire range of crack growth rates, as shown in figure 6.4. It is clear that the 80 °C specimens do not follow the same trend as the room temperature specimens. Although at the low end of the  $G_{\max}$  range the 80 °C  $G^*$  values are reasonably close to the room temperature trend, at higher  $G_{\max}$  values they curve away to become much larger, indicating a stronger dependence of  $G^*$  on  $G_{\max}$ . In addition there is a greater variability in the slope of the  $G^*$  vs  $G_{\max}$  lines for the 80 °C specimens, resulting in a greater spread of  $G^*$  values for a given  $G_{\max}$ , particularly

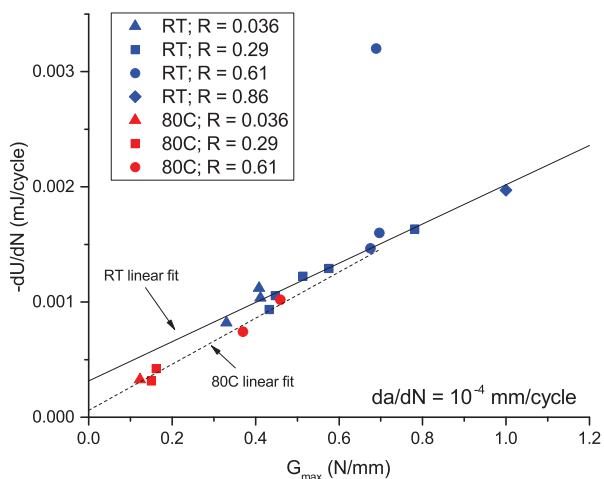


Figure 6.3: Energy dissipation as a function of  $G_{\max}$  for the room temperature (RT) specimens and the specimens tested at 80 °C (80C). The solid black line shows a linear fit through the room temperature specimens, excluding the outlier data point from experiment B-002-II (RT;  $R = 0.61$ ). The dashed line shows a linear fit through the 80 °C data.

## 6

at higher  $G_{\max}$  values. Unlike at room temperature, for the 80 °C specimens there also appears to be an  $R$ -ratio effect. For a given  $G_{\max}$ ,  $G^*$  is lower for a higher  $R$ -ratio.

These observations imply that due to the increase of temperature the material behaviour has changed, altering the relationship between resistance to crack growth and applied load that was seen for the room temperature specimens.

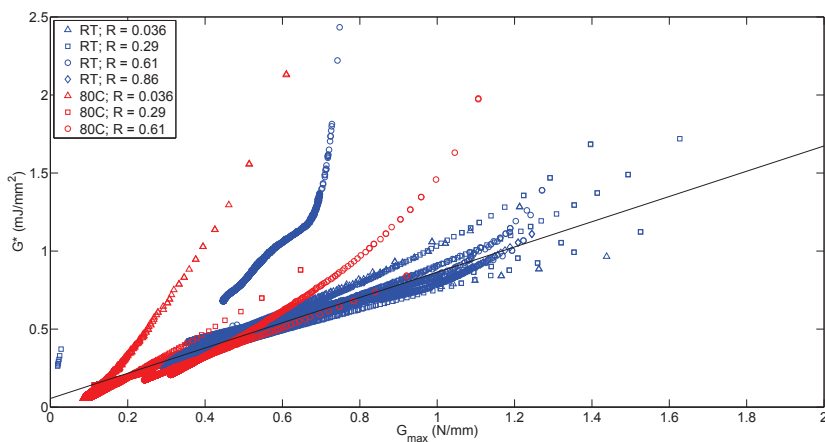


Figure 6.4:  $G^*$  values as a function of  $G_{\max}$  for the room temperature (RT) specimens and the specimens tested at 80 °C (80C). The black line shows a linear fit through the room temperature specimens, excluding the outlier datapoints from experiment B-002-II (RT;  $R = 0.61$ ).

Not only the relationship between resistance and applied load has changed however.



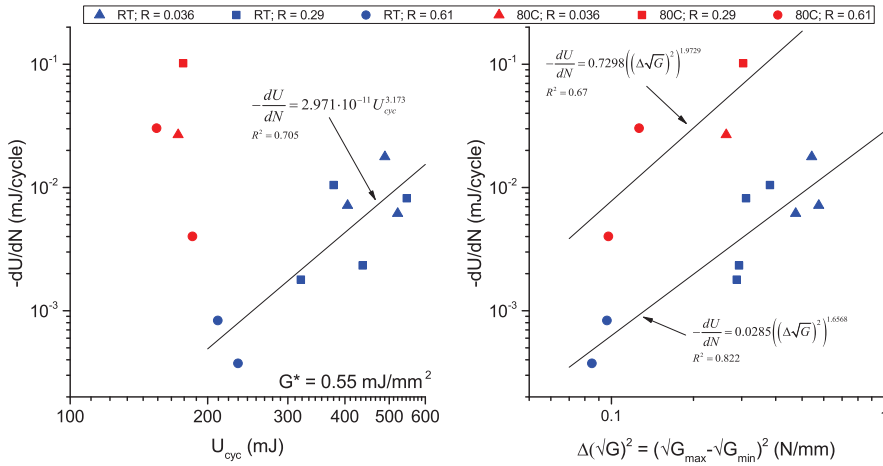


Figure 6.5: Energy dissipation as a function of  $U_{cyc}$  (left panel) and  $(\Delta\sqrt{G})^2$  (right panel) for  $G^* = 0.55 \text{ mJ/mm}^2$  for both the room temperature (RT) specimens and the specimens tested at  $80^\circ\text{C}$  (80C). Power-law fits of the different data sets and the associated correlation coefficients are also shown.

The relationship between applied load and available energy has also changed, and in fact in a more drastic manner. This is illustrated in the left panel of figure 6.5, which shows the relationship between  $dU/dN$  and  $U_{cyc}$  for  $G^* = 0.55 \text{ mJ/mm}^2$ . Where at high temperature the relationship between  $G^*$  and  $G_{\max}$  was merely altered, the relationship between  $dU/dN$  and  $U_{cyc}$  seems to have completely disappeared.

Interestingly, the relationship between  $(\Delta\sqrt{G})^2$  and  $dU/dN$  appears to remain intact, albeit altered, as shown in the right panel of figure 6.5. At a fixed value of  $G^*$ , a given value of  $(\Delta\sqrt{G})^2$  will result in a larger amount of energy dissipation, and therefore crack growth, at higher temperatures. It seems that as with thickness, changing the temperature changes the amount of energy available for crack growth for a given load cycle.

The most likely explanation for the change in the  $G^*$  vs  $G_{\max}$  and  $dU/dN$  vs  $U_{cyc}$  is the change of failure mode that was observed during fractographic investigation. For this investigation the specimens were broken apart by means of a quasi-static test on a Zwick 20 kN tensile test machine. The resulting fracture surfaces are shown in figure 6.6, and a greater magnification image of the fracture surfaces for specimens T-001 and T-003 is shown in figure 6.7.

For specimens T-001 ( $R = 0.036$ ) and T-002 ( $R = 0.29$ ) there are portions of the fracture surface where adhesive residue is present on only one of the two surfaces. This indicates that specimens T-001 and T-002 suffered adhesive failure during at least part of the fatigue test. Specimen T-003 ( $R = 0.61$ ) and the room temperature specimens suffered cohesive failure, as indicated by the presence of adhesive residue on both fracture surfaces.

This difference in failure modes explains why there is a difference in the  $G^*$  vs  $G_{\max}$  behaviour as seen in figure 6.4, and why the relationship between  $dU/dN$  and  $U_{cyc}$  for fixed  $G^*$  disappears. In both cases the failure mechanisms are different, so it is not surprising that the relationships between the applied load on the one hand, and the

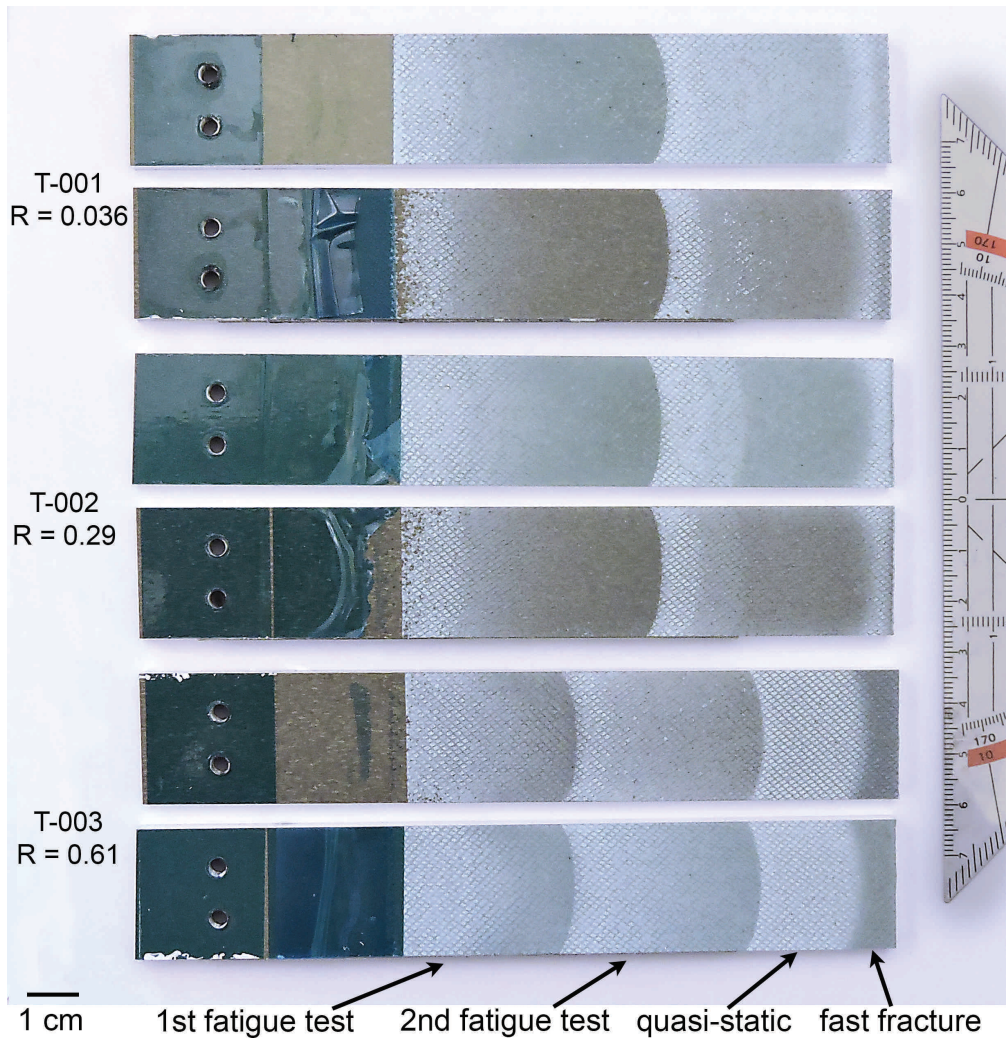


Figure 6.6: Fracture surfaces of the series T specimens (all tested at 80 °C). Two fatigue tests were performed per specimen, which is clearly visible on the fracture surfaces. The fracture surfaces formed during the quasi-static loading performed to break apart the specimens are also visible. Crack growth direction was from left to right. For specimens T-001 and T-002 one of the fracture surfaces per specimen is almost free of adhesive residue, indicating adhesive failure.

crack growth resistance and energy available for crack growth on the other hand, should change. Why there is still a relationship between  $dU/dN$  and  $(\Delta\sqrt{G})^2$  for fixed  $G^*$ , despite the disappearance of the  $dU/dN$  vs  $U_{cyc}$  relationship is unclear.

It is also worth noting that even for the experiments where cohesive failure was seen (i.e. T-003-I and T-003-II;  $R = 0.61$ ) the energy dissipation for a given  $(\Delta\sqrt{G})^2$  or  $U_{cyc}$  for fixed  $G^*$  was greater than the room temperature value. This suggests that at high temperature the amount of energy available for crack growth is increased for a given load

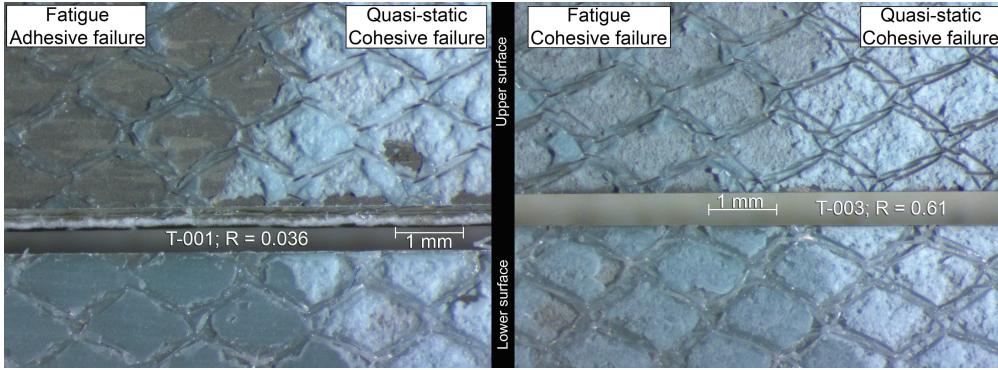


Figure 6.7: Micrograph of the fracture surfaces of specimens T-001 (left) and T-003 (right) showing the transition from fatigue to quasi-static loading. The upper and lower surfaces are shown side-by-side. Crack growth direction was from left to right. For specimen T-001 the upper surface corresponding to the fatigue test is almost free of adhesive residue, indicating adhesive failure. For specimen T-003 there is adhesive residue on both surfaces, indicating cohesive failure.

cycle, even when there is no change in the failure mode. It is possible that the reduction in yield strength due to increase of the temperature allows void formation to occur in a larger area ahead of the crack tip. In that way it might be possible to make use of strain energy stored in a larger volume of material, thus allowing more energy to be used for crack growth for a given load cycle. To further investigate this hypothesis would require a precise determination of the crack-tip stress and strain fields, as well as more understanding of the micro-mechanics of crack growth.

## 6.4. CONCLUSION

FOR the FM 94 epoxy adhesive, increasing the temperature from room temperature to 80 °C increases the crack growth rate for a given loading.

For two out of the three tested specimens, increasing the temperature changed the failure mode from cohesive to adhesive. This explains why large differences were seen between the behaviour of the 80 °C and the room temperature specimens. In particular, for the 80 °C specimens greater variability was seen in the slope of the  $G^*$  vs  $G_{\max}$  curve, than for the room temperature specimens. In addition, at 80 °C there was no longer a relationship between  $dU/dN$  and  $U_{cyc}$  for a fixed  $G^*$ . For reasons that are unclear, there did still appear to be a relationship between  $dU/dN$  and  $(\Delta\sqrt{G})^2$  at a fixed  $G^*$ .

Although there was no longer a relationship between  $dU/dN$  and  $U_{cyc}$  for a fixed  $G^*$  at 80 °C it is clear that the energy dissipation at increased temperature for a given  $U_{cyc}$  was higher than at room temperature. This implies that the energy available for crack growth for a given load cycle is greater at 80 °C than at room temperature.

In fact, for a given  $G_{\max}$ ,  $G^*$  was higher for the 80 °C specimens, than for the room temperature specimens. However, this was outweighed by the increase in available energy, in the end resulting in faster crack growth. Further investigation of the micro-mechanics is necessary to understand why higher temperatures would increase the amount of available energy.

In terms of the conceptual model presented in Chapter 3 these results imply that temperature changes both the relationship between the applied load and the crack growth resistance, and the relationship between the applied load and the available energy.

For specimens T-001 ( $R = 0.036$ ) and T-002 ( $R = 0.29$ ) there is a clear reason why this change in behaviour occurred: the failure mode changed from cohesive to adhesive. For specimen T-003 ( $R = 0.61$ ), where the failure mode remained cohesive, the  $G^*$  vs  $G_{\max}$  behaviour, i.e. the relationship between applied load and crack growth resistance, remained closer to the room temperature behaviour. In general, for a given  $G_{\max}$ , the resistance to crack growth is higher at higher temperature, but the exact relationship between load and resistance will depend on whether the failure is adhesive or cohesive.

At a given crack growth resistance value, the same load cycle (in terms of  $U_{cyc}$  or  $(\Delta\sqrt{G})^2$ ) at an elevated temperature will result in more energy being available for crack growth than at room temperature.

Taken together, for a given load cycle, increasing the temperature will increase both the resistance to crack growth, and the amount of energy available for crack growth. If the failure mode remains cohesive, the resistance will only be increased by a small amount. However, if the failure mode becomes adhesive, the resistance will become much larger. The amount of energy available becomes much larger than at room temperature regardless of whether the failure mode changes.

Although both the resistance and the available energy increase, the increase of the available energy is much larger. Increasing the temperature to 80 °C causes an increase of the resistance ( $G^*$ ) for a given load of at most a factor 2 - 4, whereas the amount of available energy increases by up to an order of magnitude. Because the available energy increases more than the resistance, the end result is that for a given load cycle, an increase in temperature results in an increase of the crack growth rate.

## REFERENCES

- [1] A. Russell, *A Damage Tolerance Assessment of Bonded Repairs to CF-18 Composite Components Part I Adhesive Properties*, Tech. Rep. Technical Memorandum 88-25 (Defence Research Establishment Pacific, 1988).
- [2] I. A. Ashcroft, D. J. Hughes, S. J. Shaw, M. A. Wahab, and A. Crocombe, *Effect of temperature on the quasi-static strength and fatigue resistance of bonded composite double lap joints*, *J Adhes* **75**, 61 (2001).
- [3] I. A. Ashcroft and S. J. Shaw, *Mode I fracture of epoxy bonded composite joints 2. Fatigue loading*, *Int J Adhes Adhes* **22**, 151 (2002).
- [4] J. A. Pascoe, *Delamination of bonded repairs - a damage tolerance approach*, (2012), Delft University of Technology, MSc thesis.
- [5] W. Chan and A. Wang, *Free-edge delamination characteristics in S2/CE9000 glass/epoxy laminates under static and fatigue loads*, in *Composite Materials: Fatigue and Fracture, Second Volume, ASTM STP 1012*, edited by P. A. Lagace (American Society for Testing and Materials, Philadelphia, 1989) pp. 270–295.



- [6] A. Sjögren and L. E. Asp, *Effects of temperature on delamination growth in a carbon/epoxy composite under fatigue loading*, Int J Fatigue **24**, 179 (2002).
- [7] Y. Shindo, A. Inamoto, F. Narita, and K. Horiguchi, *Mode I fatigue delamination growth in GFRP woven laminates at low temperatures*, Eng Fract Mech **73**, 2080 (2006).
- [8] Y. Shindo, T. Takeda, F. Narita, N. Saito, S. Watanabe, and K. Sanada, *Delamination growth mechanisms in woven glass fiber reinforced polymer composites under mode II fatigue loading at cryogenic temperatures*, Compos Sci Technol **69**, 1904 (2009).
- [9] Y. Shindo, M. Miura, T. Takeda, N. Saito, and F. Narita, *Cryogenic delamination growth in woven glass/epoxy composite laminates under mixed-mode I/II fatigue loading*, Compos Sci Technol **71**, 647 (2011).
- [10] P. Coronado, A. Argüelles, J. Viña, V. Mollón, and I. Viña, *Influence of temperature on a carbon-fibre epoxy composite subjected to static and fatigue loading under mode I delamination*, Int J Solids Struct **49**, 2934 (2012).
- [11] D. A. Burianek and S. M. Spearing, *Delamination growth from face sheet seams in cross-ply titanium/graphite hybrid laminates*, Compos Sci Technol **61**, 261 (2001).
- [12] C. D. Rans, R. C. Alderliesten, and R. Benedictus, *Predicting the influence of temperature on fatigue crack propagation in fibre metal laminates*, Eng Fract Mech **78**, 2193 (2011).
- [13] J. A. Pascoe, R. C. Alderliesten, and R. Benedictus, *Methods for the prediction of fatigue delamination growth in composites and adhesive bonds - a critical review*, Eng Fract Mech **112-113**, 72 (2013).
- [14] M. Hagenbeek, *Characterisation of Fibre Metal Laminates under Thermo-mechanical Loadings*, Ph.D. thesis, Delft University of Technology (2005).
- [15] *FM 94 adhesive film technical data sheet*, (2010), Cytec Industries.
- [16] *FM 73 adhesive film technical data sheet*, (2011), Cytec Industries.
- [17] P. Chalkley and J. van den Berg, *On obtaining design allowables for adhesives used in the bonded-composite repair of aircraft*, Tech. Rep. DSTO-TR-0608 (Defence Science and Technology Organisation, 19987).
- [18] P. Chakley and A. Baker, *Adhesives characterisation and data base*, in *Advances in the bonded composite repair of metallic aircraft structure*, Vol. 1, edited by A. Baker, L. Rose, and R. Jones (Elsevier, Oxford, 2002) pp. 87–102.
- [19] D. Bürger, *Mixed-mode Fatigue Disbond on Metallic Bonded Joints*, Phd thesis, Delft University of Technology (2015), <http://dx.doi.org/10.4233/uuid:ec4dbcd6-052d-4009-bf9e-cdcbf4614174>.



# 7

## FATIGUE CRACK GROWTH WITHIN A SINGLE CYCLE

*I have heard the mermaids singing, each to each.*

T.S. Elliot - *The Love Song of J. Alfred Prufrock*

*In analyses of fatigue crack growth it is nearly always assumed that the crack growth rate can be approximated by a value,  $da/dN$ , that is effectively the average growth rate over one cycle. The same has been done so far in this thesis. However in reality the crack growth rate is not constant during a single cycle, and crack growth may not even occur during every cycle. For a full understanding of crack growth it is necessary to better understand how crack growth progresses during a single load cycle.*

*In experiments described in this chapter the acoustic emission technique was used to gain more insight into the single cycle crack growth behaviour. Although the results are preliminary, evidence was found that crack growth occurs during the portion of a fatigue cycle where the load is above a certain threshold value. In addition the results suggest that it may be possible to determine this fatigue threshold value from quasi-static tests. To be able to gain more confidence in these conclusions, more research needs to be done on the link between the physical crack growth processes and the acoustic emission signals. This will allow more accurate interpretation of the received signals.*

### 7.1. MOTIVATION

UP to this point in this thesis, FCG has always been considered with the single fatigue cycle as the smallest time-scale. That is to say, both energy dissipation and crack growth rate have always been averaged to a single cycle. This procedure implicitly carries with it two assumptions.

The first assumption is that it is not necessary to take into account how the crack growth rate changes over the course of a single fatigue cycle, even though there is evidence that it is not constant [2]. Besides that evidence, the simple observation that fatigue loading is a cyclical phenomenon should be enough to realise that the crack growth rate is not constant within a single cycle. Of course, if the crack growth rate is not constant, the energy dissipation cannot be constant either.

The second assumption is that crack growth occurs during every cycle, or at the very least, that it may be treated as occurring during each cycle with an average rate.

Given that aerospace structures are typically required to have fatigue lives on the order of hundreds of thousands – if not millions – of cycles, these assumptions may be sufficient for a prediction model. However, from a scientific point of view they represent simplifications that obscure the actual crack growth behaviour. In order to identify which characteristics of a cycle are important for fatigue crack growth, it is important to understand how the crack growth progresses within the cycle. Does the crack only grow at maximum load? If not, does it grow only during loading or also during unloading? Does crack growth occur during the entire cycle, or is there a threshold load level below which crack growth stops?

To answer these questions, experimental techniques are needed that are able to track crack growth within one load cycle. The optical crack length measurement technique used for the previous experiments described in this thesis is insufficient for two reasons. First of all, during a single load cycle crack growth is typically on the order of  $10^{-3}$  –  $10^{-5}$  mm, which is much lower than the length resolution that can be obtained with the optical technique. Secondly, the optical measurement technique is only capable of measuring crack length at the side of the specimen. Any crack growth that occurs inside the specimen cannot be detected. Since it is possible that crack growth in the centre of the specimen occurs at a lower load level than crack growth at the side of a specimen, this is a significant drawback.

A possible solution could be to perform in-situ experiments in an SEM, which might solve the length resolution issues. However this would not solve the issue of only being able to see the side of the specimen. Furthermore, for the present research a suitable test set-up was not available. Thus a different technique was selected: acoustic emission (AE).

Acoustic emission is based on the work of Kaiser [3]. It works on the principle that crack growth (but also other types of events and/or micro-structural changes) emit ultrasonic sound-waves that can be detected by using suitable transducers. By recording when these signals are detected, it is possible to determine at what points within the fatigue cycle crack growth occurs.

The research presented in this chapter is one of the earliest (if not the earliest) uses of AE for the purpose of understanding crack growth within a single cycle. Thus many questions still remain to be answered. Nevertheless, the research can serve as a proof-



of-concept of this use of the AE technique, and some interesting results regarding crack growth behaviour were obtained.

## 7.2. SPECIMENS AND EXPERIMENTAL SET-UP

THE AE experiments were conducted on the AE series of specimens, which were of the standard DCB type described in Chapter 3. These specimens were left from the research of Bürger [4], but were of the same composition, and manufactured in the same way, as the other specimens used in this research. The specimens were again tested on the MTS 10 kN fatigue test machine.

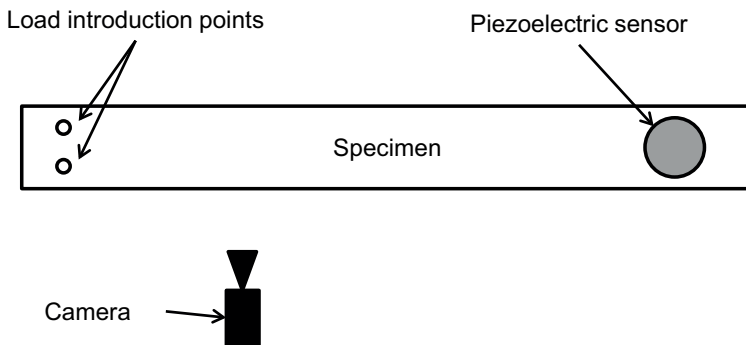


Figure 7.1: Schematic illustration of the test set-up for the acoustic emission test, showing a top-view of the specimen and the placement of the piezoelectric sensor and the camera. The load was applied normal to the plane of the illustration. The figure is not to scale [1].

An AE sensor was clamped to the specimens, as shown schematically in figure 7.1. To improve the conductivity between the sensor and the specimen, grease was applied to the surface of the specimen. The sensor used was a wide-band piezoelectric sensor, type AE1045S, with an external 34 dB pre-amplifier and a 20-1200 kHz band-pass filter. It was connected to an AMSY-6 Vallen, 8-channel AE system. The force and displacement outputs of the fatigue machine were output to the AE system, allowing them to be correlated to the recorded AE signals.

Three specimens were prepared for this experimental series, coded AE001 through AE003. However for specimen AE002 the thread of the lower bolt holes failed before any crack growth was detected. The thread failure occurred at approximately 2.1 kN of applied force. This is more than a factor of 2 higher than the force needed to cause crack growth in the other specimens. The most likely explanation is that in specimen AE002 the crack starter failed to initiate a cohesive crack in the material.

The AE system continuously monitors the sensor for signals. If the signal has a higher peak amplitude than a pre-determined threshold it is recorded. A single signal detection is referred to as a 'hit' in this thesis. For the experiments conducted on specimen AE-001 the threshold was set to 62 dB, based on previous experience with the AE system. The purpose of this threshold is to prevent the recording of noise signals. Of course having an AE threshold setting that is too high would mean that signals emitted by actual crack growth are also not recorded. Therefore the proper threshold setting was investigated

using specimen AE003, as described in more detail in the next section. As a result of this investigation, 55 dB was used as the threshold setting during the experiments on specimen AE003, with exception of the very first experiment, which used a setting of 50 dB.

In order to gain a better understanding of the crack growth a variety of load cases was selected, comprising quasi-static loading, fatigue loading at a low strain rate (i.e. 1 mm/min) and fatigue loading at a 'normal' frequency (i.e. 5 Hz, as used in the rest of this thesis). Multiple load cases were applied to each specimen. The different experiments are referred to by the number of the specimen, followed by the suffix QS (for quasi-static) or Fat (for fatigue) and a numerical index.

For the quasi-static loading the displacement was increased at 1 mm/min and then held constant either as soon as the first AE hits were detected, or as soon as a drop in the load was detected. For the fatigue loading different R-ratios were examined. A full list of the applied load cases is shown in table 7.1.

The raw and analysed experimental data is available at [5].

Table 7.1: Test matrix, listing the different experiments and the applied load cases. [1].

Experiment	Load case
AE001-QS1	QS load at 1 mm/min until the first acoustic emission signal, then displacement held constant.
AE001-QS2	QS load at 1 mm/min until drop in the force. Fatigue machine safety interlock activated before this happened. Therefore the collected data will not be discussed in this thesis. Higher capacity load cell (10 kN) installed after this test.
AE001-QS3	QS load at 1 mm/min until drop in the force, then displacement held constant.
AE001-QS4	QS load at 1 mm/min until crack length had been extended to roughly 100 mm.
AE001-QS5	QS load at 1 mm/min until drop in the force, then displacement held constant.
AE001-Fat1	5 Fatigue cycles at 1 mm/min displacement rate. $d_{max} = 1.39$ mm, $d_{min} = 0$ mm, ( $R=0$ ).
AE001-Fat2	5 Fatigue cycles at 1 mm/min displacement rate. $d_{max} = 1.39$ mm, $d_{min} = 0$ mm, ( $R=0$ ).
AE001-Fat3	5 Fatigue cycles at 1 mm/min displacement rate. $d_{max} = 1.39$ mm, $d_{min} = 0$ mm, ( $R=0$ ).
AE001-Fat4	5 Fatigue cycles at 2 mm/min displacement rate. $d_{max} = 1.39$ mm, $d_{min} = 0$ mm, ( $R=0$ ).
AE001-Fat5	5 Fatigue cycles at 1 mm/min displacement rate. $d_{max} = 1.39$ mm, $d_{min} = 0.695$ mm, ( $R=0.5$ ).
AE001-Fat6	Fatigue cycles at 5Hz. $d_{max} = 1.39$ mm, $d_{min} = 0.695$ mm, ( $R=0.5$ ). AE system recording frequency set too low, resulting in aliasing, this experiment will not be discussed in this thesis.

Table 7.1: Test matrix, listing the different experiments and the applied load cases. [1].

Experiment	Load case
AE001-Fat7	Fatigue cycles at 5Hz. $d_{max} = 1.39$ mm, $d_{min} = 0.695$ mm, ( $R=0.5$ ).
AE001-Fat8	5 Fatigue cycles at 1 mm/min displacement rate. $d_{max} = 1.39$ mm, $d_{min} = 0.695$ mm, ( $R=0.5$ ).
AE001-Fat9	5 Fatigue cycles at 1 mm/min displacement rate. $d_{max} = 7.6$ mm, $d_{min} = 0.695$ mm, ( $R=0$ ).
AE001-Fat10	5 Fatigue cycles at 1 mm/min displacement rate. $d_{max} = 7.6$ mm, $d_{min} = 3.8$ mm, ( $R=0.5$ ).
AE003-QS1	QS load at 1 mm/min in order to create a cohesive crack. Test stopped after onset of crack growth determined visually.
AE003-QS2	QS load at 1 mm/min until the first acoustic emission signal. Then displacement held constant. Test repeated with a higher AE threshold. Test repeated again, but only holding after the first cluster of signals rather than the first hit.
AE003-QS3	QS load at 1 mm/min until drop in the load, then displacement held constant.
AE003-Fat1	5 Fatigue cycles at 1 mm/min displacement rate. $d_{max} = 2.27$ mm, $d_{min} = 0$ mm, ( $R=0$ ).
AE003-Fat2	5 Fatigue cycles at 1 mm/min displacement rate. $d_{max} = 2.27$ mm, $d_{min} = 1.135$ mm, ( $R=0.5$ ).
AE003-Fat3	5 Fatigue cycles at 1 mm/min displacement rate. $d_{max} = 1.9$ mm, $d_{min} = 0$ mm, ( $R=0$ ).
AE003-Fat4	5 Fatigue cycles at 1 mm/min displacement rate. $d_{max} = 1.9$ mm, $d_{min} = 0.95$ mm, ( $R=0.5$ ).
AE003-Fat5	Fatigue cycles at 5Hz. $d_{max} = 2.27$ mm, $d_{min} = 0.95$ mm, ( $R=0.42$ ).
AE003-Fat6	Fatigue cycles at 5Hz. $d_{max} = 2.27$ mm, $d_{min} = 0$ mm, ( $R=0$ ).

### 7.3. QUASI-STATIC EXPERIMENTS

THE first quasi-static load case was the case where the displacement was held constant as soon as a hit was detected. The results are shown in figure 7.2.

For experiment AE001-QS1 there was an initial cluster of hits, which died down after the displacement was held. No crack growth was observed visually, which means these signals were either produced by a different process than crack growth, or that crack growth did occur but was too small to be visible, or did not occur on the visible surface of the specimen.

On specimen AE003 this load case was performed 3 times during experiment AE003-QS2. During the first load application an AE threshold of 50 dB was used. However this caused the detection of hits at very low load levels ( $G \approx 0.01$  N/mm). Based on the waveform these signals were interpreted as noise, and it was decided to raise the threshold to 55 dB, which was used for all subsequent experiments on AE003. During the second

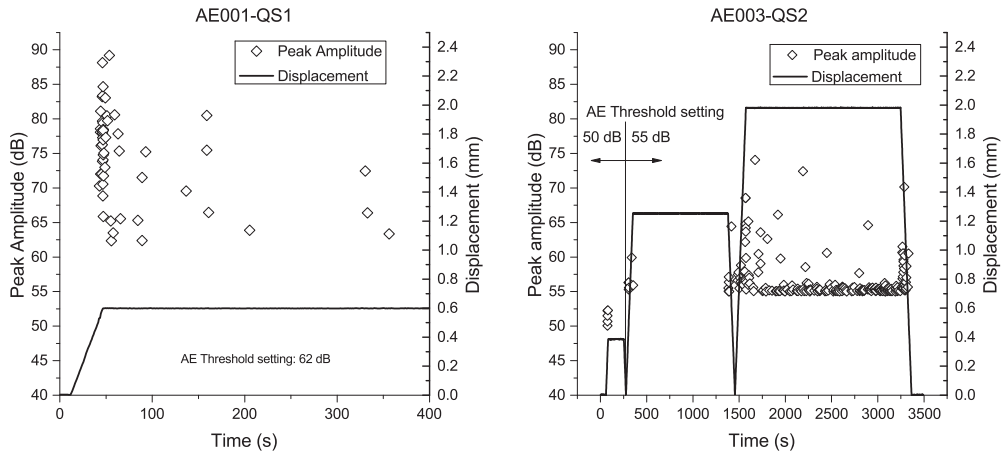


Figure 7.2: Displacement and peak amplitude of the received acoustic signals for the load case where the displacement was held as soon as the first signals were detected. This load case was performed once on specimen AE-001 (experiment AE001-QS1, left panel) and three times on specimen AE003 (experiment AE003-QS2, right panel). The detection threshold for the acoustic emission system was raised between the first and second test on specimen AE003, as analysis of the waveform suggested the signals detected during the first test were just noise. [1]

test a peak amplitude of just under 60 dB was reached during loading. No further signals were detected during the hold. However during unloading a cluster of hits was detected. The source of these signals is unknown; one possibility is that they are emitted when the crack flanks come in contact during closure of the crack.

During the third test the load was increased until a clear cluster of hits was seen. During this test some crack growth occurred, as shown in figure 7.3. There was about 0.75 mm of fast crack growth while the displacement was still increasing, followed by another 0.2 mm during the first minutes of the hold. After that both the force and the visible crack length remained constant. Nevertheless there was a constant 'baseline' of hits with a peak amplitude of around 55 dB that was not seen during the first and second load application.

It is unclear what the source of these signals is. The fact that the force remains constant seems to rule out visco-elastic effects and crack growth as sources, making it likely that this signal represents some kind of noise. In order to properly interpret these signals further research is required to be able to match the features of the signals to physical processes in the material. This was beyond the scope of the present work however. Based on the results of experiment AE003-QS2, it will be assumed in this thesis that crack growth only occurs when there are signals with a peak amplitude greater than 58 dB.

More crack growth occurs if the displacement is increased until the force decreases again. This case is shown in figures 7.4 (for specimen AE001) and 7.6 (for specimen AE003, discussed below). For both experiments on specimen AE001 (i.e. AE001-QS3 and AE001-QS5) there is a large cluster of hits that starts when a certain load level is exceeded and continues until the displacement is held. During this time there is rapid crack growth. Then the signals slowly die down: both the peak amplitude and the num-

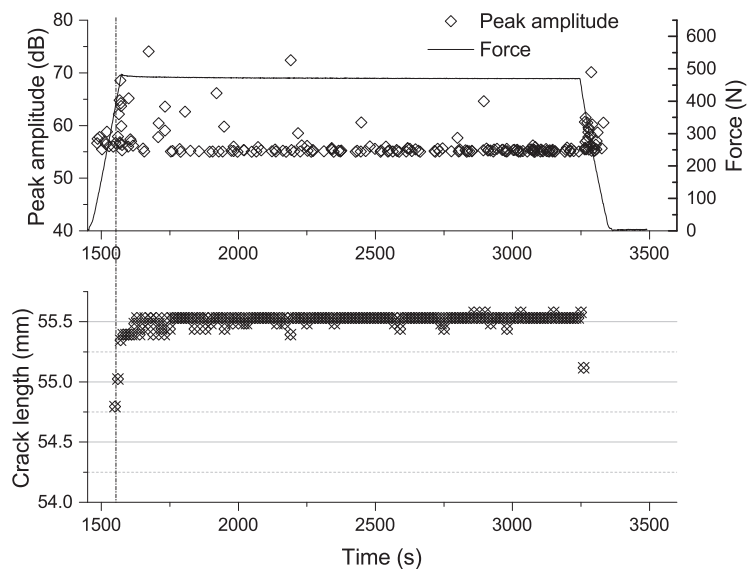


Figure 7.3: Force, peak amplitude, and crack growth for the third load application during experiment AE003-QS2. The displacement was held as soon as the first AE signals were detected. There was approximately 0.75 mm of crack growth coincident with the first cluster of AE hits above 55 dB, as indicated by the vertical line. During the first minutes of the subsequent hold the crack grew by approximately another 0.2 mm [1].

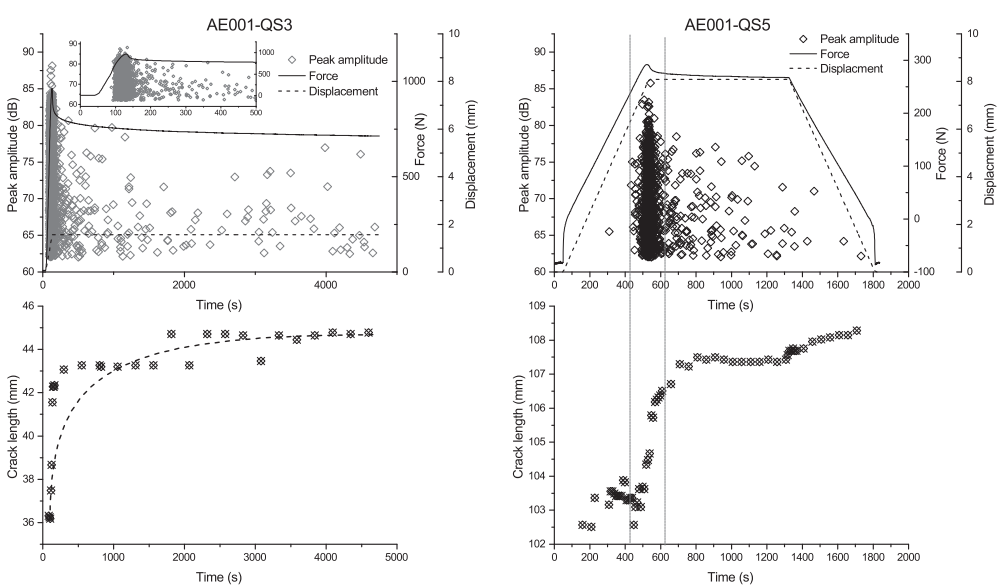


Figure 7.4: Crack length, force, and peak amplitude of the acoustic emission signals for experiments AE001-QS3 and AE001-QS5 (AE threshold: 62 dB). The dashed line on the bottom left panel is thought to better represent the actual crack growth behaviour than the data points, due to the measurement difficulties highlighted in figure 7.5 [1].

ber of hits per second decrease. The force decreases asymptotically as well, and some small amount of crack growth is detected during this period.

Unfortunately the crack progression is not entirely clear for these experiments, especially for AE001-QS3 and AE003-QS3 (which will be discussed below). This is due to the issues with the visual crack length measurements illustrated by the example shown in figure 7.5. In some cases there was no clear advance of the crack tip. Rather a faint line was seen in the photographs, which gradually became more distinct in later images. At an arbitrary level of visibility this line was considered to be part of the crack, causing a jump in the crack length.

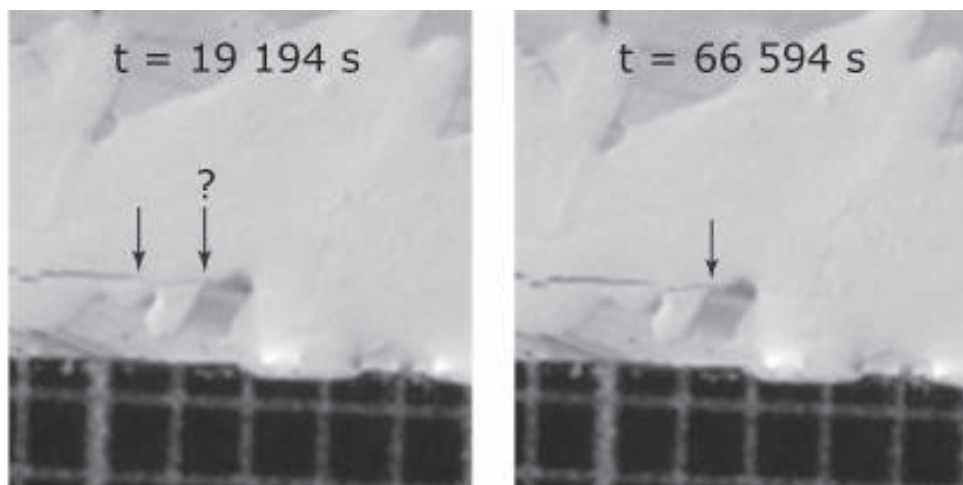


Figure 7.5: Example of the issues with crack length measurement. This figure shows a portion of two photographs taken during test AE003-QS3. At  $t = 66594$  s the crack tip is located at the arrow. However at  $t = 19194$  s it is not clear whether the left or the right arrow indicates the crack tip. No crack tip advance was obvious. Rather, the faint line between these two arrows gradually became less faint in later pictures. This causes the jump in the crack length measurements as shown in figure 7.6, even though this most likely does not reflect the actual crack growth behaviour [1]

Given that during the quasi-static experiments on series A (Section 4.5) the cracks were seen to advance continuously, and given the lack of any discontinuities in the force vs time curve, it seems unlikely that the discontinuities in the crack length measurements reflect the actual crack growth behaviour. A more likely explanation is that the crack continued to grow in the specimen, without breaking through the layer of type-writer correction fluid painted onto the side of the specimen. For future experiments it is therefore recommended to at least thin the fluid further and to investigate the possibility of conducting the tests without applying any fluid at all.

In order to further investigate if and how crack growth occurs while applying a constant load, a long duration test was performed during experiment AE003-QS3. The specimen was loaded at 1 mm/min until the force was seen to decrease. The displacement was then held constant for about 18.5 hours. Figure 7.6 shows the results. Again rapid crack growth took place while the displacement was increased, followed by a small amount of more gradual crack growth while the displacement was held. Unfortunately the exact

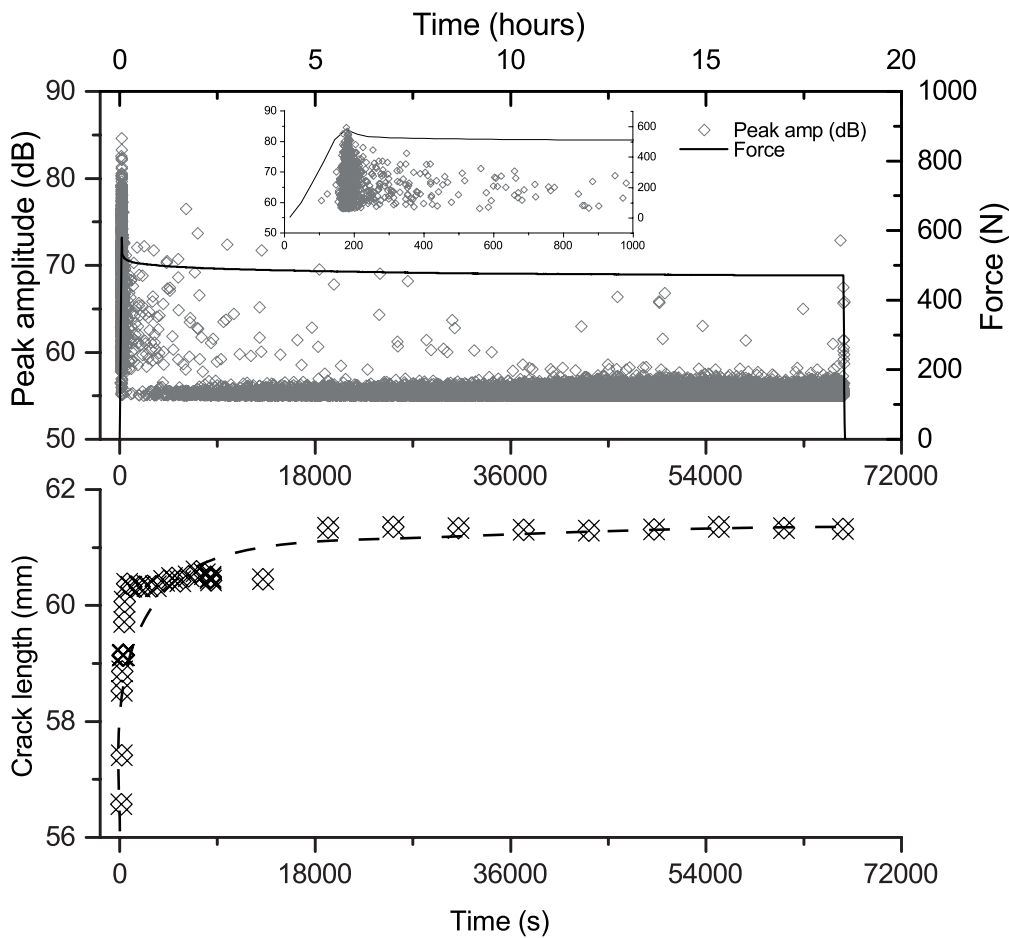


Figure 7.6: Force, crack length and peak amplitude for experiment AE003-QS3. The inset figure shows a detailed view of the time period surrounding the maximum force. The force peaks at 580 N and decays asymptotically. During the last 8960 s the force is constant at 471.56 N (load cell resolution: approximately 0.3 N). In order to prevent problems rendering the graph for publication, the data is filtered to only show 1 out of every 10 hits with a peak amplitude under 58 dB (selected based on the 58 dB signal not being associated with fatigue crack growth in the previous tests). For the full data see [5]. The dashed line is thought to more accurately approximate the actual crack growth behaviour than the data points, due to the issues discussed under figure 7.5 [1]

manner of crack growth could not be determined, due to the same measurement issue as discussed above and shown in figure 7.5.

Although for two of the experiments the exact manner of crack growth is not clear, it seems clear that crack growth can in fact continue, even if the displacement is held constant. This may also explain some of the frequency effects seen in FCG experiments. If crack growth can occur at constant load, then perhaps it matters not only what maximum load is reached, but also how long the load is above a certain threshold. For a given number of cycles, a lower frequency implies a longer time spent at high load, which might produce a different amount of crack growth.

There is also an interesting parallel between these quasi-static experiments and the earlier FCG experiments. In both cases there is a fixed amount of energy added to the system at the start of the test. During (displacement-controlled) fatigue some of this energy is constantly cycled into and out of the specimen by the fatigue machine, but the maximum total energy in the specimen only decreases. During the quasi-static test the energy is only added once, but then also decreases over time.

Thus in both cases there is an initial input of energy, part of which is dissipated by crack growth. In fact during the quasi-static tests described here the initial energy input is higher, as the displacement is increased until there is a drop in the force, whereas in the fatigue tests performed discussed earlier in this thesis, the load was chosen so that this critical force / displacement was not reached. However even though the initial energy was higher during the long duration quasi-static test (AE009-QS3) than during the fatigue tests, and the duration of the tests were comparable (18 hours for the QS tests, roughly 24 for the fatigue tests), much more crack growth occurred during the fatigue test than during the quasi-static test. Although the crack growth resistance during quasi-static growth is higher than under fatigue load (see Chapter 4), this is not enough to explain the difference in crack growth. Apparently the fact that during fatigue the load is cycled and not just held constant also plays a role.

#### 7.4. QUASI-STATIC THRESHOLD

FOR the quasi-static tests it was seen that emission of acoustic signals only started once a certain load level had been reached. Under the assumption that no crack growth can occur without acoustic emission, this observation allows the calculation of a threshold  $G$  value,  $G_{th}$ . As the force and displacement outputs were also recorded by the AE system, it was relatively straightforward to find the matching force and displacement for any given AE signal detection. The corresponding  $G$  value was then computed as:

$$G = \frac{3Pd}{2wa} \quad (7.1)$$

This is less accurate than the CC method used for the rest of this thesis (equation 3.6). However due to the smaller range of crack lengths during this test series (especially for AE003), the correct calibration factor could not be found as readily. Thus the simplicity of equation 7.1 was deemed to be acceptable, especially when comparing the AE series of test results with each other. However care should be taken when comparing the numerical SERR values from this chapter with those from previous chapters. For the previous experiments in this thesis the calibration parameter  $n$  was usually in the range



Table 7.2: Threshold SERR values measured during the quasi-static test. Values are shown for two cases: using the first AE signal with a peak amplitude over 58 dB and using the first AE signal with a peak amplitude over 62 dB. Note that for specimen AE001 the AE threshold value was 62 dB, and for AE003 the threshold was 55 dB, thus the second case allows evaluation of the effect of the lower AE threshold setting for AE003. The  $G_{Ic}$  value, determined according to the maximum force criterion of ASTM D3433, is also shown (where applicable) [1].

Experiment	$G_{th}$ (N/mm) 1st hit > 58 dB	$G_{th}$ (N/mm) 1st hit > 62 dB	$G_{Ic}$ (N/mm) ASTM D3433
AE001-QS3	0.6928	0.6928	N/A
AE001-QS4	0.7427	0.7427	1.759
AE001-QS5	0.4047	0.4047	1.314
AE003-QS2	0.2877	0.8814	N/A
AE003-QS3	0.5331	0.8294	1.534
Mean	0.532	0.7102	1.534
Standard deviation	0.171	0.1662	0.182

2–4, suggesting that the values found with equation 7.1 contain an error on the order of 30%.

As mentioned before, it was assumed that signals with a peak amplitude less than 58 dB did not correspond to crack growth, based on the results of experiment AE003-QS2. Thus the threshold  $G_{th}$  is defined in this chapter as the lowest value of  $G$  for which a signal with a peak amplitude greater than 58 dB was recorded.

For specimen AE001 an AE threshold level of 62 dB was set, which means that any signals with a peak amplitude between 58 and 62 dB were not recorded. To gauge the effect of this on the determined  $G_{th}$  value,  $G_{th}$  values were also calculated for specimen AE003, using the minimum  $G$  value for which a signal with a peak amplitude greater than 62 dB was detected. The threshold values using both a criterion of 58 dB and a criterion of 62 dB are shown in table 7.2

The measured threshold value increases when 62 dB is used as a criterion rather than 58 dB, indicating that the 62 dB AE threshold setting was too high. Using 62 dB as a criterion, AE003 seems to have a higher threshold than specimen AE001. However the difference between the mean  $G_{th}$  values for AE001 and AE003 is less than 2 times the standard deviation for the threshold value of AE001, so it can not be stated with confidence that the thresholds are in fact different.

Under quasi-static conditions it is often assumed that crack growth only occurs for  $G > G_{Ic}$ , where  $G_{Ic}$  is determined according to one of the criteria offered in ASTM standards D3433 [6] or D5528 [7]. However, as can be seen in table 7.2, using acoustic emission crack growth was detected at  $G$  values well below the ASTM-defined  $G_{Ic}$ . This suggests that although  $G_{Ic}$  is a useful value for material selection and design purposes, it should not be interpreted as the lowest  $G$  value at which cracks will grow, even under quasi-static loading.

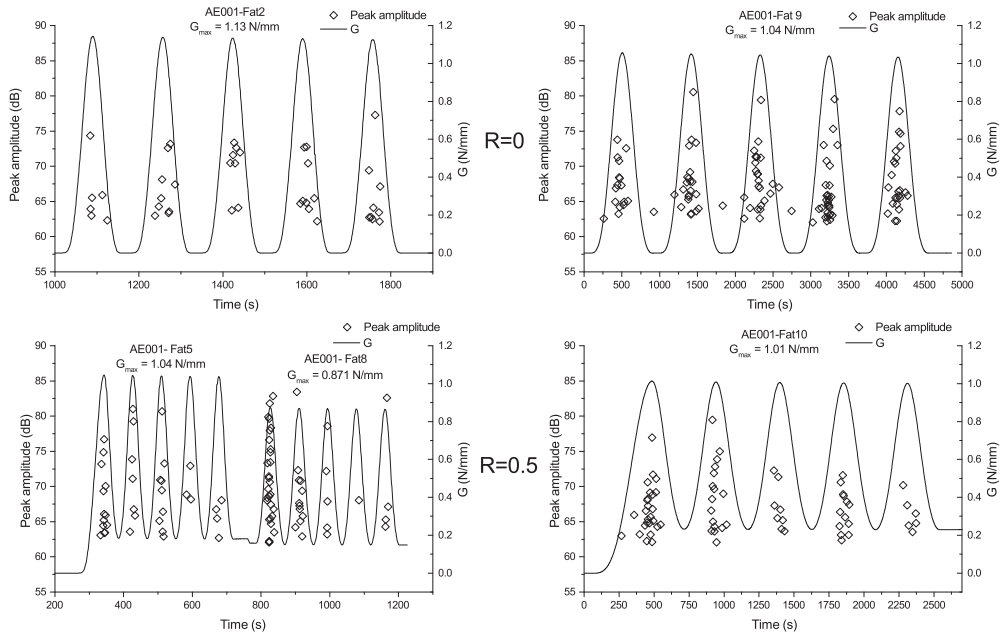


Figure 7.7: SERR and peak amplitude of AE signals for the 1mm / min fatigue tests on specimen AE001. The top row shows data for experiments conducted at  $R = 0$  and the bottom row shows data for  $R = 0.5$ . Though AE001-Fat8 seems to follow immediately after AE001-Fat5 in this representation, this was not the case in reality. The AE threshold was 62 dB.

## 7

## 7.5. FATIGUE EXPERIMENTS

IN order to investigate crack growth behaviour during fatigue, first a number of experiments were conducted on each specimen where fatigue cycles were applied with a displacement rate of 1 mm/min. This was done at both  $R = 0$  and  $R = 0.5$ . Then fatigue cycles were applied with a frequency of 5 Hz to investigate the existence of frequency effects.

The results for the low rate fatigue experiments are shown in figure 7.7 (specimen AE001) and figure 7.8 (specimen AE003). Assuming that AE hits with a peak amplitude greater than 58 dB mean crack growth, crack growth appears to occur both during loading and during unloading for specimen AE001, whereas for AE003 crack growth occurs only during loading. Crack growth appears to occur only when the  $G$  is above a certain threshold value, which will be discussed in more detail below.

For both specimens there appears to be an effect related to the  $R$ -ratio. This is most clear for the experiments on AE-003 (figure 7.8). At  $R = 0.5$  crack growth was only detected during 3 out of the 5 cycles for experiment AE003-Fat2, and in only 2 out of 5 cycles for experiment AE003-Fat4, whereas for  $R = 0$  (AE003-Fat1 and AE003-Fat3), there were multiple hits in every cycle. Also for specimen AE001 (figure 7.7) it seems that for  $R = 0$  the number of hits is roughly the same in each cycle, whereas for  $R = 0.5$  there are more hits during the first one or two cycles and fewer hits during the subsequent cycles.

The  $R$ -ratio effect appears to be stronger for specimen AE003. This is somewhat

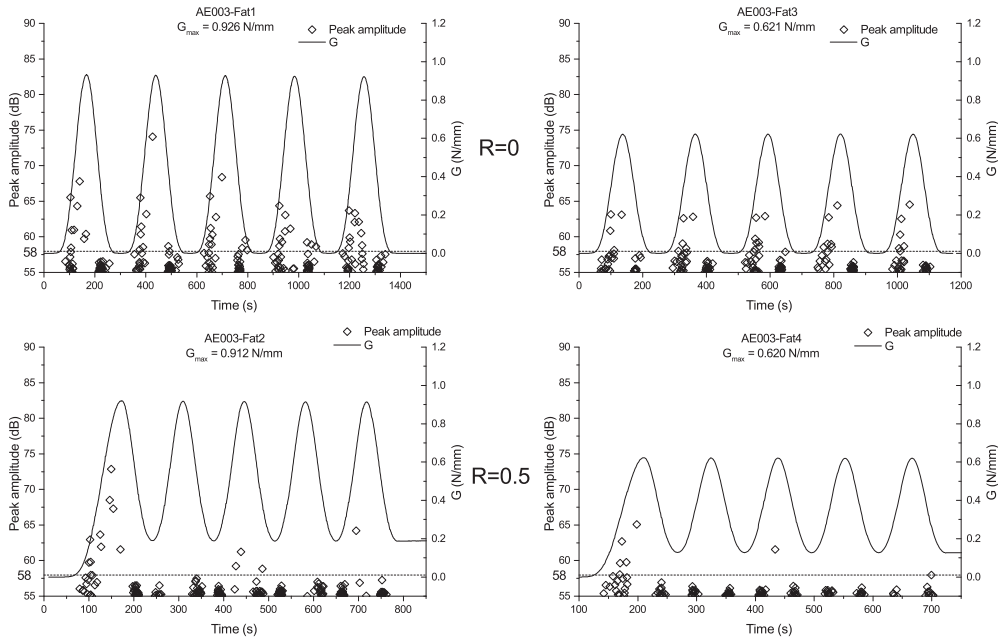


Figure 7.8: SERR and peak amplitude of AE signals for the fatigue tests on specimen AE003. The top row shows data for experiments conducted at  $R = 0$  and the bottom row shows data for  $R = 0.5$ . The AE threshold was 55 dB.

counter-intuitive, given that in absolute terms the increase of  $G_{\min}$  (and therefore the decrease of  $\Delta G$ ,  $(\Delta\sqrt{G})^2$ , and  $U_{cyc}$ ) was lower. Other than specimen variability there is no obvious hypothesis that can explain this behaviour.

Comparing specimens AE001 and AE003; during the tests on specimen AE003 fewer hits were recorded, and the peak amplitudes were lower. This is even true when  $G_{\max}$  was lower for the experiment conducted on AE001 (AE001-Fat8), than for the experiment conducted on AE003 (AE003-Fat1&2). Again specimen variability is a possible explanation. Another possible hypothesis is the effect of load history. For specimen AE001 the experiments followed quasi-static tests where the displacement was held for either 79 minutes (AE001-Fat1-5, following test AE001-QS3) or 30 minutes (AE001-Fat8-10, following AE001-QS5). In contrast the experiments on specimen AE003 (AE003-Fat1-4) were conducted after the 18.5 hour hold of experiment AE003-QS3. It is possible that during this long hold damage was created in a process zone ahead of the crack tip, which made FCG easier (i.e. require less energy per unit of growth). This would explain why the AE signals for AE003 were less energetic.

For specimen AE003 a cluster of low ( $<58$  dB) amplitude hits was detected each cycle near the minimum load, during both loading and unloading. Apart from the low amplitude, these hits do not occur when the specimen is *at* minimum load, or during the high load portion of the cycle. This suggests that these signals are related to some kind of crack opening and/or closing process and not to the crack growth itself. It is likely that these signals also occurred for specimen AE001, but were not recorded due to the higher

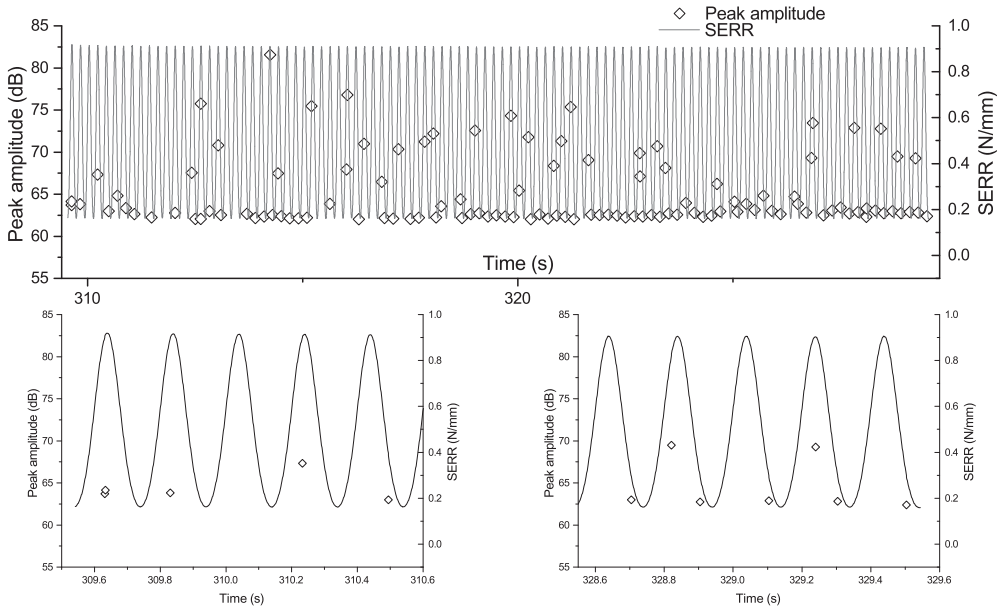


Figure 7.9: Peak amplitude and SERR values for experiment AE001-Fat7. The lower figures show the first and last 5 load cycles. AE detection threshold was 62 dB [1]

AE threshold setting of 62 dB.

From an energy point of view, it is interesting to note that the signal with the highest peak amplitude (and therefore highest energy) occurred on average for a SERR value greater than  $0.9G_{\max}$ . An exception was experiment AE003-Fat1, where the strongest signal occurred within 80% of  $G_{\max}$ . This suggests that the largest crack growth increment indeed occurs near the peak load value. However it should be noted that these signals only accounted for roughly 10-20% of the total acoustic energy received during the cycle. Thus even though the largest crack growth increment may occur near to the peak load, it does not mean that the *largest amount* of crack growth actually occurs there. After all, the total crack growth in a cycle is the summation of all the individual increments. The present results suggest that the majority of the crack growth is caused by many small increments occurring at lower load levels, rather than a single large increment occurring at or near the peak load in the cycle.

Figure 7.9 through 7.11 show the results for the 5 Hz fatigue tests. Compared to the low rate experiments there are far fewer hits per cycle, especially for AE001. Rather than having many hits per cycle there are only one or two, and in some cases there are even no hits per cycle. For AE003 again the clusters of low amplitude hits near the minimum load are seen. However compared to the low rate experiments, the amplitudes seem to be somewhat higher. This fits with the hypothesis that these signals are caused by some kind of crack opening / closing process, as a higher strain rate implies more forceful crack closure and opening. It also implies that the correct peak amplitude criterion to be used for determining the crack growth threshold may be frequency and / or strain rate dependent.

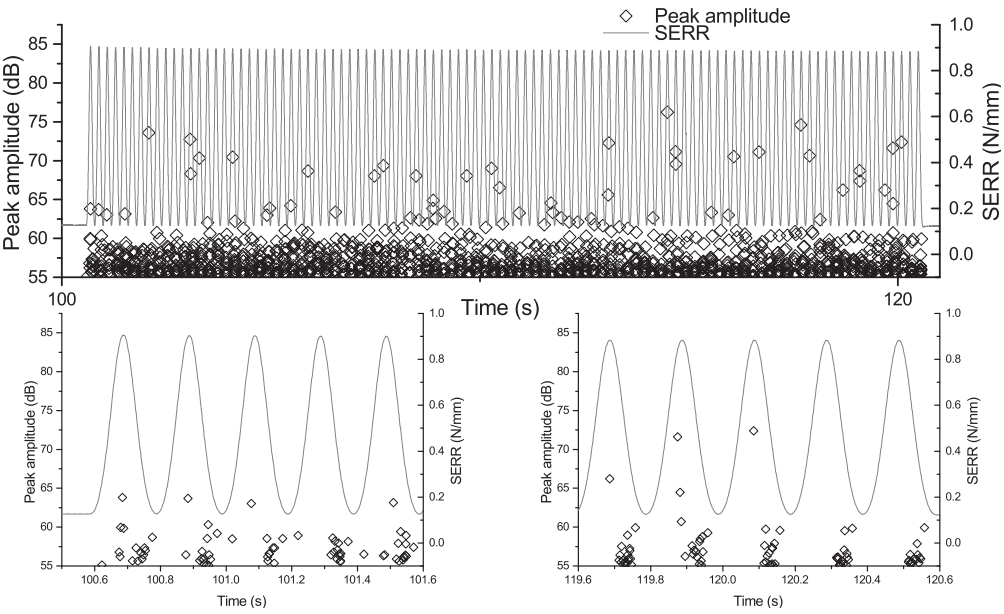


Figure 7.10: Peak amplitude and SERR values for experiment AE003-Fat5. The lower figures show the first and last 5 load cycles. AE detection threshold was 55 dB [1]

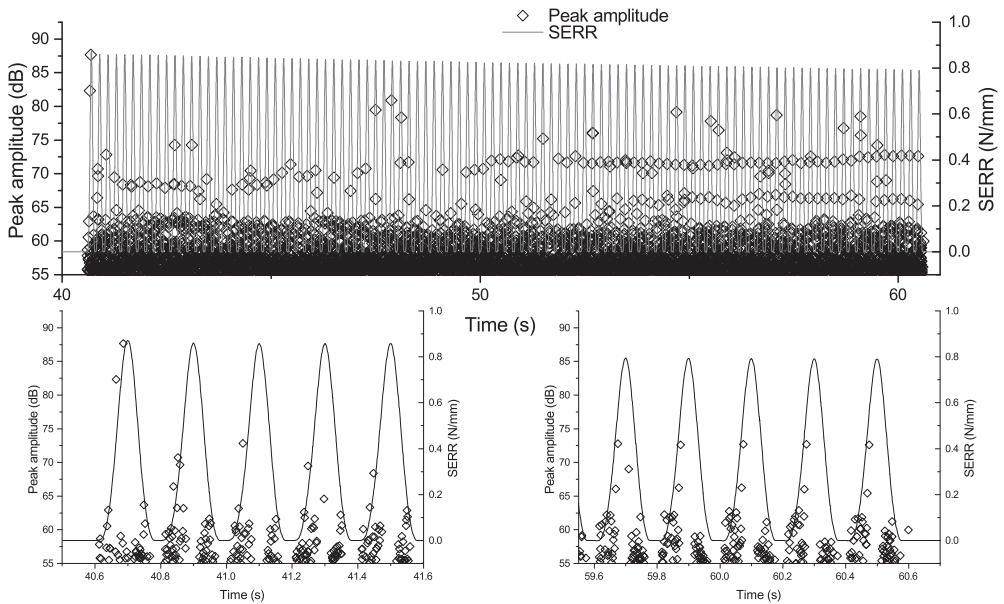


Figure 7.11: Peak amplitude and SERR values for experiment AE003-Fat6. The lower figures show the first and last 5 load cycles. AE detection threshold was 55 dB [1]

One puzzling observation is that for experiment AE003-Fat5 (5Hz,  $R = 0.42$ ) the low

amplitude signals were only observed during the unloading portion of the fatigue cycle. The reason for this is unclear, though one possibility is that the crack was not fully closed, as  $G_{\min} > 0$  during this experiment. Another option is that the signals did occur, but the amplitude was too low to cause them to be recorded.

The 5 Hz fatigue tests present an AE signal pattern that is similar to what was seen for the long duration QS hold tests. There is a more or less continuous baseline of low amplitude signals, with higher amplitude signals occurring at seemingly random intervals. For the tests at  $R > 0$  (AE001-Fat7, figure 7.9 and AE003-Fat5, figure 7.10) there were cycles where no signals were detected with a peak amplitude greater than 58 dB. From these results it is clear that crack growth does not occur every cycle, and that the crack growth rate is not a continuous function of cycle number.

The success of the existing prediction methods means that it is acceptable to use an average  $da/dN$  when investigating high-cycle fatigue. However for low cycle fatigue, and for a better overall understanding of the crack growth process, a clearer understanding of the mechanisms is needed, that can explain why the crack growth rate varies from cycle to cycle.

## 7.6. FATIGUE THRESHOLDS

As with the quasi-static experiments, a threshold value could also be determined for FCG. Again the definition of  $G_{th}$  is here: the lowest  $G$  value for which a signal with a peak amplitude greater than 58 dB (or 62 dB) was emitted. Figure 7.12 shows the threshold values measured during the low rate fatigue experiments, using both 58 dB and 62 dB peak amplitude as a criterion.

Despite the large amount of scatter it can be said that the threshold for AE003 was clearly lower than for AE001. This fits with the hypothesis proposed earlier that the long duration hold during AE003-QS3 created damage near to the crack tip, making crack growth easier. Of course specimen variability also cannot be excluded as an explanation. As would be expected, the  $R$ -ratio does not appear to affect the threshold value.

Figure 7.13 shows a comparison between the measured fatigue thresholds (using the 58 dB peak amplitude) and the values obtained from the quasi-static experiments. Although the scatter is quite large, the fatigue and quasi-static threshold values appear to match. It is also worth noting that the minimum  $G_{\max}$  values reached during the FCG tests discussed in chapter 4 were of the same order as the  $G_{th}$  values found here. This suggests that the fatigue crack growth threshold could be obtained from a quasi-static experiment, which would greatly reduce the required experimental effort. Before this can be stated with certainty however, further research is necessary to reduce the observed scatter, and to clarify what the appropriate criterion is to identify the threshold. I.e. should peak amplitude be used, and if so, which amplitude? Or should a different feature of the AE signals be used to identify crack growth? It should also be confirmed that crack growth cannot occur without causing acoustic emissions, and that any acoustic emissions that are generated are distinguishable from noise.

The threshold values measured for the 5 Hz experiments are compared to the low rate experiments in figure 7.14. Given the small number of hits, especially for specimen AE003, only tentative conclusions can be drawn from these results. However it does appear that frequency affects the crack growth threshold. This would mean that frequency

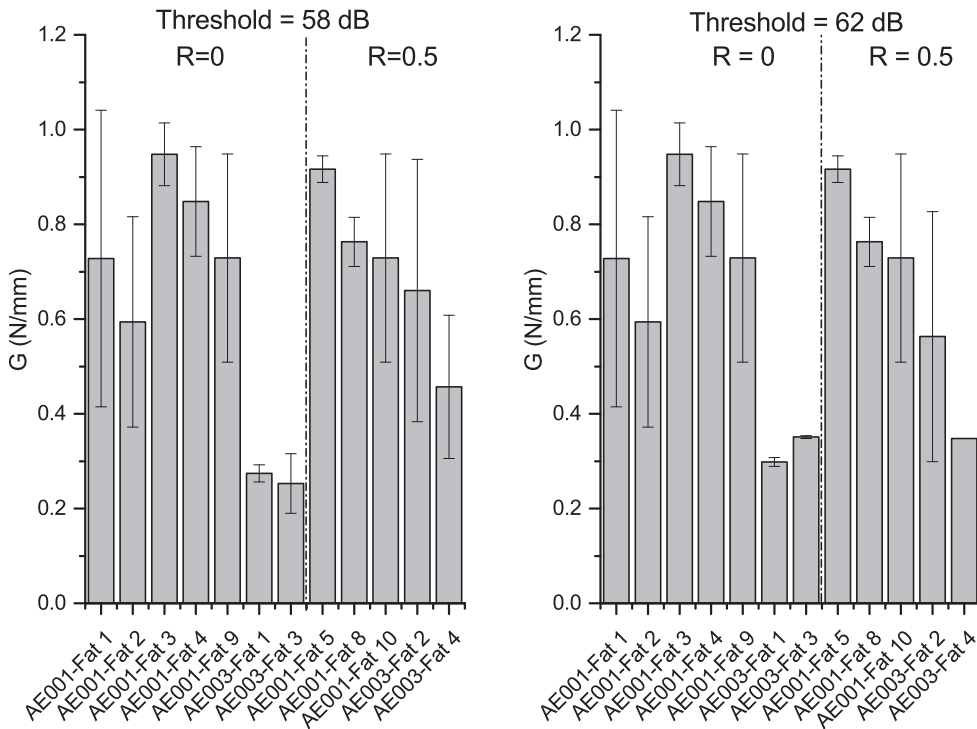


Figure 7.12: Fatigue threshold values for each fatigue experiment. The error-bars show the standard deviation. The threshold was determined by finding the lowest  $G$  value corresponding to an AE signal with a peak amplitude greater than 58 dB (left panel) or  $> 62$  dB (right panel). Each fatigue experiment represents a set of 5 cycles. Note that for specimen AE001 the AE threshold level was set to 62 dB and thus there are no differences between the left and the right panel for these experiments. For experiment AE003-Fat4 only 1 signal with a peak amplitude  $> 62$  dB was detected during the entire run of 5 cycles. This explains the lack of an error-bar for this experiment [1]

effects in fatigue are not only caused by spending a different amount of time at high load, but also by strain-rate dependence of the material response. In the present test campaign, the fatigue cycles were applied in a sinusoidal manner. However, given that both the 'dwell time' at high load, and the strain-rate appear to affect the crack growth rate, it seems likely that the pattern of the applied load matters. For example, if a trapezoidal load is applied, rather than a sinusoidal one, the load will spend more time per cycle at a high value, and the strain rates during loading and unloading will be higher. Thus a faster crack growth would be expected, due to both a longer time spent at high load, and a lower threshold value as a result of the increased strain rate.

It also appears that the crack growth threshold is not constant during fatigue, as there are large differences between the thresholds measured for the first 5 cycles and the last 5 cycles of each experiment.

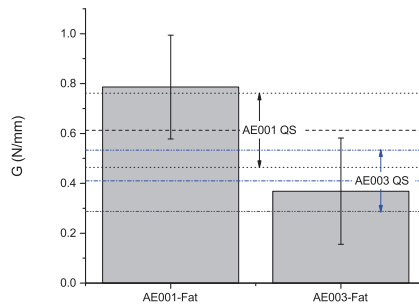


Figure 7.13: Comparison between the fatigue and quasi-static thresholds, showing the values for each specimen individually. The vertical bars show the fatigue threshold value, using 58 dB peak amplitude as the criterion. The error bars represent 1 standard deviation. Similarly the horizontal lines show the mean value  $\pm$  1 standard deviation of the quasi-static threshold (see also table 7.2) [1]

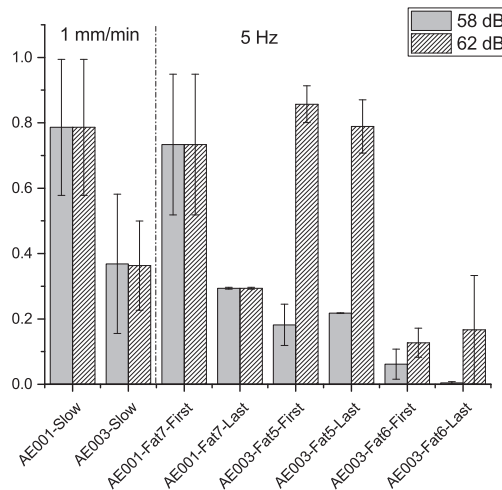


Figure 7.14: Comparison of the measured crack growth thresholds for the low rate fatigue and the 5 Hz fatigue cycles, using either 58 dB or 62 dB as the threshold criterion. For AE001 the AE threshold setting was 62 dB and so there is no difference between the 58 and the 62 dB criterion for those experiments. Threshold values were determined for the first and last 5 cycles for each 5 Hz experiment [1]

## 7.7. DISCUSSION

At present there are still some obstacles to be overcome before the AE data can be properly compared to the results presented in the previous chapters. In particular, the link between the physical crack growth processes and the received acoustic emission signals is still unclear. This makes it difficult to determine which signals indeed represent crack growth and which can be regarded as other microstructural events or noise.

This lack of understanding also prevents selection of a suitable criterion for determining the crack growth threshold,  $G_{th}$ . As was shown in this chapter, changing the peak



amplitude value used as a threshold criterion can cause large changes to the threshold value that is then found. Furthermore it should be noted that in the present research peak amplitude was selected as a criterion out of convenience. Further research should be conducted in order to confirm that peak amplitude is indeed the appropriate characteristic to use, or whether a different feature of the AE signals can more accurately be used to discriminate between crack growth and noise.

Nevertheless, it does seem clear from the results discussed in this section that, in fatigue, crack growth can occur both during loading and during unloading. The results suggest that crack growth occurs whenever the load (in terms of  $G$ ) is above a certain threshold value. It also appears that this threshold value can be determined from quasi-static tests. A remarkable feature of fatigue crack growth is that crack growth occurs, despite  $G$  not exceeding  $G_{Ic}$ . The results presented in this chapter help to explain this observation. It is not that crack growth under fatigue loading occurs at lower load levels than under quasi-static loading. Rather, under quasi-static loading, *development of a damage zone and/or crack growth also already starts for  $G$  values below  $G_{Ic}$ .*

The similarity between the fatigue and quasi-static thresholds found for these tests hold the tantalising promise that it might be possible to determine a fatigue threshold from a purely quasi-static test. This would offer a significant reduction of the time required to characterise and certify materials, as determination of the fatigue threshold currently requires long duration (and therefore expensive) tests.

However it should first be cleared up what the meaning of the threshold value in fatigue is. In section 4.4.3 it was shown that the  $dU/dN$  vs  $U_{cyc}$  behaviour that was found during the fatigue tests is incompatible with the existence of a fatigue threshold value, at least in the sense of a load value below which absolutely no crack growth occurs. On the other hand, the AE results presented here do strongly suggest that crack growth only occurs during the portion of the cycle at which the load is above a certain value.

In this chapter  $G_{th}$  was defined as the lowest  $G$  level at which AE signals were detected with a peak amplitude greater than 58 dB. Of course this does not necessarily mean there was in fact no crack growth for  $G < G_{th}$ . Thus one possibility that would reconcile the results in this chapter with the discussion in section 4.4.3 is that crack growth does in fact occur when the load is below the  $G_{th}$  as defined here, but that the resulting AE signals have a peak amplitude lower than 58 dB. Of course this case would suggest that there is in fact no absolute threshold. For practical purposes it may still be possible to define a threshold (in the sense of not exceeding a very small amount of crack growth within an operational lifetime). It may also still be possible to find the fatigue threshold on the basis of a quasi-static test in that case.

The results presented in this chapter clearly show that the fatigue crack growth rate is not constant during a single cycle; nor is crack growth an instantaneous event that occurs exactly at the peak of the load cycle. Furthermore evidence was presented that the amount of crack growth varies from cycle to cycle. When predicting the life-time of an operational structure, which is expected to last for hundreds of thousands of cycles or more, this can perhaps be ignored and an average value used instead. This does not hold however, if one wishes to gain a better understanding of the physics of fatigue crack growth.

The previous chapters have shown that there is a relationship between the applied

load on the one hand and the crack resistance and available energy on the other, but the nature of the relationship has remained unclear. The applied load itself is not constant, but continuously changes over the course of a single load cycle. Therefore to understand how it affects the resistance and the available energy, will require a better understanding of what actually happens within a single load cycle. After all, the results in this chapter have shown that crack growth is a process that involves a large part of the load cycle, or perhaps even the entire load cycle. In other words, the results in this chapter point to the need to abandon the single cycle as the smallest time-scale at which fatigue crack growth is investigated.

## REFERENCES

- [1] J. A. Pascoe, D. S. Zarouchas, R. C. Alderliesten, and R. Benedictus, *Using acoustic emission to understand fatigue crack growth within a single load cycle*, Int J Fract (2016), under review.
- [2] P. White, *Molecular dynamic modelling of fatigue crack growth in aluminium using LEFM boundary conditions*, Int J Fatigue **44**, 141 (2012).
- [3] J. Kaiser, *Erkenntnisse und folgerungen aus der messung von geräuschen bei zugbeanspruchung von metallischen werkstoffen*, Archiv für das Eisenhüttenwesen **24**, 43 (1953).
- [4] D. Bürger, *Mixed-mode Fatigue Disbond on Metallic Bonded Joints*, Phd thesis, Delft University of Technology (2015), <http://dx.doi.org/10.4233/uuid:ec4dbcd6-052d-4009-bf9e-cdcbf4614174>.
- [5] J. A. Pascoe, D. Zarouchas, and R. C. Alderliesten, *Acoustic emission during crack growth in FM94 epoxy*, (2016), available via: <http://dx.doi.org/10.4121/uuid:8cb928b4-4dc9-4420-8adc-f1273c9fd7c5>.
- [6] ASTM Standard D3433-99, *Standard test method for fracture strength in cleavage of adhesives in bonded metal joints*, (2012), ASTM International, West Conshohocken, PA, USA.
- [7] ASTM Standard D 5528/ D 5528-01, *Standard test method for mode I interlaminar fracture toughness of unidirectional fiber-reinforced polymer matrix composites*, (2007), ASTM International, West Conshohocken, PA, USA.

# 8

## CONCLUSIONS AND RECOMMENDATIONS

*'The story so far'. Maybe it's all we can ever hope for.*

Neil Gaiman - *The Sandman* Vol. 2

*The main conclusions of this thesis are summarised. This thesis has demonstrated the use of the measurement of strain energy dissipation to understand more about the crack growth processes. In relation to the conceptual model presented in Chapter 3, it was shown that the amount of energy required per unit of crack growth depends on the maximum load (i.e.  $G_{\max}$ ), whereas the amount of energy available depends on the load range  $(\Delta\sqrt{G})^2$  or  $U_{\text{cyc}}$ .*

*Recommendations are given for future research. This should focus on generating more insight into the crack growth processes, rather than on just generating more predictions of crack growth. In addition, the strain energy approach should be extended to verify whether it can also be applied to investigate the effect of loading mode, and of environmental effects other than temperature.*

## 8.1. CONCLUSIONS

THIS section summarises the main conclusions of this thesis. The following topics are discussed:

- The appropriate physical interpretation of similitude parameters based on LEFM.
- The correlation between crack growth rate and energy dissipation.
- The effect of adhesive thickness.
- The effect of temperature.
- Fatigue crack growth in a single cycle.

### 8.1.1. PHYSICAL INTERPRETATION OF LEFM PARAMETERS

Over the last five decades, the main focus of research into fatigue crack growth has been the prediction of the crack growth rate for a given load cycle. Using the similitude principle, a variety of methods have been developed that are capable of producing the desired predictions. However, it should be remembered that the similitude principle is merely a tool to determine when a valid comparison can be made between two structures. In fatigue crack growth, similitude parameters have been selected purely on the basis of their consistency, rather than on any deeper physical justification. This is the reason that models for fatigue crack growth rely on empirical correlations, with little to no explanation of the mathematical form of these relationships.

Although empirical correlations can provide good predictions if supported by appropriate experimental data, the danger is that it is unknown under which conditions similitude will no longer hold. To avoid inadvertently violating similitude, extensive test databases may be necessary, which requires large and costly test campaigns. A proper understanding of the underlying physics could help cut down the number of experiments required to calibrate models for FCG, and may also lead to more accurate modelling. The first step towards a proper understanding of the physics, is a correct understanding of how to interpret the similitude parameters that are used.

Because the only requirement of a similitude parameter is consistency (i.e. the same value of the parameter always results in the same material behaviour), the validity of a certain similitude parameter does not automatically imply a specific physical interpretation. In particular, just because  $(\Delta\sqrt{G})^2$ ,  $\Delta\sqrt{J}$ , and  $\Delta K$  are successful similitude parameters<sup>1</sup>, does not mean it is correct to interpret them as the crack driving force, as has been done recently [1, 2].

Under quasi-static load conditions Eshelby has shown that the  $J$ -integral, and thus by extension  $G$ , can be interpreted as a driving force for crack growth [3–5]. However this does not trivially carry over to the fatigue load case. In particular, under fatigue loading the load applied to the specimen is time-dependent, and thus it stands to reason that the crack driving force should also be.

<sup>1</sup> Note that for small scale yielding conditions, these parameters are equivalent.

Since the load is cyclical, it is of course not impossible that a time-independent parameter could characterise the crack driving force, so  $(\Delta\sqrt{G})^2$  and  $\Delta K$  are not disqualified on that count. However, it is mathematically impossible for  $(\Delta\sqrt{G})^2$  and  $\Delta K$  to uniquely define a load cycle. It is well established in literature, and again shown in the present thesis, that the crack growth rate is affected by the mean load. Thus any description of the crack driving force must include the mean load in the description of the driving force itself, which is something that  $(\Delta\sqrt{G})^2$  and  $\Delta K$  fail to do.

All of the above does not invalidate the use of LEFM to provide similitude parameters, nor the use of those parameters to make crack growth predictions. However it is important not to assign inappropriate physical interpretations to these parameters. Furthermore the argument above, as well as the arguments presented in section 4.2.2, should make it clear that it is inappropriate to rely on only a single similitude parameter for predicting crack growth, as at least two parameters are required to uniquely define a load cycle.

### 8.1.2. CORRELATION OF ENERGY DISSIPATION AND CRACK GROWTH RATE

A strong correlation was found between the strain energy dissipation per cycle and the crack growth rate. This correlation has also been shown for mode I delamination in CFRP [6, 7] and mode I fatigue crack growth in aluminium [8]. From the measured energy dissipation, both the total amount of energy available for crack growth, and the amount of energy required per unit of crack growth ( $G^*$ ) can be determined.

$G^*$  can be interpreted as the material's crack growth resistance. It was found that  $G^*$  is not constant during a fatigue test. The experimental results showed a linear correlation between  $G^*$  and  $G_{\max}$ . The most likely hypothesis to explain this is that at higher  $G_{\max}$  values, more plasticity is created in the vicinity of the crack tip, and/or damage mechanisms are activated that do not contribute to crack growth. As a result more energy is dissipated per unit of crack growth. Fractographic evidence was presented that supported this hypothesis.

Since  $G^*$  only represents the material's crack growth resistance, to find the actual crack growth rate it is also necessary to know how much energy is available for crack growth. From the experiments it was found that for a fixed value of  $G^*$ , the energy dissipation per cycle,  $dU/dN$ , (which is assumed to equal the energy available for crack growth) shows a power-law correlation with  $(\Delta\sqrt{G})^2$ ,  $\Delta G$ ,  $U_{tot}$ , or  $U_{cyc}$ . The coefficients and exponents of these correlations both appear to be a linear function of  $G^*$ . However, more statistical analysis and possibly more experimental data is necessary to confirm this.

In terms of the traditional LEFM parameters, it appears that  $G_{\max}$  provides a measure of the material's crack growth resistance in a given cycle, and  $(\Delta\sqrt{G})^2$  provides a measure of the amount of available energy. More research is needed to find the actual relationships between the applied load on the one hand and the resistance and available energy on the other.

### 8.1.3. EFFECT OF THICKNESS

The effect of changing the adhesive thickness was investigated by producing specimens with three different adhesive thicknesses. It was found that for the range of thicknesses

tested, adhesive thickness does not affect the relationship between applied load and crack growth resistance (i.e.  $G^*$  vs  $G_{\max}$ ). In contrast, the relationship between applied load and energy dissipation for a fixed  $G^*$ , (i.e.  $dU/dN$  vs  $(\Delta\sqrt{G})^2$ ) is affected by adhesive thickness. At increased thickness more energy will be dissipated for a given  $(\Delta\sqrt{G})^2$  value. Combined with the lack of change in the  $G^*$  vs  $G_{\max}$  relationship this results in a faster crack growth rate for a given load cycle. For a given load cycle the resistance to crack growth stays the same, but the amount of energy available increases.

Fatigue crack growth in an adhesive bond was also compared to delamination in GFRP specimens. The same epoxy resin was used as respectively adhesive and matrix material. Again the  $G^*$  vs  $G_{\max}$  relationship was not affected, whereas the  $dU/dN$  vs  $(\Delta\sqrt{G})^2$  relationship was. This suggests that the relationship between applied load and crack growth resistance is mainly a material property, whereas the relationship between applied load and available energy for crack growth is also related to specimen geometry.

#### 8.1.4. EFFECT OF TEMPERATURE

To investigate the effect of changing material properties, a number of fatigue crack growth experiments were performed at a temperature of 80 °C. For the majority of these experiments adhesive failure was observed, rather than cohesive failure. This means that the results of these experiments are not directly comparable to the results obtained at room temperature.

At 80 °C  $G^*$  for a given  $G_{\max}$  was higher than at room temperature. This is likely mainly due to the switch from a cohesive failure mode to an adhesive one. For the experiments where the failure mode was still cohesive, the  $G^*$  vs  $G_{\max}$  curves were close to the room temperature curves. Regardless of whether the failure mode changed or not, at 80 °C there was no longer a correlation between  $dU/dN$  vs  $U_{cyc}$  for a given  $G^*$ . Curiously, there still appeared to be a correlation between  $dU/dN$  and  $(\Delta\sqrt{G})^2$ . Why this should be so is not clear.

In other words, the temperature appears to have a small effect on the relationship between applied load and resistance, unless the failure mode changes, in which case the effect is large. On the other hand the temperature strongly affects the relationship between applied load and the amount of energy available.

Thus for a given load cycle (i.e. combination of  $G_{\max}$  and  $(\Delta\sqrt{G})^2$ ), at 80 °C the resistance to crack growth ( $G^*$ ) is higher than at room temperature, especially if the failure mode becomes adhesive, rather than cohesive. However, the amount of energy available for crack growth is also higher. Since the amount of available energy increases more quickly than the resistance, the end result is that for a given load cycle the crack growth will be faster at 80 °C than at room temperature.

#### 8.1.5. FATIGUE CRACK GROWTH IN A SINGLE CYCLE

Acoustic emission was used to investigate when fatigue crack growth occurs within a single cycle. The results are somewhat tentative due to the large amounts of scatter, pointing to a need to refine the experimental technique. Nevertheless the potential of the technique was shown, and some preliminary conclusions can be drawn.

It appears the crack growth can occur both during the loading portion and the un-

loading portion of the fatigue cycle. Acoustic emissions thought to be caused by crack growth were only detected when the load (in terms of  $G$ ) was above a certain threshold. This suggests the existence of a load threshold, and that the portion of the fatigue cycle below that load does not contribute to crack growth. However, results from earlier fatigue tests suggest that the entire load cycle is in fact important. One way to reconcile these findings is if crack growth can occur below the load threshold identified during the acoustic emission tests. This is possible if crack growth occurring below the load threshold does not emit acoustic signals, or emits signals that were not detected, or were discarded, with the equipment settings used in this experiment. At present, these possibilities can not be discounted. Further work is necessary in order to be able to match the received acoustic signals to specific mechanisms and events in the material.

For many practical purposes a threshold value is defined which does not correspond to absolutely no crack growth occurring, but merely to ensuring that the amount of crack growth will remain sufficiently small during the operational life time of the structure. Even if acoustic emission can not detect all crack growth, it may be useful to establish such an 'engineering' threshold. Comparing quasi-static and fatigue tests, acoustic signals were detected when the load was increased above the same  $G$  value in both cases. This suggests that a fatigue threshold can be determined from a purely quasi-static test. It also means that the physical interpretation of  $G_{Ic}$  should be re-evaluated, as even under quasi-static conditions crack growth occurs for  $G < G_{Ic}$ .

### 8.1.6. FINAL CONCLUSIONS

The results presented in this thesis show that measuring strain energy dissipation is a useful method to characterise fatigue crack growth, and allows more insight into the underlying physical processes. Using strain energy allows one to separate the effect of merely applying a different load cycle from actual changes in the material behaviour. Furthermore, the strain energy approach presented in this thesis allowed the resistance to crack growth and the energy available for crack growth to be examined separately.

The conceptual model introduced in section 3.1, and shown schematically in figure 8.1, works well as a framework for understanding fatigue crack growth. According to this model the amount of crack growth in a cycle follows from the total amount of energy available for crack growth, and the amount of energy required per unit of crack growth (i.e. the crack growth resistance). Both the available energy and the crack growth resistance depend on the applied load cycle. In particular, the crack growth resistance appears to be related the maximum load, whereas the available energy appears to depend on the load range and/or the cyclic work applied during the load cycle.

The resistance to crack growth seems to mainly depend on  $G_{max}$ , i.e. on the peak load reached in a cycle. The robustness of the relationship between  $G^*$  and  $G_{max}$  suggests that it is principally a material parameter. On the other hand the amount of available energy seems to depend mainly on  $(\Delta\sqrt{G})^2$  or  $U_{cyc}$ . This relationship appears to depend more on geometry and environmental factors, rather than purely on the material.

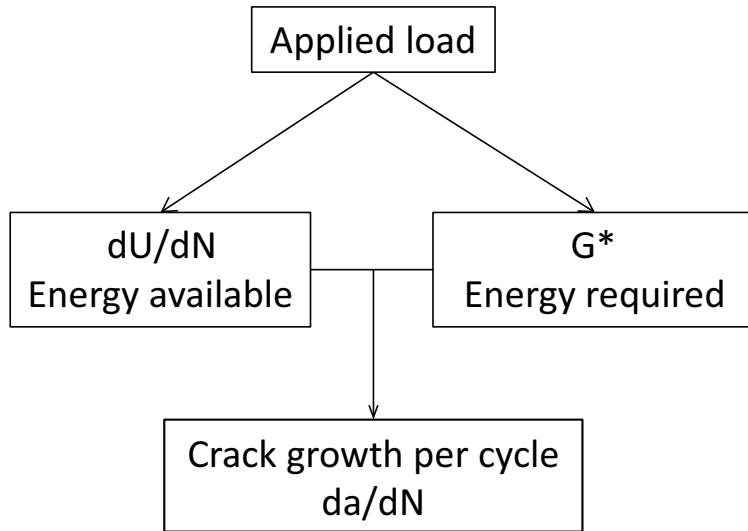


Figure 8.1: Diagram of the conceptual model for fatigue crack growth developed in this thesis.

## 8.2. RECOMMENDATIONS

This thesis has highlighted the need to improve the understanding of the physical processes underlying fatigue crack growth. It has attempted to provide some steps towards doing this, but much further research still needs to be done. This section will provide the author's view on what directions future research into fatigue crack growth should take.

### 8.2.1. CRITERIA FOR A GOOD FATIGUE MODEL

First of all it is good to establish what criteria a good model of fatigue crack growth should meet, in order to provide a good understanding of fatigue crack growth, rather than just a good prediction.

Firstly, a good model should relate the crack growth rate to a complete and unique description of the load cycle. If an incomplete description of the load cycle is used (e.g. only  $G_{\max}$  or only  $(\Delta\sqrt{G})^2$  by themselves), a rigorous justification should be given why the other information about the load cycle can be neglected. In light of the results and discussion presented in this thesis, it seems very unlikely that a good model for understanding crack growth can be formulated without taking the entire load cycle into account.

Secondly, a good model should be able to explain why only a finite amount of crack growth occurs during a single fatigue cycle. If the load cycle is described in terms of the work performed during that cycle, this condition is easy to fulfil. However if a model is based on some measure of the crack driving *force* then this point requires more attention. A force induces an acceleration, and not simply a displacement. Thus to correctly model the fact that the amount of crack growth in a single cycle is finite, some kind of time integral of the crack driving force would be required.



### 8.2.2. FUTURE RESEARCH DIRECTIONS

The above criteria apply regardless of which approach to understanding fatigue crack growth is chosen. To continue specifically with the strain energy approach used in this thesis, the next step would be to gain a better understanding of how the applied load affects the required and available energies. This thesis has shown there is a relationship between  $G^*$  and  $G_{\max}$ , and between  $dU/dN$  and  $(\Delta\sqrt{G})^2$  or  $U_{cyc}$ . However why these relationships exist, and why they have the mathematical form that was found, is not yet clear. Thus the first order of business should be to investigate these relationships.

Understanding these relationships requires a better understanding of the micro-mechanics of crack growth, which can be developed analytically, numerically, and experimentally. Analytically, continuum mechanics and a proper application of the configurational force approach may provide a mathematical framework for interpreting the results from this thesis. Additionally, analytical micro-mechanical approaches may help relate a given far-field load to a specific amount of energy dissipation at the crack tip.

If the crack-tip geometry is too complex to investigate using analytical approaches, numerical approaches may offer a solution. In particular, a multi-scale approach may help to understand how a far-field load translates to a local strain energy distribution and energy dissipation at the crack tip. At present a challenge that needs to be overcome before good numerical models can be made, is that there is a lack of good models of the material behaviour, especially for adhesives. Even bulk material properties are difficult to find for adhesives. When they can be found, it is unclear how to translate these properties to the behaviour of a thin adhesive film such as found in an adhesive bond. New experimental procedures are needed that can provide the required input for numerical models.

Experimental methods should be used not only to provide material models for use in numerical analysis, but also to better characterise the crack growth process. An obvious step would be to apply the procedures used in this thesis to characterise crack growth in other material types, and under different load and environmental conditions; e.g. to examine the effect of loading-mode, or of humidity. Further data is also required to properly validate some of the preliminary conclusions of this thesis, e.g. the difference in delamination growth behaviour for different fibre angles in GFRP.

Apart from that, more experimental data is needed on fatigue crack growth behaviour within a single cycle. This thesis has shown that acoustic emission is a promising technique to gain more insight on this matter, but monitoring the crack tip at a very high magnification (in an SEM if necessary and possible) during an entire load cycle may also be useful. The magnification should be high enough to be able to reliably identify the amount of crack growth that occurs during a single fatigue cycle, i.e. on the order of  $10^{-4} - 10^{-6}$  mm/cycle. The time resolution of the crack tip measurements should ideally be such that there are multiple measurements during a single cycle. This would allow a full characterisation of the crack growth behaviour, which at present is usually limited to the average behaviour over a course of a single cycle, which itself is derived from the average behaviour over some number of cycles (in this thesis: 100 – 1000). Consideration should also be given to the necessity of measuring the crack surface area, rather than just the crack length. Of course the analytical, numerical, and experimental approaches are not exclusive, but should be pursued in parallel so that the various approaches can

inform each other.

### 8.2.3. CONCRETE NEXT STEPS

The previous section has given a broad overview of the kinds of research that are needed to in order to develop a more complete understanding of fatigue crack growth. But what are the immediate follow-ups to this thesis that hold the greatest promise to deliver results? In the author's view, the most pressing concern is to elucidate the relationship between the applied load and the crack growth resistance and the available energy.

This could be approached by a strategy based on the work of Eshelby [3–5]. Eshelby used physical principles to provide a justification for interpreting  $G$  as a driving force for crack growth under quasi-static conditions. By means of the energy momentum tensor, Eshelby was able to relate a far-field load to a local driving force on discontinuities in the material. Under quasi-static load, the far-field loading can be regarded as constant, resulting in a constant driving force.

In fatigue the far-field load is time-dependent, and therefore the crack driving force is as well. Thus Eshelby's work should be extended in order to be able to take this time-dependence into account. In this way a time-dependent driving force can hopefully be derived based on the time-dependent far-field load. Once a time-dependent expression for the driving-force is obtained, the acceleration of the crack tip can be found. The acceleration can then be integrated to provide the crack growth behaviour over the desired number of cycles.

To validate the model(s) developed based on this configurational force approach experimental results are needed that are able to describe the evolution of the crack over the course of a single cycle. These should be obtained taking into account the points raised in the previous section.

Over the past decades, research into fatigue crack growth, especially in adhesives and FRP composites, has focussed on generating predictions. This skips the necessary intermediate steps of properly characterising and understanding what is happening in the material. It is the author's hope that this thesis will contribute to a renewed interest in generating not mere predictions of fatigue crack growth, but true understanding.

## REFERENCES

- [1] R. Jones, A. J. Kinloch, and W. Hu, *Cyclic-fatigue crack growth in composite and adhesively-bonded structures: The FAA slow crack growth approach to certification and the problem of similitude*, Int J Fatigue **88**, 10 (2016).
- [2] W. Ochensberger and O. Kolednik, *Physically appropriate characterization of fatigue crack propagation rate in elastic-plastic materials using the J-integral concept*, Int J Fract **192**, 25 (2015).
- [3] J. D. Eshelby, *The force on an elastic singularity*, Philosophical Transactions of the Royal Society of London A: Mathematical, Physical and Engineering Sciences **244**, 87 (1951).
- [4] J. D. Eshelby, *Energy relations and the energy-momentum tensor in continuum me-*

- chanics*, in *Inelastic behaviour of solids*, edited by M. Kanninen, W. Adler, A. Rosenfield, and R. Jaffee (McGraw-Hill, New York, 1970).
- [5] J. D. Eshelby, *The elastic energy-momentum tensor*, Journal of Elasticity **5**, 321 (1975).
- [6] L. Yao, R. C. Alderliesten, M. Zhao, and R. Benedictus, *Discussion on the use of the strain energy release rate for fatigue delamination characterization*, Composites Part A **66**, 65 (2014).
- [7] L. Amaral, L. Yao, R. Alderliesten, and R. Benedictus, *The relation between the strain energy release in fatigue and quasi-static crack growth*, Eng Fract Mech **145**, 86 (2015).
- [8] D. Pasman, *Fatigue crack growth in solid round metallic bars with a shoulder fillet* (Delft University of Technology, Delft, 2015) MSc thesis.



**A**

## **CURVE FIT PARAMETERS AND ADDITIONAL DATA**

Mean values and standard deviations of the measured  $R_p$  and  $R_d$  values for the experiments presented in this thesis are shown in tables A.1 through A.3.

Table A.1: Mean values and standard deviation of  $R_p$  and  $R_d$  for the standard thickness room temperature fatigue tests. The grouping used in presentation of the data is also shown.

Specimen	$R_d$		$R_p$		Group
	Mean	Standard deviation	Mean	Standard deviation	
B-001-II	0.10	$4.0 \cdot 10^{-4}$	0.036	0.0060	$R = 0.036$
B-002-I	0.88	$4.6 \cdot 10^{-4}$	0.86	0.0015	$R = 0.86$
B-002-II	0.74	$3.5 \cdot 10^{-4}$	0.61	0.015	$R = 0.61$
C-001-I	0.33	0.0010	0.29	0.0047	$R = 0.29$
C-002-D	0.67	0.0087	0.61	0.010	$R = 0.61$
D-002-I	0.29	$2.8597 \cdot 10^{-4}$	0.29	0.0017	$R = 0.29$
E-001-I	0.29	0.012	0.24	0.012	$R = 0.29$
E-001-II	0.29	$3.6 \cdot 10^{-4}$	0.27	0.0021	$R = 0.29$
E-002-I	$2.3 \cdot 10^{-4}$	$6.3 \cdot 10^{-4}$	-0.022	0.0056	$R = 0.036$
E-002-II	$-9.3 \cdot 10^{-5}$	$4.5 \cdot 10^{-4}$	0.014	0.0047	$R = 0.036$
E-003-I	0.61	$7.6 \cdot 10^{-4}$	0.60	0.0029	$R = 0.61$
E-003-II	0.61	$3.94 \cdot 10^{-4}$	0.62	0.0027	$R = 0.61$

Table A.2: Mean values and standard deviation of  $R_p$  and  $R_d$  for the increased thickness room temperature fatigue tests. Series G contained 2 adhesive layers, and series H contained 1.5 layers.

Specimen	$R_d$		$R_p$	
	Mean	Standard deviation	Mean	Standard deviation
G-002-I	0.29	0.0015	0.25	0.0043
G-006-III	0.036	$3.7 \cdot 10^{-4}$	$-2.8 \cdot 10^{-4}$	0.015
G-008-I	0.61	$7.4 \cdot 10^{-4}$	0.47	0.0047
G-009-I	0.61	$6.2 \cdot 10^{-4}$	0.56	0.0043
G-010-I	0.86	$6.0 \cdot 10^{-4}$	0.82	0.0014
H-002-I	0.033	0.0012	0.0054	0.0067
H-003-I	0.29	$8.4 \cdot 10^{-4}$	0.24	0.0038
H-006-I	0.61	$6.9 \cdot 10^{-4}$	0.56	0.0040
H-008-I	0.86	$4.04 \cdot 10^{-4}$	0.83	0.0012

Crack length versus number of cycles was fit according to:

$$a = \alpha N^\beta \quad \text{or} \quad \alpha N^\beta + \gamma \quad (\text{A.1})$$

The obtained curve fit parameters are shown in tables A.4 through A.6. A value  $\gamma = 0$  implies that a two-parameter power-law was selected as the model to be used in the curve fit.

Table A.3: Mean values and standard deviation of  $R_p$  and  $R_d$  for the 80 °C fatigue tests.

Specimen	$R_d$		$R_p$	
	Mean	Standard deviation	Mean	Standard deviation
T-001-I	-0.0020	$8.1 \cdot 10^{-4}$	-0.030	0.0091
T-002-I	0.29	$7.8 \cdot 10^{-4}$	0.12	0.0051
T-002-II	0.29	$6.6 \cdot 10^{-4}$	0.29	0.0038
T-003-I	0.61	$7.3 \cdot 10^{-4}$	0.53	0.0036
T-003-II	0.61	$3.9 \cdot 10^{-4}$	0.56	0.0032

Table A.4: Curve-fit parameters for the  $a$  versus  $N$  functions for the standard thickness room temperature fatigue tests.

Specimen	$\alpha$	$\beta$	$\gamma$
B-001-II	93.28	0.03884	0
B-002-I	54.49	0.016	0
B-002-II	79.25	0.01556	0
C-001-I	47.55	0.04882	0
C-002-D	49.15	0.03588	0
D-002-I	535	0.009855	-464.1
E-001-I	61.95	0.04621	-20.21
E-001-II	54.69	0.0532	34.41
E-002-I	-248.9	-0.0234	289.1
E-002-II	30.99	0.07673	80.28
E-003-I	13.5	0.08129	37.16
E-003-II	15.63	0.08088	57.42

Similarly the strain energy versus number of cycles was fit according to:

$$U = \alpha N^\beta \quad \text{or} \quad \alpha N^\beta + \gamma \quad (\text{A.2})$$

The obtained curve fit parameters are shown in tables A.7 through A.12. A value  $\gamma = 0$  implies that a two-parameter power-law was selected as the model to be used in the curve fit.

For the compliance calibration method used to calculate the SERR compliance calibration parameters are required, as described in ASTM D5528 [2]. The parameters used in this thesis are listed in tables A.13 through A.15

Table A.5: Curve-fit parameters for the  $a$  versus  $N$  functions for the increased thickness fatigue tests [1].

Specimen	$\alpha$	$\beta$	$\gamma$
G-002-I	42.79	0.03788	0
G-006-III	0.2818	0.3663	138.2
G-008-I	0.009334	0.5101	58.73
G-009-I	6.024	0.1219	39.56
G-010-I	61.01	0.0003143	0
H-002-I	43.79	0.04914	0
H-003-I	1.72	0.2145	57.72
H-006-I	0.00911	0.5406	58.42
H-008-I	0.004994	0.52863	60.9

Table A.6: Curve-fit parameters for the  $a$  versus  $N$  functions for the 80 °C fatigue tests.

Specimen	$\alpha$	$\beta$	$\gamma$
T-001-I	36.81	0.06456	0
T-002-I	41.98	0.05123	0
T-002-II	72.51	0.03946	0
T-003-I	39.63	0.03812	0
T-003-II	65.47	0.03347	0

Table A.7: Curve-fit parameters for the  $U_{cyc}$  versus  $N$  functions for the standard thickness room temperature fatigue tests.

Specimen	$\alpha$	$\beta$	$\gamma$
B-001-II	1858	-0.136	0
B-002-I	345	-0.061	0
B-002-II	492.1	-0.1133	0
C-001-I	1528	-0.1248	0
C-002-D	749.6	-0.1013	0
D-002-I	1812	-0.131	0
E-001-I	1355	-0.138	-33.59
E-001-II	1961	-0.1475	8.262
E-002-I	1679	-0.1482	-31.65
E-002-II	1360	-0.1096	-82.15
E-003-I	701.1	-0.1017	-27.02
E-003-II	1479	-0.02712	-839.8



Table A.8: Curve-fit parameters for the  $U_{tot}$  versus  $N$  functions for the standard thickness room temperature fatigue tests.

Specimen	$\alpha$	$\beta$	$\gamma$
B-001-II	22.33	-0.3223	0
B-002-I	686.9	-0.03044	0
B-002-II	960.2	-0.2099	0
C-001-I	107.4	-0.1248	0
C-002-D	394.2	-0.09102	0
D-002-I	2005	-0.1322	0
E-001-I	1377	-0.1316	-44.43
E-001-II	2099	-0.1439	-3.85
E-002-I	1679	-0.1482	-31.6
E-002-II	1357	-0.1085	-86.24
E-003-I	1197	-0.05165	-361.1
E-003-II	6403	-0.007873	-5456

Table A.9: Curve-fit parameters for the  $U_{cyc}$  versus  $N$  functions for the increased thickness fatigue tests.

Specimen	$\alpha$	$\beta$	$\gamma$
G-002-I	729.7	-0.09976	-83.11
G-006-III	1912	-0.1553	-37.7
G-008-I	672.2	-0.1284	0
G-009-I	977	-0.18888	55.53
G-010-I	-0.2288	0.1686	79.5
G-010-II	4824	-0.6333	104
H-002-I	972.9	-0.155	-9.965
H-003-I	841.6	-0.1311	-10.24
H-006-I	604.3	-0.1319	23.12
H-008-I	7986	-0.5571	111

Table A.10: Curve-fit parameters for the  $U_{tot}$  versus  $N$  functions for the increased thickness fatigue tests.

Specimen	$\alpha$	$\beta$	$\gamma$
G-002-I	775.7	-0.08145	-145.4
G-006-III	1972	-0.1609	-27
G-008-I	890.4	-0.1314	0
G-009-I	-1325	0.01719	1857
G-010-I	-	-	-
G-010-II	4619	-0.53	329
H-002-I	972.1	-0.1547	-10.3
H-003-I	859.3	-0.124	-20.2
H-006-I	765	-0.08141	-71.26
H-008-I	10540	-0.4644	359.7

Table A.11: Curve-fit parameters for the  $U_{cyc}$  versus  $N$  functions for the 80 °C fatigue tests.

Specimen	$\alpha$	$\beta$	$\gamma$
T-001-I	2430	-0.3792	54.42
T-002-I	768.9	-0.2785	33.8
T-002-II	496.5	-0.0758	-84.74
T-003-I	418.3	-0.1809	32.32
T-003-II	1122	-0.2408	65.41

Table A.12: Curve-fit parameters for the  $a$  versus  $N$  functions for the 80 °C fatigue tests.

Specimen	$\alpha$	$\beta$	$\gamma$
T-001-I	2625	-0.3879	35.16
T-002-I	773.5	-0.2773	34.09
T-002-II	578.6	-0.06143	-151.5
T-003-I	500.6	-0.1555	33.77
T-003-II	1596	-0.2425	100.7

Table A.13: CC Correction parameters for the room temperature specimens.

Specimen	$n$
B-001-II	3.267
B-002-I	1.863
B-002-II	3.936
C-001-I	3.198
C-002-D	2.741
D-002-I	3.122
E-001-I	2.832
E-001-II	3.769
E-002-I	3.060
E-002-II	3.868
E-003-I	3.160
E-003-II	3.635

Table A.14: CC Correction parameters for the increased thickness specimens.

Specimen	$n$
G-002-I	3.887
G-006-III	2.909
G-008-I	3.388
G-009-I	2.696
G-010-I	3
H-002-I	3.14
H-003-I	2.467
H-006-I	2.696
H-008-I	2.98

Table A.15: CC Correction parameters for the increased temperature tests.

Specimen	$n$
T-001-I	2.316
T-002-I	2.898
T-002-II	3.027
T-003-I	3.183
T-003-II	4.113

## REFERENCES

- [1] N. Zavatta, *Influence of adhesive thickness on adhesively bonded joints under fatigue loading*, (2015), MSc thesis, Università di Bologna, available from [http://amslaurea.unibo.it/9713/1/zavatta\\_nicola\\_tesi.pdf](http://amslaurea.unibo.it/9713/1/zavatta_nicola_tesi.pdf).
- [2] ASTM Standard D 5528/ D 5528-01, *Standard test method for mode I interlaminar fracture toughness of unidirectional fiber-reinforced polymer matrix composites*, (2007), ASTM International, West Conshohocken, PA, USA.

# B

## EFFECT OF $R$ -RATIO FOR CONSTANT $(\Delta\sqrt{G})^2$ AND $\Delta G$

From the definitions of  $R$  and  $G$ , it follows that:

$$G_{\min} = R^2 G_{\max} \quad (\text{B.1})$$

$$\Delta G = (1 - R^2) G_{\max} \quad (\text{B.2})$$

$$(\Delta\sqrt{G})^2 = (1 - R)^2 G_{\max} \quad (\text{B.3})$$

$$(\text{B.4})$$

Thus when keeping  $\Delta G$  constant and changing the  $R$ -ratio one has

$$\Delta G_2 = \Delta G_1 \quad (\text{B.5})$$

$$(1 - R_2^2) G_{\max,2} = (1 - R_1^2) G_{\max,1} \quad (\text{B.6})$$

$$G_{\max,2} = \frac{(1 - R_1^2)}{(1 - R_2^2)} G_{\max,1} \quad (\text{B.7})$$

or, setting  $R_1 = 0, R_2 = R$

$$G_{\max} = \frac{1}{(1 - R^2)} G_{\max, R=0} \quad (\text{B.8})$$

Similarly, for constant  $(\Delta\sqrt{G})^2$

$$G_{\max} = \frac{1}{(1 - R)^2} G_{\max, R=0} \quad (\text{B.9})$$

The mean  $G$  is given by

$$\frac{1 + R^2}{2} G_{\max} \quad (\text{B.10})$$

Since

$$\frac{1}{(1 - R)^2} > \frac{1}{(1 - R^2)} \quad (\text{B.11})$$

changing  $R$  while keeping  $(\Delta\sqrt{G})^2$  constant has a larger effect on  $G_{\max}$ , and therefore also on the mean  $G$  value, than changing  $R$  while keeping  $\Delta G$  constant. In other words, the ‘ $R$ -ratio effect’ when using  $(\Delta\sqrt{G})^2$  as a similitude parameter will be larger than when using  $\Delta G$ .

With regards to the cyclic energy one can write:

$$U_{cyc} = \frac{1}{2} P_{\max} d_{\max} - \frac{1}{2} P_{\min} d_{\min} \quad (\text{B.12})$$

$$= (1 - R^2) P_{\max} d_{\max} \quad (\text{B.13})$$

$$= (1 - R^2) \frac{G_{\max}}{\eta} \quad (\text{B.14})$$

$$\eta = \frac{\frac{2wa}{n}}{\quad} \quad (\text{B.15})$$

using equation 3.6 for  $G$ .

Thus if keeping  $\Delta G$  constant and changing  $R$ , and keeping in mind equation B.8, one has

$$U_{cyc} = (1 - R^2) \frac{G_{\max}}{\eta} \quad (\text{B.16})$$

$$= \frac{(1 - R^2)}{(1 - R^2)} \frac{1}{\eta} G_{\max, R=0} \quad (\text{B.17})$$

$$U_{cyc} = \frac{1}{\eta} G_{\max, R=0} \quad (\text{B.18})$$

In other words, if  $\Delta G$  is constant,  $U_{cyc}$  is also constant, for any  $R$  ratio, whereas  $G_{\max}$  and therefore  $G^*$  will increase.

# ACKNOWLEDGEMENTS

Although a PhD thesis is supposedly a proof of mastery for a single person, producing a PhD thesis is by no means a solo effort. On these pages I'd like to thank all those who made this thesis possible.

First of all, René Alderliesten, my daily supervisor. Thank you for your support and interest. Thank you for all the discussions, whether they were scheduled or 2 minute quick questions that turned into half-hour debates. Thank you for having a door that was always open, despite all your other responsibilities.

Next my promotor, Rinze Benedictus. Thank you for your interest, not only in my research, but in my development as a person and professional scientist as well. Thank you also for the trust you placed in me.

There is a lot of paperwork surrounding the PhD process, from employment contracts to travel requests, and the only reason I was able to navigate it smoothly was our department secretary, Gemma. Gemma, thank you!

My PhD thesis involved a lot of lab-work, which would have been impossible without the help of the lab and workshop technicians, and the lab secretary. Bart, Berjan, Berthil, Bob, Cees, Ed, Frans, Fred, Gertjan, Hans, Johan, Lijing, Marianne and Misja, thank you for all your help with questions big and small.

I had a most enjoyable time as a member of the Structural Integrity & Composites group, and this was in no small part due to my wonderful friends and colleagues, both inside and outside the group. So Adrián the Viking, Small Adrián, Andrei, Andy, Aubryn, Bea, Bernhard, Calvin, Chirag, Cornelis, Chunsen, Daniel, Daniella, Derek, Dimitrios, Eirini, Fabricio, Freek, Freddy, Genevieve, Gillian, Greg, Gustavo, Hans, Hamideh, Huajie, Ilias, Ilhan, Irene, Jonathan, Jos, Julia, Julian, Julien, Keisuke, Kiki, Konstantin, Lei, Leila, Liaojun, Liesbeth, Lucas, Marcello, Marcias, Maria, Maria Pia, Maro, Martine, Mayank, Megan, Michiel, Michiel, Morteza, Nat, Natcha, Niels, Nikos, Nikos, Otto, Paola, Pedro, Ping, Roger, Romina, Sofia, Sotiris, Tian, Taylor, Vassilis, Vincent, Vincenius, Wandong, Zahid, and everyone I've forgotten to mention (sorry!). I have a message...foooooor *you*: Bedankt! Danke! Dhonnobad! Domo arigato! Дякую! Ευχαριστώ! Gracias! Grazie! Kòp kun! Merci! Mersi! Obrigado! Спасибо! Terima kasih! Thank you! 谢谢! for all the BBQs, birthday parties, cakes, coffe breaks, dinners, drinks, lunches, and general fun! Without you the faculty would be a boring place to work, don't ever change!

Thank you Daniel for teaching me the basics of the experimental techniques I used.

Thank you Dimitrios for your help with the acoustic emission measurements.

Thank you Tony Kinloch and Rhys Jones for our e-mail discussions, and for accepting a grad student as an equal partner in your scientific debates.

Thank you Gordon Williams for agreeing to sit on my thesis committee, although later events prevented that.

Thank you Ana, Erica, and Laurens of (at the time) TU Delft and Downside-up for your mentoring and your help developing my 'soft' skills.

Thank you to my students: Ali, Jur, Muhammad, Nicola, and Tijn, for your hard work and enthusiasm. Thank you for the chance to sharpen my ideas, and for all the useful data you provided me.

Thank you to Annemiek and all the staff at the 4TU.Centre for Research Data for your enthusiasm and your help with making my data available online.

Thank you Anne for your help with the cover.

Thank you Eirini for spotting that typo.

Thank you to the NWO for funding my project and to the Mosaic desk for their helpful response to any inquiries.

Last, but most certainly not least, dear Mum and Dad, thank you for all your support, and for teaching me to always do my best.

John-Alan



# CURRICULUM VITAE

## John Alan PASCOE

The author was born in Hilversum, the Netherlands, on the 7<sup>th</sup> of April 1987. In 2005 he graduated *cum laude* from the Gemeentelijk Gymnasium Hilversum. He then enrolled in the Aerospace Engineering programme at Delft University of Technology, where he obtained a Bachelor of Science degree *cum laude* in 2008.

The author remained at TU Delft for his master's degree, except for a three month internship at the Defence Science and Technology Organisation in Melbourne, Australia, under supervision of Mr G. Swanton and Mr L. Molent. After returning from his internship, the author worked on his master's thesis, entitled: 'Delamination of Bonded Repairs - A Damage Tolerance Approach'. This work was performed under the supervision of Dr R. Rodi and Dr Ir R.C. Alderliesten. As a result of this thesis, the author obtained the degree of Master of Science *cum laude* in Aerospace Engineering from TU Delft in May 2012.

After obtaining his MSc degree, the author was employed as a researcher at TU Delft for six months, working on a software package for crack growth predictions in fibre metal laminates.

In July 2012 the Netherlands Organisation for Scientific Research (NWO) awarded the author a Mosaic grant to fund the PhD research project that resulted in this thesis. The author started this project at TU Delft in October 2012, under supervision of Prof Dr Ir R. Benedictus as promotor and Dr Ir R.C. Alderliesten as co-promotor and daily supervisor.



# LIST OF PUBLICATIONS

## JOURNAL PAPERS

5. **J.A. Pascoe**, R. C. Alderliesten, R. Benedictus, *On the physical interpretation of the R-ratio effect and the LEFM parameters used for fatigue crack growth in adhesive bonds*, Under review at the International Journal of Fatigue, (2016).
4. **J.A. Pascoe**, D.S. Zarouchas, R. C. Alderliesten, R. Benedictus, *Using acoustic emission to understand fatigue crack growth within a single load cycle*, Under review at the International Journal of Fracture, (2016).
3. **J.A. Pascoe**, R.C. Alderliesten, R. Benedictus, *On the relationship between disbond growth and the release of strain energy*, [Engineering Fracture Mechanics](#) **133**, 1-13 (2015).
2. **J.A. Pascoe**, R.C. Alderliesten, R. Benedictus, *Methods for the Prediction of Fatigue Delamination Growth - A Critical Review*, [Engineering Fracture Mechanics](#) **112-113**, 72-96 (2013).
1. **J.A. Pascoe**, C.D. Rans, R. Benedictus, *Characterizing fatigue delamination growth behaviour using specimens with multiple delaminations: the effect of unequal delamination lengths*, [Engineering Fracture Mechanics](#) **109**, 150-160 (2013).

## CONFERENCE PAPERS

3. **J.A. Pascoe**, R.C. Alderliesten, R. Benedictus, *Characterising resistance to fatigue crack growth in adhesive bonds by measuring release of strain energy*, [Procedia Materials Science](#) (21<sup>st</sup> European Conference on Fracture) **2**, 80-87 (2016).
2. **J.A. Pascoe**, R.C. Alderliesten, R. Benedictus, *Towards Understanding Fatigue Disbond Growth via Cyclic Strain Energy*, [Procedia Materials Science](#) (20<sup>th</sup> European Conference on Fracture) **3**, 610-615 (2014).
1. **J.A. Pascoe**, C.D. Rans, R.C. Alderliesten, R. Benedictus, *Fatigue Disbonding of Bonded Repairs - An Application of the Strain Energy Approach*, in: A. Brot (ed.), *Proceedings of the 27<sup>th</sup> Symposium of the International Committee on Aeronautical Fatigue and Structural Integrity* (2013).